

January 01, 2014

## Multicomponent dark matter: possible signatures at colliders, satellites, and underground experiments

Gregory Peim  
*Northeastern University*

---

### Recommended Citation

Peim, Gregory, "Multicomponent dark matter: possible signatures at colliders, satellites, and underground experiments" (2014). *Physics Dissertations*. Paper 42. <http://hdl.handle.net/2047/d20003279>

This work is available open access, hosted by Northeastern University.

Multicomponent Dark Matter: Possible Signatures at Colliders, Satellites, and  
Underground Experiments

A dissertation presented

by

Gregory Peim

to

The Department of Physics

In partial fulfillment of the requirements for the degree of  
Doctor of Philosophy

in the field of

Physics

Northeastern University  
Boston, Massachusetts  
August 19, 2013

©  
Gregory Peim, 2013  
ALL RIGHTS RESERVED

Multicomponent Dark Matter: Possible Signatures at Colliders, Satellites, and  
Underground Experiments

by

Gregory Peim

ABSTRACT OF DISSERTATION

Submitted in partial fulfillment of the requirement  
for the degree of Doctor of Philosophy in Physics  
in the College of Science of  
Northeastern University,  
August 19, 2013

# Abstract

Collider and dark matter phenomenology of the Higgs boson, Supersymmetry, Stueckelberg extensions to the Standard Model as well as to the Minimal Supersymmetric Standard Model, and exotic TeV size scalars with naturalness implications in the context of multicomponent dark matter and asymmetric dark matter models are investigated. The measurement of signals of new physics at dark matter direct detection experiments as well as colliders (Large Hadron Collider, TeVatron, and a future muon collider) were discussed and explored in depth with a focus on the prospects for the discovery of new physics. The details of multicomponent dark matter models and each components role in the calculation of the dark matter relic density are analyzed.

# Acknowledgement

I would like to thank my advisor, Professor Pran Nath, for all that I have learned from him and all the time he has invested into me. The contents of this thesis would have never happened if it was not for his enthusiasm, dedication, guidance, and support. His commitment and enjoyment to research has greatly influenced me and I hope I still have such passion for my work years into the future.

I would like to express my gratitude to the other members of my Thesis Committee, Professor George Alverson, Professor Brent Nelson, and Professor Darien Wood for their help and patience during my Ph.D. studies. I believe we had many fruitful interactions that developed me as a researcher as well as an individual and I would like to thank you for being so understanding.

I would also like to thank my collaborators, Sujeet Akula, Dr. Baris Altunkaynak, Dr. Ning Chen, Dr. Daniel Feldman, Dr. Wan-Zhe Feng, Professor Katherine Freese, Dr. Michael Holmes, Mengxi Liu, and Dr. Zuowei Liu, with whom the research contained in this thesis would not have happened. Thank you for the constant encouragement on all the projects we worked on.

A lot of this could not happen without the help of the Physics department, specifically Lindsay Day, Tom Hamrick, Alina Mak, Suzanne Robblee, Professor Mark Williams, and Nancy Wong. Additionally, I would like to thank the Gordon En-

gineering Leadership Program for providing me with support during my last year. Most of all Marlys Vaughn, Professor Stephen McKnight, Professor Simon Pitts, Professor Steve McGonagle, Professor Steven Klosterman, and Amy Manley. I learned a lot from you and I would like to thank you for all the time you invested into me.

I am very grateful to the people who made sure that I enjoyed Boston rather than work all the time in a windowless office including Darin Baumgartel, Laura Bulgryn, Matthew Chasco, Julio Chapeton, Dana Eiesland, David Falta, Kate Foss, Rohan Gala, Arda Halu, Dr. Benjamin Jurke, Molee Leng, Dr. Micah McCauley, Dr. Thaya Paramanathan, Francisco Reynoso, Rachel Rosenberg, Pammy Taylor, and Dr. Dashun Wang.

Finally, and most of all, I would like to thank my family for their encouragement and their endless support.

# Contents

<b>Abstract</b>	<b>3</b>
<b>Acknowledgement</b>	<b>5</b>
<b>Table of contents</b>	<b>7</b>
<b>List of figures</b>	<b>10</b>
<b>List of tables</b>	<b>14</b>
<b>1 Introduction and Overview</b>	<b>15</b>
<b>2 The Standard Model</b>	<b>18</b>
2.1 Particle Masses in the Standard Model . . . . .	19
2.2 Challenges of the Standard Model . . . . .	20
<b>3 Asymmetric Dark Matter in the Standard Model</b>	<b>21</b>
3.1 Introduction . . . . .	21
3.2 Cosmic coincidence and asymmetric dark matter . . . . .	23
3.3 Analysis in the Standard Model framework . . . . .	26
3.3.1 $T > T_{\text{EWPT}}$ . . . . .	27
3.3.2 $T < T_{\text{EWPT}}$ . . . . .	29
3.3.3 Determining the Asymmetric dark matter mass . . . . .	32
3.4 Asymmetric dark matter in a Stueckelberg extension of the SM . . . .	38
3.4.1 Resonant annihilation of symmetric dark matter . . . . .	39

<b>4</b>	<b>Supersymmetry</b>	<b>47</b>
4.1	Minimal Supersymmetric Standard Model Overview . . . . .	47
4.2	$R$ -Parity . . . . .	49
<b>5</b>	<b>Multicomponent Dark Matter</b>	<b>51</b>
5.1	Introduction . . . . .	51
5.2	Multicomponent Hidden Sector Models . . . . .	53
5.2.1	Multicomponent $U(1)_X$ model . . . . .	53
5.2.2	Two component dark matter: Majorana + Dirac . . . . .	58
5.2.3	Three component dark matter: Dirac and two spin-0 particles	58
5.2.4	Four component dark matter: Majorana, Dirac, and two spin-0 particles . . . . .	59
5.3	Multicomponent Leptophilic $U(1)_X \times U(1)_C$ model . . . . .	60
5.4	Relic Density in a Two Component Model . . . . .	68
<b>6</b>	<b>Asymmetric Dark Matter in the MSSM</b>	<b>71</b>
6.1	Introduction . . . . .	71
6.2	Analysis in supersymmetric framework . . . . .	73
6.2.1	$T > M_{\text{SUSY}}$ . . . . .	73
6.2.2	$T_1 > T > M_2 > T_{\text{EWPT}}$ . . . . .	74
6.2.3	The AsyDM mass: SUSY case . . . . .	75
6.3	Asymmetric dark matter in a Stueckelberg extension of the MSSM . .	77
6.4	Decay of the $\rho$ . . . . .	81
<b>7</b>	<b>Early Search for SUSY at the LHC</b>	<b>84</b>
7.1	Introduction . . . . .	84
7.2	Standard Model Backgrounds at $\sqrt{s} = 7 \text{ TeV}$ . . . . .	84
7.3	Sparticle production cross sections at $\sqrt{s} = 7 \text{ TeV}$ . . . . .	85

7.4	Signature Analysis and SUSY Discovery Reach at $\sqrt{s} = 7\text{TeV}$ and $1\text{fb}^{-1}$ . . . . .	89
7.5	LHC Reach with $35\text{pb}^{-1}$ of Data . . . . .	90
7.6	Implications of The Early LHC Constraints . . . . .	96
<b>8</b>	<b>Signatures</b>	<b>100</b>
8.1	Asymmetric Dark Matter Signatures at Colliders . . . . .	100
8.1.1	$Z'$ exchange contribution to $\mu^+\mu^- \rightarrow e^+e^-$ at loop level . . . . .	102
8.2	The Predictive Higgs Pole Model . . . . .	105
8.2.1	Signatures of the Higgs-pole region at the LHC . . . . .	107
8.3	Higgs discovery implications . . . . .	110
8.3.1	Implications for mSUGRA . . . . .	110
8.3.2	125 GeV Higgs boson and dark matter . . . . .	114
<b>9</b>	<b>Conclusions</b>	<b>118</b>
9.1	Multicomponent Dark Matter . . . . .	119
9.2	Asymmetric Dark Matter . . . . .	119
9.3	Early Discovery Potential of the LHC . . . . .	120
9.4	LHC SUSY Searches . . . . .	121
9.5	Higgs Discovery at the LHC . . . . .	122
9.6	Further Research . . . . .	123
	<b>Bibliography</b>	<b>124</b>

# List of Figures

- 3.1 An exhibition of the thermal relic density of  $\bar{\psi}$  as a function of  $M_{Z'}$  in the model with gauged  $L_\mu - L_\tau$  for different values of the coupling constant. The left panel shows the case  $\gamma = 0$  and the right panel shows  $\gamma = 1.3 \times 10^{-10}$ . In both cases, the analysis shows that the component of dark matter that is thermally produced can be efficiently depleted by resonant annihilation via the  $Z'$  pole. . . . . 46
- 6.1 An exhibition of the depletion of the MSSM neutralino dark matter below 10% of the WMAP relic density for cold dark matter. Parameter points are displayed by their light CP even Higgs mass and the yellow band corresponds to 10% of the WMAP-7 observed limit. The left panel shows the parameter points of mSUGRA and the right panel shows the non-universal gaugino parameter points. All parameter points shown pass the general constraints. . . . . 81
- 6.2 A generic diagram showing the decay of the  $\rho$  to one of the final states which could be  $\mu^+\mu^-$ ,  $\nu_\mu\bar{\nu}_\mu$ ,  $\tau^+\tau^-$ ,  $\nu_\tau\bar{\nu}_\tau$  via exchange of sleptons, charginos and neutralinos at one loop. . . . . 82
- 7.1 An exhibition of the sparticle production cross sections at the LHC at  $\sqrt{s} = 7$  TeV for mSUGRA as a function of the universal gaugino mass  $m_{1/2}$  at the GUT scale when  $m_0 = 500$  GeV,  $A_0 = 0$ ,  $\tan\beta = 20$  and  $\text{sign}(\mu) = +1$ . Left panel: production cross sections of  $\tilde{g}\tilde{g}$ ,  $\tilde{g}\tilde{q}$ ,  $\tilde{q}\tilde{q}$  (solid red, dashed green, dashed blue lines). Middle panel: production cross sections for  $\tilde{g}\chi^\pm$ ,  $\tilde{g}\chi^0$  (solid red, dashed green lines). Right panel: production cross sections for  $\chi^\pm\chi^\pm$ ,  $\chi^\pm\chi^0$ ,  $\chi^0\chi^0$  (solid red, dashed green, dashed blue lines). . . . . 88
- 7.2 Contour plots with constant values of  $\log(\sigma_{SUSY}/\text{fb})$  for  $\sigma_{SUSY}$  in  $m_{\tilde{g}} - m_{\chi^\pm}$  mass plane for the case with nonuniversalities in the gaugino sector. Gaugino masses  $m_1$ ,  $m_2$ , and  $m_3$  vary up to 1 TeV. First panel from left:  $m_0 = 250$  GeV,  $\tan\beta = 10$  while  $A_0 = 0$ ,  $\text{sign}(\mu)=+1$ ; second panel from left:  $m_0 = 250$  GeV,  $\tan\beta = 30$ ; third panel from left:  $m_0 = 1000$  GeV,  $\tan\beta = 10$ ; fourth panel from left:  $m_0 = 1000$  GeV,  $\tan\beta = 30$ . . . . . 90

- 7.3 A reach plot for mSUGRA using the Standard Model backgrounds given in Table 7.1 at the LHC with  $\sqrt{s} = 7 \text{ TeV}$  with  $1 \text{ fb}^{-1}$  of integrated luminosity. The mSUGRA parameters used are  $A_0 = 0$ ,  $\tan \beta = 45$ ,  $\text{sign}(\mu) = 1$ . The condition used for a signal to be observable is  $S > \max(5\sqrt{B}, 10)$  where  $B$  stands for the Standard Model background. Early LHC reaches at  $1 \text{ fb}^{-1}$  for the gluino ( $\tilde{g}$ ), the chargino ( $\tilde{\chi}_1^\pm$ ), the neutralino ( $\chi_1^0$ ), the stau ( $\tilde{\tau}_1$ ), and the stop ( $\tilde{t}_1$ ) are exhibited in the inset where the  $y$ -axis is plotted on a logarithmic scale. . . . . 91
- 7.4 Left: Reach plot with  $35 \text{ pb}^{-1}$  of integrated luminosity using the ATLAS cuts discussed in the text with different  $\tan \beta$  and  $A_0$ :  $A_0 = 0$  and  $\tan \beta = 3$  (dashed line);  $A_0 = 0$  and  $\tan \beta = 45$  (solid green line);  $A_0 = 2m_0$  and  $\tan \beta = 45$  (solid red line). For comparison we give the ATLAS observed limit ( $A_0 = 0$  and  $\tan \beta = 3$ ) (solid blue line). Right: Reach plot with  $35 \text{ pb}^{-1}$  of integrated luminosity of data using the ATLAS 0 lepton cuts. For comparison we give the ATLAS observed limit (red dashed line). . . . . 93
- 7.5 Top left panel: Number of signal events in the  $m_0 - m_{1/2}$  plane for the case  $A_0 = 0, \tan \beta = 3$  using the 1 lepton ATLAS cuts in the  $m_0 - m_{1/2}$  plane. The dark areas correspond to number of events greater than 2 with the actual numbers indicated along the vertical line to the right while the white areas are filled with models but have number of events smaller than 2. Top right panel: Same as the left panel except that the plot is  $m_{\tilde{g}}$ (gluino) –  $m_{\tilde{q}}$ (squark) mass plane for the lightest squark of the first 2 generations. The square region in the left panel becomes squeezed into the polygon-like region in the physical mass plane in the right panel. One may note that the ATLAS constraints do not rule out a low mass gluino on the scale of order 400 GeV for heavy squarks. Bottom left panel: The same as the top left panel except that the analysis is done using 0 lepton ATLAS cuts. Bottom right panel: Same as the top right panel except that the analysis is done using the 0 lepton ATLAS cuts. The (red) stars correspond to channel D. In channel D we find maximally 51 events over the space scanned after a requirement that the number of events be at least 15 before cuts. However, when only considering models not already excluded by channels A and C, the number of events in channel D is maximally 18. . . . . 95

7.6	<p>Upper left panel: An exhibition of the allowed models indicated by grey (dark) dots in the <math>m_0 - m_{1/2}</math> plane when only flavor and collider constraints are imposed. The region excluded by ATLAS (as well as CMS) lies below the thick black curve in the left hand corner. Upper right panel: same as the left upper panel except that only an upper bound on relic density of <math>\Omega h^2 \leq 0.14</math> is imposed. Lower left panel: Same as the upper left panel except that the relic density constraint as in the upper right panel is also applied. This panel exhibits that most of the parameter space excluded by ATLAS is already excluded by the collider/ flavor and relic density constraints. The dark region below the ATLAS curve is the extra region excluded by ATLAS which was not previously excluded by the indirect constraints. Lower right panel: The analysis of this figure is similar to the lower left panel except that models with <math> \mu  &lt; 500</math> GeV are exhibited in green. . . . .</p>	97
8.1	<p>Left: Leptonic final states in a <math>\mu^+\mu^-</math> collider where the <math>\mu^+\mu^- \rightarrow l\bar{l}</math>, with <math>l = \mu, \nu_\mu, \tau, \nu_\tau</math>, final state arising from direct channel poles involving <math>Z'</math>. The <math>Z'</math> pole does not allow for a <math>e^+e^-</math> final state and thus the relative production cross section for <math>\mu^+\mu^- \rightarrow \tau^+\tau^-</math> vs <math>\mu^+\mu^- \rightarrow e^+e^-</math> can be used to detect the existence of a <math>L_\mu - L_\tau</math> gauged boson. Right: A similar analysis is possible for <math>\rho</math> but its production is suppressed relative to <math>Z'</math> since it must be produced at the loop level. . .</p>	101
8.2	<p>An exhibition of the relative strength of the <math>\tau^+\tau^-</math> vs <math>e^+e^-</math> signal at a muon collider. The presence of a detectable <math>Z'</math> resonance in the <math>\mu^+\mu^- \rightarrow \tau^+\tau^-</math> channel provides a smoking gun signature for the gauged <math>L_\mu - L_\tau</math> AsyDM model. A similar resonance is also present in the <math>\mu^+\mu^- \rightarrow \mu^+\mu^-</math> channel while <math>\mu^+\mu^- \rightarrow e^+e^-</math> cross section shows no such enhancement in the <math>Z'</math> region. . . . .</p>	101
8.3	<p><math>Z' - \gamma</math> and <math>Z' - Z</math> exchange via <math>\mu^+\mu^-, \nu_\mu\bar{\nu}_\mu, \tau^+\tau^-, \nu_\tau\bar{\nu}_\tau</math> loops. . . .</p>	103
8.4	<p>Left: Distribution of the ratio of the effective mass peak to the gluino mass. The models plotted here are the 700 model subset and the peak is found after adding the SM background and applying a cut as discussed in the text. We find the peak to be at <math>1.57 \pm 0.085</math>. Right: Distribution of the ratio of effective mass peak to the mass difference between the two lightest neutralinos under the same cut. The mass difference between the two lightest neutralinos corresponds to the upper bound of the edge in the OSSF dilepton invariant mass plot. We find the peak to be at <math>12.50 \pm 0.721</math>. . . . .</p>	109

- 8.5 Left panels: plots of the 2D posterior probability densities,  $1\sigma$  and  $2\sigma$  contours are also drawn. Right panels: plots of the profile likelihoods. Top: in the  $m_0 - m_{1/2}$  plane. Middle: in the  $A_0/m_0 - \tan\beta$  plane. Bottom: in the  $m_A - \tan\beta$  plane. The posterior mean is marked by a large dot while the best-fit point is shown by a circled 'X'. The color bar above the top panel gives the relative likelihood which increases left-to-right. . . . . 113
- 8.6 Left panels: plots of the 2D posterior probability densities,  $1\sigma$  and  $2\sigma$  contours are also drawn. Right panels: plots of the profile likelihoods. Top: in the  $m_{\tilde{g}} - m_{\tilde{q}}$  plane. Upper-middle: in the  $m_{\tilde{q}} - m_{\tilde{\chi}_1^\pm}$  plane. Lower-middle: in the  $m_{\tilde{\tau}_1} - m_{\tilde{t}_1}$  plane. Bottom: in the  $\mu - m_{\tilde{g}}$  plane. The posterior mean is marked by a large dot while the best-fit point is shown by a circled 'X'. The color bar above the top panel gives the relative likelihood which increases left-to-right. . . . . 115
- 8.7 Plots of  $\mathcal{R} \equiv (\Omega h^2) / (\Omega h^2)_{\text{WMAP}}$  vs the neutralino mass  $m_{\tilde{\chi}_1^0}$ . The left panel presents the 2D posterior PDF, and the right panel presents the profile likelihood. The analysis shows that virtually all of credible region of mSUGRA will be probed by the SuperCDMS and XENON-1T experiments. The color bar above the panels gives the relative likelihood which increases left-to-right. . . . . 116

# List of Tables

3.1	A list of three models which allow for generation of asymmetric dark matter in an extension of the Standard Model. . . . .	26
3.2	A display of the various interactions that allow a transfer of the $B - L$ asymmetry from the Standard Model sector to the dark matter sector.	37
4.1	Table showing the quantum numbers for the Standard Model particles and their super-partners. Please note that the table is done using $Q_{EM} = T_3 + \frac{1}{2}Y$ . . . . .	48
7.1	An exhibition of the Standard Model backgrounds computed in this work at $\sqrt{s} = 7$ TeV. All processes were generated using MADGRAPH 4.4. Our notation here is that $\ell = e, \mu, \tau$ , and $all = \ell, \nu, jets$ . Cuts1-Cuts4 indicated in the table are defined in (7.1). In the background analysis we eliminate double counting between the process $W^\pm + t\bar{b}$ ( $\bar{t}b$ ) and $t\bar{t}$ by subtracting out double resonant diagrams of $t\bar{t}$ when calculating $W^\pm + t\bar{b}$ ( $\bar{t}b$ ). . . . .	86
8.1	General predictions for the sparticle masses for the models with $m_0 \leq 10$ TeV satisfying all phenomenological constraints discussed in the text. It is further found that $m_0 \geq 1.05$ TeV, and the scalar masses are bounded as : $m_{\tilde{t}_1} \geq 323$ GeV, $m_{\tilde{b}_1} \geq 706$ GeV, $m_{\tilde{\tau}_1} \geq 484$ GeV, $m_{\tilde{q}} \geq 1070$ GeV, $m_{\tilde{\nu}} \geq 1050$ GeV, and $m_A \geq 187$ GeV. . . . .	107
8.2	Typical size of dominant branching ratios of the sparticles with the largest production modes emerging from proton-proton collision at the LHC over a subset of 700 models. Here $u, d$ includes the first 2 generations of quarks and $l$ includes all 3 generations of leptons (hence the factors of 2 and 3 in the Table). The factor of 4 includes $u, d$ and the conjugate modes for the charginos. In addition to the three dominant sparticles arising from proton-proton collisions (the three cases considered in the Table), a small subset of models are found to produce light stops ( $m_{\tilde{t}_1} \sim 350$ GeV) at the LHC which decay via $\tilde{t}_1 \rightarrow (t\tilde{\chi}_1^0, b\tilde{\chi}_1^-, t\tilde{\chi}_2^0)$ respectively, depending on the particular model point. . . . .	108

# Chapter 1

## Introduction and Overview

With the Large Hadron Collider (LHC) having accumulated a substantial amount of integrated luminosity [1], dark matter direct detection experiments collecting data [2], and the Planck satellite releasing its observations [3], particle physics finds itself in a very exciting data enriched era. The field recently surpassed a milestone with the July 2012 announcement of a  $5\sigma$  detection of a boson around 125 GeV, with preliminary results indicating a Higgs boson [4–8]. The content of this thesis is directly tied to the new wave of data that has come forth from the LHC and dark matter related experiments.

The Standard Model (SM) [9–16] of electroweak and strong interactions has been successful in explaining a large amount of data in particle physics. Specifically the Standard Model is in excellent agreement with the high precision data from various collider experiments including the large electron-positron collider (LEP), TeVatron, and the LHC. The Standard Model is based on the gauge group  $SU(3)_C \times SU(2)_L \times U(1)_Y$ , where  $SU(3)_C$  is the gauge group of the strong color interaction,  $SU(2)_L$  is the gauge group of the weak chiral interaction, and  $U(1)_Y$  is the hypercharge fac-

tor. In the Standard Model, the electroweak gauge symmetry of  $SU(2)_L \times U(1)_Y$  is spontaneously broken to the electromagnetic gauge group  $U(1)_{EM}$ , by the Higgs mechanism [17–20]. The mechanism introduces a new  $SU(2)_L$  scalar doublet that develops a vacuum expectation value and gives mass to the  $W^\pm$  gauged boson as well as the  $Z^0$  gauged boson and keeps the photon massless. After the symmetry is broken, a residual  $CP$ -even scalar field is left and is known as the Higgs boson. The recent discovery of the Higgs boson at the LHC marks a milestone in that all the particles predicted in the Standard Model have now been discovered.

However, the theory is not perfect and fails to provide an explanation of a variety of observed phenomena in nature. This includes the existence of cold dark matter, dark energy, baryon and anti-baryon asymmetry in the Universe, as well as neutrino masses and mixing. From a theoretical viewpoint the Standard Model fails to explain gravity, the Higgs fine-tuning, and why there are only 3 generations of quarks and leptons. The contents of this thesis focuses mainly on trying to explain the existence of cold dark matter as well as the anti-baryon asymmetry in the Universe and will touch on the inclusion of gravity and the Higgs fine-tuning.

First, let us begin by exploring what dark matter is. In the 1930s, when studying the rotational curves of galaxies and comparing that motion to the amount of visible light (coming from the stars) it was found that the curves could only be explained by additional mass which interacted gravitationally with other visible objects. This observation can be explained by introducing a new type of matter, i.e. dark matter (DM) which interacts gravitationally (and I will assume it also interacts weakly, i.e. WIMP). Thus dark matter must be electromagnetically neutral.

Experimental data has found that there are more baryons than anti-baryons in the Universe. Why is this? How did this come about? Additionally it is interesting to

investigate if there is some underlying principle why the ratio of the dark matter relic density to baryonic relic density is  $\sim 5$ , which is called the cosmic coincidence. The focus of this thesis is to explain the cosmic coincidence by using the assumption that  $B - L$  excess in the visible sector has been generated in the early universe which can then generate (asymmetric) dark matter (AsyDM) carrying a non-vanishing  $B - L$ . Dark matter, however, could be multicomponent consisting not only of dark matter from AsyDM but also of other species such as the neutralino, which is the leading dark matter candidate in supersymmetry/supergravity theories.

Further elaboration of the above three paragraphs is the focus of this thesis and it is organized in the following manner. In Chapter 2, I give a very brief overview of the Standard Model including how the masses are generated and the challenges. Next, the Stueckelberg mechanism is used to extend the Standard Model to generate a dark matter candidate that can explain the cosmic coincidence (Chapter 3). The analysis is done at different temperature scales and the depletion of the symmetric component is explored. In Chapter 4, a brief introduction is given of supersymmetry. In Chapter 5 we extend the Minimal Supersymmetric Standard Model using a Stueckelberg mechanism which introduces the possibility of multicomponent dark matter. We then revisit asymmetric dark matter in Chapter 6 for the Minimal Supersymmetric Standard Model case. In Chapter 7 we explore the possibility of detecting supersymmetry at the LHC as well as the implications of the results at the LHC and in Chapter 8 we explore signatures that can be used to test models discussed in earlier chapters. Conclusions are given in Chapter 9.

# Chapter 2

## The Standard Model

In this chapter we give a short overview of the Standard Model (SM) [9, 10, 13, 14, 21] and for readers who would like a more in-depth introduction should see [16]. The Standard Model of particle physics combines all the known interactions (the electromagnetic, the weak, and the strong interaction) except gravity. The theory has been tested very extensively and has excellent agreement with experimental data. Most recently, (July 2012), the last remaining particle (the Higgs boson) seems to have been discovered at the LHC [4–8].

The Standard Model contains in it three generations of spin- $\frac{1}{2}$  fermions (quarks and leptons), spin-1 bosons (gluon, photon,  $W^\pm$ , and  $Z^0$ ) as well as a spin-0 scalar (Higgs Boson) and the theory is based on the gauge group  $SU(3)_C \times SU(2)_L \times U(1)_Y$ , which determine the interactions of the Standard Model particles. Here  $C$  stands for color,  $L$  stands for left chiral, and  $Y$  stands for hypercharge. The interactions are governed by 8  $SU(3)_C$  gauge fields (“strong interaction”), 3  $SU(2)_L$  gauge field (“weak interaction”), and 1  $U(1)_Y$  gauge field (“hypercharge interaction”). The electromagnetic charge derives from these fields by the Gell-Mann-Nishijima rela-

tion

$$Q_{\text{EM}} = T_3 + \frac{1}{2}Y \quad (2.1)$$

where  $Y$  is the generator of the  $U(1)_Y$  group and  $T_3$  is a generator of the  $SU(2)_L$  group.

## 2.1 Particle Masses in the Standard Model

To give mass to the “known” particles in the Standard Model one uses the Higgs mechanism [17–20], which introduces an additional scalar  $SU(2)_L$  doublet of the form

$$\phi = \begin{pmatrix} H^+ \\ H^0 \end{pmatrix} \quad (2.2)$$

with a potential

$$V(\phi) = -\mu^2 \phi^\dagger \phi + \lambda (\phi^\dagger \phi)^2 \quad (2.3)$$

where  $\mu^2, \lambda > 0$ . The tachyonic mass term for the Higgs field gives rise to a spontaneous symmetry breaking. This results in a non-vanishing vacuum expectation value (VEV).

$$\langle \phi \rangle_0 = \begin{pmatrix} 0 \\ v/\sqrt{2} \end{pmatrix} \quad (2.4)$$

where  $v = \mu/\sqrt{\lambda}$ . This means  $H^0$  can be redefined as  $(v + h)/\sqrt{2}$  and the tree level mass of the Higgs is  $m_h^2 = 2\mu^2 > 0$ .

## 2.2 Challenges of the Standard Model

The Standard Model is a very well tested theory and its theoretical predictions agree with experimental measurement with a high precision. However, many phenomena remain unexplained in the Standard Model. Astrophysical experiments have detected the existence of cold dark matter and dark energy. The Standard Model cannot explain either of these observations. In the Standard Model neutrinos are massless and do not mix. However, atmospheric and solar neutrino experiments have observed neutrinos oscillating between flavor, which implies that they have a non-zero mass. The Universe has an imbalance of matter over anti-matter. The Standard Model does not provide a sufficient explanation of this. As mentioned earlier, the Standard Model does not include gravity. A complete theory of particle physics should include all fundamental forces. The square of the Higgs mass gets quantum corrections of the form  $m_h^2(\Lambda) = m_h^2 + c\Lambda^2$ . To be consistent with the observed electroweak phenomena, the bare mass term  $m_h^2$  needs to cancel the correction term to high precision.

The focus of the rest of the thesis is the exploration of cold dark matter in a multicomponent picture. The implications of multicomponent dark matter in direct detection and their tests at colliders will also be discussed.

# Chapter 3

## Asymmetric Dark Matter in the Standard Model

### 3.1 Introduction

In this chapter we will discuss asymmetric dark matter. The majority of this analysis comes directly from [22]. To begin let us consider one of the outstanding puzzles in particle physics and cosmology that relates to the so called cosmic coincidence, i.e., the apparent closeness of the amount of baryon asymmetry to the amount of dark matter in the Universe. Thus the WMAP-7 result, with RECFAST version 1.5 to calculate the recombination history [2], gives the baryonic relic density to be  $100\Omega_{\text{B}}h_0^2 = 2.255 \pm 0.054$  and the dark matter relic density to be  $\Omega_{\text{DM}}h_0^2 = 0.1126 \pm 0.0036$ , which leads to

$$\frac{\Omega_{\text{DM}}h_0^2}{\Omega_{\text{B}}h_0^2} = 4.99 \pm 0.20. \quad (3.1)$$

The closeness of  $\Omega_{\text{DM}}h_0^2$  and  $\Omega_{\text{B}}h_0^2$  points to the possibility that the baryonic matter and dark matter may have a common origin; a possibility that has been noted for some time [23–27]. Dark Matter models of this type are called asymmetric dark matter (AsyDM).

In this chapter we analyze this issue in the framework of a Stueckelberg  $U(1)$  extension of the Standard Model [28, 29]. There are two main constraints in building models with asymmetric dark matter. First, we need a mechanism for transferring a  $B - L$  asymmetry produced in the early universe to dark matter. Second, we must have a mechanism for depleting the symmetric component of dark matter generated via thermal processes.

The above issues have been discussed in the literature in a variety of works (for a review see [30] and references with in). The models based on the Stueckelberg extensions discussed here are different from the ones considered previously both in terms of the mechanism for depletion of the symmetric component of dark matter. Specifically, we consider a  $U(1)_X$  extension of the Standard Model gauge group which is anomaly free. Further, we consider dark matter candidates which will carry lepton number but not a baryon number, and are singlets of the Standard Model gauge group. In the leptonic sector it is known [31, 32] that for the Standard Model case we may choose one of the linear combinations  $L_e - L_\mu$ ,  $L_\mu - L_\tau$ ,  $L_e - L_\tau$  to be anomaly free and can be gauged. Here we consider a gauged  $L_\mu - L_\tau$  in the discussion of asymmetric dark matter as this choice is the more appropriate one for the analysis here. Specifically, we will consider a  $U(1)_X$ ,  $X = L_\mu - L_\tau$  Stueckelberg extension of the Standard Model.

## 3.2 Cosmic coincidence and asymmetric dark matter

For the analysis in this chapter we will assume that a  $B - L$  asymmetry has been generated in the early universe. It will not be speculated on how this asymmetry came about as it could be by any number of different processes such as baryogenesis or leptogenesis [33]. The asymmetry is then transferred to the dark sector at high temperatures via an interaction of the form [34]

$$\mathcal{L}_{\text{asy}} = \frac{1}{M_{\text{asy}}^n} \mathcal{O}_{\text{DM}} \mathcal{O}_{\text{asy}}, \quad (3.2)$$

where  $M_{\text{asy}}$  is the scale of this interaction,<sup>1</sup> and  $\mathcal{O}_{\text{asy}}$  is an operator constructed from Standard Model fields which carries a non-vanishing  $B - L$  quantum number while  $\mathcal{O}_{\text{DM}}$  carries the opposite  $B - L$  quantum number. This interaction would decouple at some temperature greater than the dark matter mass. As the Universe cools, the dark matter asymmetry freezes on order of the baryon asymmetry, which explains the observed relation between baryon and dark matter densities.

At the temperature where Equation (3.3) is operational, and using the fact that the chemical potential of particles and anti-particles are different, the asymmetry in

---

<sup>1</sup>In the radiation-dominated era, the Hubble expansion rate is given by  $H \sim T^2/M_{\text{Pl}}$ , where  $M_{\text{Pl}} = 2.435 \times 10^{18}$  GeV is the reduced Plank mass. For an interaction suppressed by a factor  $1/M_{\text{asy}}^n$ , the interaction rate at temperature  $T$  is  $\Gamma(T) \sim T^{2n+1}/M_{\text{asy}}^{2n}$ . Thus, the interaction will decouple if  $\Gamma < H$ , i.e., when

$$M_{\text{asy}}^{2n} > M_{\text{Pl}} T^{2n-1}. \quad (3.3)$$

the particle and antiparticle number densities is given by

$$\begin{aligned}
n_i - \bar{n}_i &= \frac{\mathfrak{g}_i}{2\pi^2} \int_0^\infty dq q^2 \left[ (e^{(E_i(q)-\mu_i)/T} \pm 1)^{-1} - (e^{(E_i(q)+\mu_i)/T} \pm 1)^{-1} \right] \\
&\equiv \frac{\mathfrak{g}_i T^3}{6} \times \begin{cases} \beta\mu_i c_i(b) & \text{bosons,} \\ \beta\mu_i c_i(f) & \text{fermions,} \end{cases} \quad (3.4)
\end{aligned}$$

where  $n_i$  and  $\bar{n}_i$  denote the equilibrium number density of particle and antiparticle respectively,  $\mathfrak{g}_i$  counts the degrees of freedom of the particle,  $E_i(q) = \sqrt{q^2 + m_i^2}$  where  $m_i$  is the mass of particle  $i$ ,  $\mu_i$  is the chemical potential of the particle ( $-\mu_i$  is the chemical potential of the antiparticle), and  $+1$  ( $-1$ ) in the denominator is for the case when the particle is a fermion (boson). In the ultra relativistic limit ( $T \gg m_i$ ) the mass of the particle can be dropped. For the analysis done throughout this chapter we will use the approximation of a weakly interacting plasma where  $\beta\mu_i \ll 1$ , and  $\beta \equiv 1/T$  and one has

$$n_i - \bar{n}_i \sim \frac{\mathfrak{g}_i T^3}{6} \times \begin{cases} 2\beta\mu_i + \mathcal{O}((\beta\mu_i)^3) & \text{bosons,} \\ \beta\mu_i + \mathcal{O}((\beta\mu_i)^3) & \text{fermions.} \end{cases} \quad (3.5)$$

In the limit where Equation (3.5) holds we have  $c_i(b) = 2, c_i(f) = 1$ . This limit is a useful approximation as it simplifies the analysis of the chemical potentials that are needed in the generation of dark matter. However, full analysis can be easily done by using the exact expression of Equation (3.4). The mass of the dark matter is constrained by the experimental ratio of dark matter to baryonic matter given in Equation (3.1). Defining  $B$  to be the total baryon number in the Universe and  $X$  to

be the total dark matter number, we obtain

$$\frac{\Omega_{\text{DM}}}{\Omega_{\text{matter}}} = \frac{X \cdot m_{\text{DM}}}{B \cdot m_{\text{B}}} \approx 5, \quad (3.6)$$

so that the dark particle mass is given by

$$m_{\text{DM}} \approx 5 \cdot \frac{B}{X} \cdot 1 \text{ GeV}. \quad (3.7)$$

Applying the general thermal equilibrium method [35], it is not difficult to express  $B$  and  $X$  in terms of the chemical potentials and then find their ratio. We note one subtlety is that while  $X$  and  $B - L$  (where by  $B - L$  we mean the  $B - L$  in the Standard Model sector) are conserved after the interaction in Equation (3.2) decouples,  $B$  is not. Thus, for example, the top quark would drop out from the thermal bath at some temperature  $T_t$  and one must solve the new set of  $\mu$  equations at  $T < T_t$  which would affect the computation of  $B$  although  $B - L$  is conserved. Typically one takes  $T_t$  to be  $M_t$  but it could be somewhat lower. Specifically, as the temperature drops below  $M_t \sim 173 \text{ GeV}$ , the top quark becomes semi-relativistic but could still be involved in the thermal equilibrium constraints. Further, as the temperature falls below the temperature where sphaleron processes decouple,  $B$  and  $L$  would be separately conserved down to the current temperatures. Thus the relevant  $B$  to compute the dark matter mass in Equation (3.7) would be the baryon number below the sphaleron temperature which we label  $B_{\text{final}}$ . It is useful to express  $X$  and  $B_{\text{final}}$  in terms of  $B - L$  so that  $X = x(B - L)$  and  $B_{\text{final}} = b(B - L)$  where  $b$  is to be determined later (see Equation (3.28)). Thus, Equation (3.7) can be rewritten as

$$m_{\text{DM}} \approx 5 \cdot \frac{b}{x} \cdot 1 \text{ GeV}. \quad (3.8)$$

Model A	SM	$T_{\text{int}} > T_{\text{EWPT}}$
Model B		$T_{\text{EWPT}} > T_{\text{int}} > M_t$
Model C		$T_t > T_{\text{int}} > M_W$

Table 3.1: A list of three models which allow for generation of asymmetric dark matter in an extension of the Standard Model.

In this chapter we will discuss three broad classes of models labeled Models A-C (see Table 3.1). For Models A, the asymmetry transfer interaction, of the form of Equation (3.2), is active only above the electroweak phase transition (EWPT) scale, i.e.,  $T_{\text{int}} > T_{\text{EWPT}}$  ( $T_{\text{EWPT}} \sim 200 \text{ GeV} - 300 \text{ GeV}$  where the Higgs gets its VEV). For Model B and C, the interaction which transfers the asymmetry could be active *also* below the EWPT scale, i.e.,  $T_{\text{EWPT}} > T_{\text{int}}$ . More specifically, in Model B we consider the temperature regime  $T_{\text{EWPT}} > T_{\text{int}} > M_t$ , and in Model C we discuss  $T_t > T_{\text{int}} > M_W$  where  $M_W$  is the mass of  $W$  boson. These three cases are summarized in Table 3.1. There can be additional subcases for these models corresponding to different choices of the  $B - L$  transfer in Equation (3.2).

### 3.3 Analysis in the Standard Model framework

In this section we will determine the dark matter mass in terms of the  $B - L$  asymmetry in the Standard Model framework utilizing Equation (3.8) for Models A-C. As mentioned above, we will discuss three different temperature regimes where the  $B - L$  transfer takes place. It should be noted that the dark matter mass depends only on the  $(B - L)$ -charge of the operator  $\mathcal{O}_{\text{asy}}$  that enters in Equation (3.2) and not on other particulars of the interaction. We will give several examples of the operator  $\mathcal{O}_{\text{asy}}$  and compute the dark matter mass for each example.

### 3.3.1 $T > T_{\text{EWPT}}$

First we consider the case when the temperature is above the electroweak phase transition scale,  $T_{\text{EWPT}}$ . In this case the following fields are in the relativistic plasma in the early universe: three generations of left-handed lepton doublets  $L_i$  and quark doublets  $q_i$ , three generations of right-handed charged leptons  $e_i$  and up and down-type quarks  $u_i$  and  $d_i$  ( $i = 1, 2, 3$ ), and a complex Higgs doublets  $H_i = (h_i^+, h_i^0)^T$ . Since the  $Z$  boson and the photon couple to particle and anti-particle pairs they have a vanishing chemical potential. Further, in this temperature regime,  $SU(2)_L$  symmetry is unbroken, the  $W$  and  $Z$  are part of the same gauge multiplet which requires that the chemical potential of the  $W$  vanishes as well. The chemical potential of the gluon is zero and different color quarks carry the same chemical potential. The flavor (CKM) mixing among quarks ensures that the chemical potential of quarks in different generations are equal. However for the lepton sector, there is no such flavor mixing in the absence of neutrino masses [36]. Thus each of the lepton numbers ( $L_e, L_\mu, L_\tau$ ) for the three generations are separately conserved. Our notation is as follows:  $\mu_{L_i}, \mu_{e_i}$  denote the chemical potentials of left-handed and right-handed leptons while  $\mu_{q_i}, \mu_{u_i}, \mu_{d_i}$  stand for the chemical potential of left-handed and right-handed quarks. We assume that the chemical potential of all generations is the same and thus drop the subscript  $i$  and use  $\mu_H$  for the chemical potential of the Higgs doublet.

The Yukawa couplings

$$\mathcal{L}_{\text{Yukawa}} = g_{e_i} \bar{L}_i H e_i + g_{u_i} \bar{q}_i H^c u_i + g_{d_i} \bar{q}_i H d_i \quad (3.9)$$

yield the following relations among the chemical potentials

$$\mu_H = \mu_L - \mu_e = \mu_q - \mu_d = \mu_u - \mu_q. \quad (3.10)$$

Sphaleron processes ( $\mathcal{O}_{\text{sph}} \sim \prod_{i=1,2,3} q_i q_i q_i L_i$ ) give us one additional relation,

$$3\mu_q + \mu_L = 0. \quad (3.11)$$

The temperature where the sphaleron processes decouple is estimated to be [37]

$$T_{\text{Sph}} \sim \left[ 80 + 54 \times \frac{m_h}{120 \text{ GeV}} \right] \text{ GeV}. \quad (3.12)$$

It is very likely that  $T_{\text{Sph}}$  lies below  $T_{\text{EWPT}}$ , and thus the sphaleron processes are always active at  $T > T_{\text{EWPT}}$ . Finally, the hypercharge neutrality condition requires the total hypercharge of the Universe to be zero<sup>2</sup>

$$3\mu_q + 6\mu_u - 3\mu_d - 3\mu_L - 3\mu_e + 2\mu_H = 0. \quad (3.13)$$

Solving Equation (3.9) to Equation (3.13) we can express all the chemical potentials in terms of the chemical potential of one single field, e.g.,  $\mu_L$ . Specifically one finds

---

<sup>2</sup> The hypercharge of the Universe used in deducing Equation (3.13) is computed as follows:

$$Y = 3 \times \left[ 2 \times 3 \times \frac{1}{3} \mu_q + 3 \times \frac{4}{3} \mu_u + 3 \times \left(-\frac{2}{3}\right) \mu_d + 2 \times (-1) \mu_L + (-2) \mu_e \right] + 2 \times 2 \mu_H,$$

where the factor of 3 outside the first brace indicates summation over quark and lepton generations while inside the brace the factor of 3 for quarks indicates summing over colors, the factor of 2 for  $q, L$  and  $H$  counts two fields inside the doublets, and the additional factor of 2 for the Higgs is due to it being bosonic (see Equation (3.5)).

for Model A (suppressing a factor of  $\beta T^3/6$ )

$$B_A = 3 \times [2\mu_q + (\mu_u + \mu_d)] = -4\mu_L, \quad (3.14)$$

$$L_A = 3 \times (2\mu_L + \mu_e) = \frac{51}{7}\mu_L, \quad (3.15)$$

so that  $(B - L)_A = -\frac{79}{7}\mu_L$ .

### 3.3.2 $T < T_{\text{EWPT}}$

Now we consider the case when the temperature is below the EWPT scale. After the Higgs gets its VEV, and the  $SU(2)_L \times U(1)_Y$  symmetry is broken, one has  $W^\pm$ ,  $Z$ , the photon and the Higgs scalar ( $h$ ) as the physical particles in the thermal bath. Again, since the  $Z$  and the photon only couple to two particles with opposite chemical potentials, their chemical potentials are zero. For temperatures above the top quark mass, the relativistic plasma includes three generations of left-handed and right-handed up-type and down-type quarks ( $u_{iL}$ ,  $u_{iR}$ ,  $d_{iL}$  and  $d_{iR}$ ), three generations of left-handed leptons ( $e_{iL}$  and  $\nu_i$ ) and right-handed charged leptons ( $e_{iR}$ ),  $i = 1, 2, 3$ . As in Section 3.3.1, we will assume that the chemical potentials are generation independent. Thus dropping the generation index we will use  $\mu_{u_L}, \mu_{u_R}, \mu_{d_L}, \mu_{d_R}$  to denote the chemical potentials of left-handed and right-handed up-type and down-type quarks,  $\mu_{e_L}$  and  $\mu_\nu$  for left-handed leptons,  $\mu_{e_R}$  for right-handed charged leptons,  $\mu_W$  for  $W^+$ , and  $\mu_h$  for  $h$ .

In the analysis below we make the following approximations:

1. At  $T_{\text{EWPT}} > T > M_t$ , we still treat the top quark as relativistic gas.
2. At  $T_t > T > M_W$ , we treat the  $W$  boson as relativistic (all other particles,

which have non-vanishing chemical potentials, are very light so the limit in Equation (3.5) holds for them).

3. We assume  $T_t > T_{\text{Sph}}$ , i.e., the top quark drops out of the thermal bath before the sphaleron processes decouple.

For  $T < T_{\text{EWPT}}$ , the Yukawa couplings have the form

$$\mathcal{L}_{\text{Yukawa}} = g_e \bar{e}_{iL} h e_{iR} + g_{u_i} \bar{u}_{iL} h u_{iR} + g_{d_i} \bar{d}_{iL} h d_{iR} + h.c., \quad (3.16)$$

and since the Higgs boson is a real field and can couple to, for example, both  $\bar{e}_{iL} e_{iR}$  and  $\bar{e}_{iR} e_{iL}$ , we get

$$0 = \mu_h = \mu_{u_L} - \mu_{u_R} = \mu_{d_L} - \mu_{d_R} = \mu_{e_L} - \mu_{e_R}. \quad (3.17)$$

Thus, the chemical potentials of left-handed and right-handed quarks/charged leptons are equal. The gauge interactions involving  $W$  bosons ( $\mathcal{L} \sim W_\mu \bar{f} \gamma^\mu f$ ) provide us the following relations,

$$\mu_W = \mu_{u_L} - \mu_{d_L} \quad (W^+ \leftrightarrow u_L + \bar{d}_L), \quad (3.18)$$

$$\mu_W = \mu_\nu - \mu_{e_L} \quad (W^+ \leftrightarrow \nu_i + \bar{e}_{iL}). \quad (3.19)$$

The sphaleron processes give us one additional equation,

$$\mu_{u_L} + 2\mu_{d_L} + \mu_\nu = 0. \quad (3.20)$$

Since  $SU(2)_L$  symmetry is broken below the EWPT scale, hypercharge is no longer a good quantum number. Further, the neutrality of the Universe now requires the

total electrical charge to be zero<sup>3</sup>

$$2(\mu_{u_L} + \mu_{u_R} + \mu_W) - (\mu_{d_L} + \mu_{d_R} + \mu_{e_L} + \mu_{e_R}) = 0. \quad (3.22)$$

Solving the new set of equations one finds for Model B

$$B_B = 3 \times [(\mu_{u_L} + \mu_{u_R}) + (\mu_{d_L} + \mu_{d_R})] = -\frac{36}{7}\mu_e, \quad (3.23)$$

$$L_B = 3 \times (\mu_{e_L} + \mu_{e_R} + \mu_\nu) = \frac{75}{7}\mu_e, \quad (3.24)$$

where we have expressed the results in terms of  $\mu_e \equiv \mu_{e_L} = \mu_{e_R}$ , and  $(B - L)_B = -\frac{111}{7}\mu_e$ .

When the temperature drops below  $T_t$ , the top quark drops out from the thermal bath, and we are left with just five flavors of quarks. In this case ( $T_t > T > M_W$ ) one must treat the first two generations and the third generations separately. For the first two generations the analysis of Equation (3.17) to Equation (3.20) still holds. For the remaining third generation leptons, we assume as before that the chemical potentials are identical to those for the first two generation leptons. Further, we note that the charge current process  $W^+ \leftrightarrow u_L + \bar{b}_L$  provides us with the relations  $\mu_W = \mu_{u_L} - \mu_{b_L}$  and  $\mu_{b_L} = \mu_{d_L}$ . Thus we can treat Model C similar to Model B with only one modification to the charge neutrality condition, which now becomes

$$4(\mu_{u_L} + \mu_{u_R}) + 6\mu_W - 3(\mu_{d_L} + \mu_{d_R} + \mu_{e_L} + \mu_{e_R}) = 0. \quad (3.25)$$

---

<sup>3</sup>The result of Equation (3.22) follows from the computation of the total charge  $Q$  which is given by

$$Q = 3 \times \left[ 3 \times \frac{2}{3}(\mu_{u_L} + \mu_{u_R}) + 3 \times \left(-\frac{1}{3}\right)(\mu_{d_L} + \mu_{d_R}) + (-1)(\mu_{e_L} + \mu_{e_R}) \right] + 2 \times 3\mu_W, \quad (3.21)$$

where again, the factors of 3 for fermions outside the big brace indicates summing over generations, the other factor of 3 for quarks stands for summing over colors. For the  $W$  boson, 2 is the boson factor as given by Equation (3.5) and 3 is the degrees of freedom of  $W$ .

Solving these equations we obtain for Model C

$$B_C = 2(\mu_{u_L} + \mu_{u_R}) + 3(\mu_{d_L} + \mu_{d_R}) = -\frac{90}{19}\mu_e, \quad (3.26)$$

$$L_C = 3 \times (\mu_{e_L} + \mu_{e_R} + \mu_\nu) = \frac{201}{19}\mu_e, \quad (3.27)$$

and  $(B - L)_C = -\frac{291}{19}\mu_e$ . We note that the sphaleron processes will decouple below  $T_{\text{Sph}}$  as mentioned already. Subsequently the baryon and lepton numbers would be separately conserved. Equation (3.17) to Equation (3.19), and Equation (3.25) to Equation (3.27) would remain valid at  $T_{\text{Sph}} > T > M_W$ .

Following our assumptions given earlier, the top quark drops out of the thermal bath before sphaleron processes decouple. After the sphaleron processes decouple,  $B$  and  $L$  would be separately conserved. In other words, the ratio of  $B/(B - L)$  would freeze as soon as the sphaleron processes are no longer active. Thus, we obtain

$$b = \frac{B_{\text{final}}}{B - L} = \left( \frac{B}{B - L} \right)_C = \frac{30}{97} \approx 0.31. \quad (3.28)$$

### 3.3.3 Determining the Asymmetric dark matter mass

We discuss now in further detail the mechanism by which  $B - L$  is transferred from the Standard Model sector to the dark matter sector and the determination of the dark matter mass. We consider the most general interaction which transfers the  $B - L$  asymmetry to dark matter at a high temperature:

$$\mathcal{L}_{\text{asy}}^{\text{SM}} = \frac{1}{M_{\text{asy}}^n} X^k \mathcal{O}_{\text{asy}}^{\text{SM}}, \quad (3.29)$$

where the operator  $\mathcal{O}_{\text{asy}}^{\text{SM}}$  is constructed from the Standard Model fields, has a  $(B - L)$ -charge  $Q_{B-L}^{\text{SM}}$ , and  $X$  is the dark particle and has a  $(B - L)$ -charge  $Q_{B-L}^{\text{DM}} = -Q_{B-L}^{\text{SM}}/k$ . The power of  $X$  can only be 2 or greater to ensure the stability of the asymmetric dark matter.

The parameterization of the asymmetric dark matter sector by the charge  $Q_{B-L}^{\text{DM}}$  is useful and we will utilize it in our analysis below. Also useful is the parameterization of the interactions in terms of the number of doublets and singlets that enter in  $\mathcal{O}_{\text{asy}}^{\text{SM}}$ , i.e.,  $N_q, N_L, N_H$  numbers of  $q, L, H$  doublets and  $N_u, N_d, N_e$  numbers of  $u_R, d_R, e_R$  singlets which are all active above the EWPT scale. Equation (3.29) leads to the following constraints [38]

$$N_q \mu_q + N_L \mu_L + N_u \mu_u + N_d \mu_d + N_e \mu_e + N_H \mu_H + k \mu_X = 0, \quad (3.30)$$

$$\frac{1}{3} N_q + \frac{1}{3} N_u + \frac{1}{3} N_d - N_L - N_e + k Q_{B-L}^{\text{DM}} = 0, \quad (3.31)$$

$$\frac{1}{3} N_q + \frac{4}{3} N_u - \frac{2}{3} N_d - N_L - 2N_e + N_H = 0. \quad (3.32)$$

Here Equation (3.30) arises from the  $\mu$  equilibrium of Equation (3.29), Equation (3.31) arises from the total  $(B - L)$ -charge conservation of the interaction, and Equation (3.32) arises from the hypercharge conservation and the condition that the asymmetric dark matter must have zero hypercharge. Together with Equation (3.10) to Equation (3.13), for Model A we obtain

$$\mu_X^{\text{A}} = -\frac{11}{7} Q_{B-L}^{\text{DM}} \mu_L. \quad (3.33)$$

If  $X$  is fermionic dark matter (FDM), we find,

$$x_{\text{A}} = \frac{X_{\text{A}}}{(B - L)_{\text{A}}} = \frac{k \mu_X^{\text{A}}}{-\frac{79}{7} \mu_L} = -\frac{11}{79} Q_{B-L}^{\text{SM}}. \quad (3.34)$$

Using Equation (3.8) and Equation (3.28), we obtain

$$m_{\text{FDM}}^{\text{A}} \approx -\frac{11.11 \text{ GeV}}{Q_{B-L}^{\text{OSM}}}. \quad (3.35)$$

If the  $B - L$  transfer interaction is also active below the EWPT scale, the treatment is similar. Assuming  $\mathcal{O}_{\text{asy}}^{\text{SM}}$  has  $N_u, N_d, N_e, N_\nu, N_W$  numbers of  $u, d, e, \nu, W^+$  fields and recalling that at  $T < T_{\text{EWPT}}$ , the left-handed and right-handed quarks and charged leptons have the same chemical potentials, one finds the following constraints

$$N_u \mu_u + N_d \mu_d + N_e \mu_e + N_\nu \mu_\nu + N_W \mu_W + k \mu_X = 0, \quad (3.36)$$

$$\frac{1}{3} N_u + \frac{1}{3} N_d - N_e - N_\nu + k Q_{B-L}^{\text{DM}} = 0, \quad (3.37)$$

$$\frac{2}{3} N_u - \frac{1}{3} N_d - N_e + N_W = 0. \quad (3.38)$$

We note that the last condition is from the charge neutrality of the operator  $\mathcal{O}_{\text{asy}}^{\text{SM}}$ . Together with Equation (3.17) to Equation (3.22), we obtain for Model B,

$$\mu_X^{\text{B}} = -\frac{11}{7} Q_{B-L}^{\text{DM}} \mu_e. \quad (3.39)$$

The fermionic dark matter mass in this model reads

$$m_{\text{FDM}}^{\text{B}} \approx -\frac{15.60 \text{ GeV}}{Q_{B-L}^{\text{OSM}}}. \quad (3.40)$$

For Model C where the top quark is out of the thermal bath, we find

$$\mu_X^{\text{C}} = -\frac{29}{19} Q_{B-L}^{\text{DM}} \mu_e. \quad (3.41)$$

and

$$m_{\text{FDM}}^{\text{C}} \approx -\frac{15.52 \text{ GeV}}{Q_{B-L}^{\text{OSM}}}. \quad (3.42)$$

Now we consider the simplest example of the  $B - L$  transfer interaction ( $Q_{B-L}^{\text{OSM}} = -1$ )

$$\mathcal{L}_{\text{asy}} = \frac{1}{M_{\text{asy}}^3} \psi^3 LH, \quad (3.43)$$

where  $\psi$  is the fermionic dark matter (which carries a lepton number of  $-1/3$ ) and  $\psi^3 \equiv \bar{\psi}^c \psi \bar{\psi}^c$ . If this interaction is only active above the EWPT scale then the dark matter mass in Model A, and more appropriately in Model A<sub>1</sub> since the interaction of Equation (3.43) is being used (see Table 3.2 which also includes a list of additional interactions), are computed to be

$$m_{\psi} = 11.11 \text{ GeV} \quad \text{Model A}_1. \quad (3.44)$$

If this interaction is also active below the EWPT scale, the dark matter masses in Models B and C are:

$$m_{\psi} = 15.60 \text{ GeV} \quad \text{Model B}_1; \quad m_{\psi} = 15.52 \text{ GeV} \quad \text{Model C}_1. \quad (3.45)$$

Further, applying Equation (3.3) and the bounds in Table 3.1 one can estimate the mass scales for these interactions:

$$M_{\text{asy}}^{\text{A}_1/\text{D}_1} \gtrsim 1.2 \times 10^5 \text{ GeV}, \quad (3.46)$$

$$1.2 \times 10^5 \text{ GeV} \gtrsim M_{\text{asy}}^{\text{B}_1} \gtrsim 0.9 \times 10^5 \text{ GeV}, \quad (3.47)$$

$$0.9 \times 10^5 \text{ GeV} > M_{\text{asy}}^{\text{C}_1} \gtrsim 0.4 \times 10^5 \text{ GeV}. \quad (3.48)$$

In the analysis above we focused on asymmetric fermionic dark matter. For bosonic dark matter, the masses would be half the fermionic ones, c.f., Equation (3.5). As an example, we consider now an interaction with a higher dimensional operator  $\mathcal{O}_{\text{asy}}^{\text{SM}}$ .

$$\mathcal{L}_{\text{asy}} = \frac{1}{M_{\text{asy}}^n} X^2 (LH)^2. \quad (3.49)$$

In this case, the dark matter could be either a fermion ( $X = \psi$ ,  $n = 4$ ) or a boson ( $X = \phi$ ,  $n = 3$ ). This interaction gives rise to Models A<sub>2</sub>-C<sub>2</sub> and Models A<sub>3</sub>-C<sub>3</sub>. As examples, for Models A<sub>2</sub> and A<sub>3</sub> where  $T_{\text{int}} > T_{\text{EWPT}}$ , applying Equation (3.35) we find that the dark matter masses are

$$m_\psi = 5.55 \text{ GeV} \quad \text{Model A}_2; \quad m_\phi = 2.78 \text{ GeV} \quad \text{Model A}_3. \quad (3.50)$$

We explain now briefly the equality of asymmetric dark mass for the Models A<sub>1</sub>, A<sub>4</sub>, A<sub>5</sub>, A<sub>6</sub>. From Equation (3.2) we can write

$$\mu_{\mathcal{O}_{\text{DM}}} + \mu_{\mathcal{O}_{\text{asy}}^{\text{SM}}} = 0. \quad (3.51)$$

For Models A<sub>1</sub>, A<sub>4</sub>-A<sub>6</sub> we have

$$LH (A_1) : \quad \mu_{\mathcal{O}_{\text{asy},1}^{\text{SM}}} = \mu_L + \mu_H, \quad (3.52)$$

$$LLe^c (A_4) : \quad \mu_{\mathcal{O}_{\text{asy},4}^{\text{SM}}} = 2\mu_L - \mu_e, \quad (3.53)$$

$$Lqd^c (A_5) : \quad \mu_{\mathcal{O}_{\text{asy},5}^{\text{SM}}} = \mu_L + \mu_q - \mu_d, \quad (3.54)$$

$$u^c d^c d^c (A_6) : \quad \mu_{\mathcal{O}_{\text{asy},6}^{\text{SM}}} = -\mu_u - 2\mu_d. \quad (3.55)$$

$\frac{1}{M^n} X^k \mathcal{O}_{\text{asy}}^{\text{SM}}$	Model	DM Mass	Model	DM Mass	Model	DM Mass
$\frac{1}{M^3} \psi^3 LH$	A <sub>1</sub>	11.11 GeV	B <sub>1</sub>	15.60 GeV	C <sub>1</sub>	15.52 GeV
$\frac{1}{M^4} \psi^2 (LH)^2$	A <sub>2</sub>	5.55 GeV	B <sub>2</sub>	7.80 GeV	C <sub>2</sub>	7.76 GeV
$\frac{1}{M^3} \phi^2 (LH)^2$	A <sub>3</sub>	2.78 GeV	B <sub>3</sub>	3.90 GeV	C <sub>3</sub>	3.88 GeV
$\frac{1}{M^5} \psi^3 LLe^c$	A <sub>4</sub>	11.11 GeV	B <sub>4</sub>	15.60 GeV	C <sub>4</sub>	15.52 GeV
$\frac{1}{M^5} \psi^3 Lqd^c$	A <sub>5</sub>	11.11 GeV	B <sub>5</sub>	15.60 GeV	C <sub>5</sub>	15.52 GeV
$\frac{1}{M^5} \psi^3 u^c d^c d^c$	A <sub>6</sub>	11.11 GeV	B <sub>6</sub>	15.60 GeV	C <sub>6</sub>	15.52 GeV

Table 3.2: A display of the various interactions that allow a transfer of the  $B - L$  asymmetry from the Standard Model sector to the dark matter sector.

From the  $\mu$  equations Equation (3.10) and Equation (3.11), it is easy to see that

$$\mu_{\mathcal{O}_{\text{asy},1}^{\text{SM}}} = \mu_{\mathcal{O}_{\text{asy},4}^{\text{SM}}} = \mu_{\mathcal{O}_{\text{asy},5}^{\text{SM}}} = \mu_{\mathcal{O}_{\text{asy},6}^{\text{SM}}}. \quad (3.56)$$

Equation (3.56) implies that the dark matter has the same mass for the Models A<sub>1</sub>,A<sub>4</sub>-A<sub>6</sub>. Similar analysis holds for Models B<sub>1</sub>,B<sub>4</sub>-B<sub>6</sub> and C<sub>1</sub>,C<sub>4</sub>-C<sub>6</sub>.

We summarize all our results in Table 3.2, where we list the dark matter mass for the various interactions<sup>4</sup> that can transfer the  $B - L$  asymmetry from the Standard Model sector to the dark matter sector. We note that for the first five interactions, the dark matter carries lepton number, while for the last one, it carries a baryon number.

---

<sup>4</sup>In the first column of Table 3.2,  $L$ ,  $H$  and  $q$  stand for  $SU(2)_L$  doublets as discussed in  $T > T_{\text{EWPT}}$  regime (Model A). When the temperature drops below EWPT scale (Model B and Model C), since  $SU(2)_L$  symmetry is broken, these interactions should be rewritten in terms of the contents of the original doublets. We omit this step for simplicity.

### 3.4 Asymmetric dark matter in a Stueckelberg extension of the SM

As discussed in the Introduction, one of the major problems for an acceptable AsyDM model is to have an efficient mechanism for the annihilation of dark matter that is produced thermally. In general one has

$$\Omega_{\text{DM}} = \Omega_{\text{DM}}^{\text{asy}} + \Omega_{\text{DM}}^{\text{sym}}, \quad (3.57)$$

where  $\Omega_{\text{DM}}^{\text{asy}}$  is the relic density of asymmetric dark matter (which carries a nonzero  $(B - L)$ -charge) and  $\Omega_{\text{DM}}^{\text{sym}}$  is the relic density of dark matter which is produced thermally. For the asymmetric dark matter to be the dominant component, the symmetric component of dark matter must be significantly depleted. Specifically we will use the criteria that  $\Omega_{\text{DM}}^{\text{sym}} / \Omega_{\text{DM}} < 0.1$ .<sup>5</sup> Thus we investigate if the symmetric component of dark matter produced by thermal processes can be annihilated efficiently. We accomplish this via the exchange of a gauge field using the Stueckelberg formalism where the gauge field couples to  $L_\mu - L_\tau$ .

For illustration let us consider Model A<sub>1</sub>, which is governed by the interaction Equation (3.43) operating at  $T_{\text{int}} > T_{\text{EWPT}}$ . The corresponding dark matter mass is 11.11 GeV. Further, we require the dark matter particles  $\psi$  to have a non-vanishing  $\mu$  or  $\tau$  lepton number. The total Lagrangian is given by

$$\mathcal{L} = \mathcal{L}_{\text{SM}} + \mathcal{L}_{U(1)} + \mathcal{L}_{\text{St}}, \quad (3.58)$$

---

<sup>5</sup>The analysis of previous sections was based on the assumption  $\Omega_{\text{DM}}^{\text{asy}} / \Omega_{\text{matter}} \approx 5$ . Inclusion of a small contribution (i.e.,  $\leq 10\%$ ) of symmetric component to dark matter will proportionately affect the determination of the dark matter mass. It is straightforward to take account of this contribution but we do not carry it out explicitly as it is a relatively small effect.

where  $\mathcal{L}_{U(1)}$  is the kinetic energy for the gauge field for the  $L_\mu - L_\tau$  symmetry, and for  $\mathcal{L}_{St}$  we assume the following form:

$$\mathcal{L}_{St} = -\frac{1}{2}(M_C C_\mu + \partial_\mu \sigma)^2. \quad (3.59)$$

In the unitary gauge the massive vector boson field will be called  $Z'$  and its interaction with fermions in the theory is given by

$$\mathcal{L}_{int} = \frac{1}{2}g_C Q_C^\psi \bar{\psi} \gamma^\mu \psi C_\mu + \frac{1}{2}g_C Q_C^f \bar{f} \gamma^\mu f C_\mu, \quad (3.60)$$

where  $f$  runs over  $\mu$  and  $\tau$  families and  $Q_C^\mu = -Q_C^\tau$ .

### 3.4.1 Resonant annihilation of symmetric dark matter

We discuss now the details of the annihilation of the symmetric component of dark matter. We will show that the relic density for such dark matter can be reduced significantly below the WMAP value with resonant annihilation via the  $Z'$  pole, i.e., via the process  $\psi\bar{\psi} \rightarrow Z' \rightarrow f\bar{f}$ .<sup>6</sup> Thus, by using Equation (3.60) one can compute the  $\psi\bar{\psi} \rightarrow f\bar{f}$  annihilation cross section and using the Breit-Wigner form for a resonance one has

$$\begin{aligned} \sigma_{\psi\bar{\psi} \rightarrow f\bar{f}} &= a_\psi \left| \left( s - M_{Z'}^2 + i\Gamma_{Z'} M_{Z'} \right) \right|^{-2}, \\ a_\psi &= \frac{\beta_f (\frac{1}{2}g_C^2 Q_C^\psi Q_C^f)^2}{64\pi s \beta_\psi} \left[ s^2 \left( 1 + \frac{1}{3}\beta_f^2 \beta_\psi^2 \right) + 4M_\psi^2 (s - 2m_f^2) + 4m_f^2 (s + 2M_\psi^2) \right]. \end{aligned} \quad (3.61)$$

---

<sup>6</sup>While the thermal dark matter can annihilate into second and third generation leptons at the tree-level, such an annihilation into the first generation leptons can come about only at the loop level involving the second and third generation leptonic loops. Thus the annihilation of thermal dark matter into first generation leptons is significantly suppressed relative to the annihilation into the second and the third generation leptons.

where  $\beta_{f,\psi} = (1 - 4m_{f,\psi}^2/s)^{1/2}$ . The relevant partial  $Z'$  decay widths are given by

$$\Gamma(Z' \rightarrow f\bar{f}) = \left(\frac{1}{2}g_C Q_C^f\right)^2 r_f \frac{M_{Z'}}{12\pi}, \quad f = \mu, \nu_\mu, \tau, \nu_\tau \quad (3.63)$$

$$\Gamma(Z' \rightarrow \psi\bar{\psi}) = \left(\frac{1}{2}g_C Q_C^\psi\right)^2 \frac{M_{Z'}}{12\pi} \left(1 + \frac{2M_\psi^2}{M_{Z'}^2}\right) \left(1 - \frac{4M_\psi^2}{M_{Z'}^2}\right)^{1/2} \Theta(M_{Z'} - 2M_\psi), \quad (3.64)$$

where  $r_f = 1$  for  $f = \mu, \tau$  and  $r_f = 1/2$  for  $f = \nu_\mu, \nu_\tau$ . A constraint on  $g_C$  comes from the contribution of the  $Z'$  to  $g_\mu - 2$  [39, 40], which is given by

$$\Delta(g_\mu - 2) = \left(\frac{1}{2}g_C Q_C^\mu\right)^2 \frac{m_\mu^2}{6\pi^2 M_{Z'}^2}. \quad (3.65)$$

In the analysis here we impose the constraint that the  $Z'$  boson contribution be less than the experimental ( $4\sigma$ ) deviation of  $\Delta a_\mu \equiv \Delta((g_\mu - 2)/2) = (3.0 \pm 0.8) \times 10^{-9}$  [39, 40], which is the constraint commonly adopted in analysis of supergravity based models.

The relic densities of  $\psi$  and  $\bar{\psi}$  are governed by the Boltzmann equations. For our analysis we will carry out an explicit thermal averaging over the Breit-Wigner pole. It is convenient to work with the Boltzmann equations for the quantities  $f_\psi \equiv n_\psi/(\mathfrak{h}T^3)$ , and  $f_{\bar{\psi}} \equiv n_{\bar{\psi}}/(\mathfrak{h}T^3)$  where  $n_\psi$  ( $n_{\bar{\psi}}$ ) is the number density of particle  $\psi$  ( $\bar{\psi}$ ) and the combination  $\mathfrak{h}T^3$  appears in the entropy per unit volume, i.e.,  $s = (2\pi^2/45)\mathfrak{h}T^3$  where  $\mathfrak{h}$  is the entropy degrees of freedom. The Boltzmann equations obeyed by  $f_\psi$  and  $f_{\bar{\psi}}$  take the form

$$\frac{df_\psi}{dx} = \alpha \langle \sigma v \rangle (f_\psi f_{\bar{\psi}} - f_\psi^{\text{eq}} f_{\bar{\psi}}^{\text{eq}}), \quad (3.66)$$

$$\frac{df_{\bar{\psi}}}{dx} = \alpha \langle \sigma v \rangle (f_\psi f_{\bar{\psi}} - f_\psi^{\text{eq}} f_{\bar{\psi}}^{\text{eq}}), \quad (3.67)$$

where  $x = k_B T / m_\psi$  in which  $k_B$  is the Boltzmann constant and hereafter we set  $k_B = 1$ , and  $\alpha$  is given by

$$\alpha(T) = \sqrt{90} m_\psi M_{\text{Pl}} \frac{\hbar}{\sqrt{g} \pi} \left( 1 + \frac{1}{4} \frac{T}{g} \frac{dg}{dT} \right), \quad (3.68)$$

where  $g$  is the degrees of freedom that enter in the energy per unit volume, i.e.,  $\rho = \frac{\pi^2}{30} g T^4$ , where  $T(t) = T_\gamma(t)$  is the photon temperature. Numerically  $\alpha(T) = 6.7 \times 10^{20} \text{ GeV}^2$  for  $g = \hbar = 68$  at  $T = 0.5 \text{ GeV}$ .  $\langle \sigma v \rangle$  is the thermally averaged cross section

$$\langle \sigma v \rangle = \frac{\int_0^\infty dv (\sigma v) v^2 e^{-v^2/4x}}{\int_0^\infty dv v^2 e^{-v^2/4x}}. \quad (3.69)$$

Further, in Equation (3.66) and Equation (3.67)  $f_\psi^{\text{eq}}$  and  $f_{\bar{\psi}}^{\text{eq}}$  are values of  $f_\psi$  and  $f_{\bar{\psi}}$  at equilibrium. Now one can obtain the result from Equation (3.66) and Equation (3.67) that the difference of  $f_\psi$  and  $f_{\bar{\psi}}$ , i.e.,

$$\gamma \equiv f_\psi - f_{\bar{\psi}}, \quad (3.70)$$

is a constant. Assuming that the asymmetric dark matter currently constitutes a fraction  $\lambda$  of the dark matter relic density, one can evaluate  $\gamma$  to be

$$\gamma \simeq \lambda \frac{5\rho_c}{6\hbar T^3 m_\psi} \equiv \lambda \gamma_0, \quad \gamma_0 \approx 1.3 \times 10^{-10} \quad (m_\psi \sim 10 \text{ GeV}), \quad (3.71)$$

where the  $5/6$  in  $\gamma_0$  is due to Equation (3.1).

It is now straightforward to obtain the individual relic densities for  $\psi$  and  $\bar{\psi}$ . Thus one integrates Equation (3.66) and Equation (3.67) from the freeze-out temperature to the current temperature of  $T_\gamma^0 = 2.73 \text{ K}$ . In the integration we will make the following

approximation which is conventionally done, i.e., we move  $\alpha$  out of the integral and replace it with  $\alpha(x_f)$ , i.e., by the value of  $\alpha$  at the freeze-out temperature. The matter density of  $\psi$  at current temperature is given by  $\rho_\psi = m_\psi n_\psi(x_0)$  where  $x_0 = T_\gamma^0/m_\psi$  and  $T_\gamma^0$  is the current photon temperature of 2.73 K. The relic density then is

$$\Omega_\psi = m_\psi n_\psi(x_0)/\rho_c, \quad (3.72)$$

where  $\rho_c$  is the critical matter density so that  $\rho_c = (3 \times 10^{-12} \text{ GeV})^4 h_0^2$  where  $h_0$  is the Hubble parameter. The integration of Equation (3.66) straightforwardly gives

$$\Omega_\psi h_0^2 = 2.2 \times 10^{-11} \sqrt{\mathfrak{g}(x_f)} \mathfrak{h}(x_0, x_f) \left( \frac{T_\gamma}{2.73} \right)^3 \left( \frac{1}{\xi} - \frac{f_{\bar{\psi}}(x_f)}{\xi f_\psi(x_f)} e^{-\xi J(x_f)} \right)^{-1}, \quad (3.73)$$

where

$$J(x_f) \equiv \int_{x_0}^{x_f} \langle \sigma v \rangle dx, \quad \mathfrak{h}(x_0, x_f) \equiv \frac{\mathfrak{h}(x_0)}{\mathfrak{h}(x_f)} \left[ 1 + \frac{1}{4} \left( \frac{T}{\mathfrak{g}} \frac{d\mathfrak{g}}{dT} \right)_{x_f} \right]^{-1}, \quad (3.74)$$

and  $\xi \equiv \alpha(x_f)\gamma$  where  $\alpha(x_f)$  is the value of  $\alpha$  evaluated at the freeze-out temperature, and where  $\mathfrak{g}(x_f)$  ( $\mathfrak{h}(x_f)$ ) are the energy (entropy) degrees of freedom at freeze out and  $\mathfrak{h}(x_0)$  is the entropy degrees of freedom at the current temperature. The derivative term  $\frac{1}{4} \left( \frac{T}{\mathfrak{g}} \frac{d\mathfrak{g}}{dT} \right)_{x_f}$  is small and is often dropped, while  $\mathfrak{h}(x_0) = 3.91$  [36, 41] and we estimate  $\mathfrak{h}(x_f) \sim \mathfrak{g}(x_f)$  given  $T_f$ . As discussed below  $x_f$  is typically of size  $\sim 1/20$  and thus  $T_f = m_\psi x_f \sim 0.5 \text{ GeV}$  for  $m_\psi \sim 10 \text{ GeV}$ . Now for  $T_f \sim 0.5 \text{ GeV}$ ,  $\mathfrak{h}(x_f) \sim 68$  which gives  $\mathfrak{h}(x_0, x_f) \sim 1/17.5$ . The quantities  $f_\psi(x_f)$  ( $f_{\bar{\psi}}(x_f)$ ) are  $f_\psi$  ( $f_{\bar{\psi}}$ ) evaluated at freeze out. Analogous to the relic density for  $\psi$ , we can get the relic

density of  $\bar{\psi}$  by integration of  $\bar{\psi}$  and we obtain

$$\Omega_{\bar{\psi}} h_0^2 = 2.2 \times 10^{-11} \sqrt{g(x_f)} \mathfrak{h}(x_0, x_f) \left( \frac{T_\gamma}{2.73} \right)^3 \left( \frac{f_\psi(x_f)}{\xi f_{\bar{\psi}}(x_f)} e^{\xi J(x_f)} - \frac{1}{\xi} \right)^{-1}. \quad (3.75)$$

The total dark matter relic density is

$$\Omega_{\text{DM}} = \Omega_\psi + \Omega_{\bar{\psi}}. \quad (3.76)$$

From Equation (3.73) and Equation (3.75) one obtains the ratio of the current relic densities of  $\bar{\psi}$  and  $\psi$  to be

$$\frac{\Omega_{\bar{\psi}} h_0^2}{\Omega_\psi h_0^2} = \frac{f_{\bar{\psi}}(x_f)}{f_\psi(x_f)} e^{-\xi J(x_f)}. \quad (3.77)$$

The front factor  $f_{\bar{\psi}}(x_f)/f_\psi(x_f)$  in Equation (3.77) takes into account the asymmetry that exists at the freeze-out temperature. The size of this effect is estimated at the end of this section and could be as much as 20%, and thus significant.

Discussed now is the evaluation of the freeze-out temperature. We adopt here the definition of [42] where the freeze-out temperature  $T_f$  is defined as the temperature where the annihilation rate per unit volume equals the rate of change of the number density. This implies

$$\frac{df_{\bar{\psi}}^{\text{eq}}}{dx} = \alpha \langle \sigma v \rangle f_\psi^{\text{eq}} f_{\bar{\psi}}^{\text{eq}}, \quad \text{at } x = x_f = T_f/m_\psi, \quad (3.78)$$

where  $f_{\bar{\psi}}^{\text{eq}}$  takes the form

$$f_{\bar{\psi}}^{\text{eq}}(x) = a_{\bar{\psi}} x^{-3/2} e^{-1/x}, \quad (3.79)$$

where  $a_{\bar{\psi}} = g_{\bar{\psi}}(2\pi)^{-3/2} h^{-1}(T) \approx 9.3 \times 10^{-4} g_{\bar{\psi}}$  around  $T = 0.5 \text{ GeV}$ , and  $g_{\bar{\psi}}$  denotes

the degrees of freedom of the dark particle ( $g_\psi = g_{\bar{\psi}} = 4$  for Dirac spinors). The freeze-out temperature is then determined by the relation

$$(x_f^{-1/2} - \frac{3}{2}x_f^{1/2})e^{1/x_f} = \alpha\langle\sigma v\rangle(a_{\bar{\psi}} + \gamma x_f^{3/2}e^{1/x_f}). \quad (3.80)$$

For the case of no asymmetry, i.e., in the limit  $\gamma \rightarrow 0$ , Equation (3.80) reduces down to the well-known result [42]. One may compare the analysis of the freeze-out temperature given by Equation (3.80) with the one using the alternate criterion [43]

$$\Delta(x_f) = cf_{\bar{\psi}}^{\text{eq}}(x_f), \quad (3.81)$$

where  $\Delta(x) \equiv (f_{\bar{\psi}}(x) - f_{\bar{\psi}}^{\text{eq}}(x))$  and  $c$  is order unity. Using Equation (3.79) in Equation (3.81) one gets

$$(x_f^{1/2} - \frac{3}{2}x_f^{-1/2} - \alpha\gamma\langle\sigma v\rangle x_f^{3/2})e^{1/x_f} = \alpha a_{\bar{\psi}}c(c+2)\langle\sigma v\rangle. \quad (3.82)$$

For  $\gamma = 0$ , Equation (3.82) reduces to the result of [43] while  $\gamma \neq 0$  gives the correction due to asymmetry. Further, we see that Equation (3.82) reduces to Equation (3.80) when  $c = \sqrt{2} - 1$ . To compute the sensitivity of the freeze-out temperature on the asymmetry it is useful to utilize the scale factor  $\lambda$  defined in Equation (3.71). On using Equation (3.80) we can obtain an approximate expression for  $dx_f/d\lambda$  so that

$$\frac{dx_f}{d\lambda} \simeq -a_{\bar{\psi}}^{-1}\gamma_0 x_f^{7/2}e^{1/x_f}. \quad (3.83)$$

From above we can compute the first order correction to the freeze-out temperature due to the asymmetry. To the leading order one has

$$x_f \simeq x_f^0 \left[ 1 - a_{\bar{\psi}}^{-1}\gamma(x_f^0)^{5/2}e^{1/x_f^0} \right], \quad (3.84)$$

where  $x_f^0$  is the zeroth order of the  $x_f$ , i.e., when  $\gamma = 0$ . We note that the correction to the freeze-out temperature due to asymmetry is independent of  $\langle\sigma v\rangle$  to leading order. Using  $a_\psi = 3.7 \times 10^{-3}$ ,  $x_f = 1/17.5$  and  $\gamma = \gamma_0 = 1.3 \times 10^{-10}$ , one finds that the correction to  $x_f$  is around a percent for the choice of the parameters given. Further, as  $\gamma$  (and hence  $\xi$ )  $\rightarrow 0$ , one has  $\frac{f_\psi(x_f)}{f_{\bar{\psi}}(x_f)} \rightarrow 1$  and in this limit one has

$$\Omega_\psi h_0^2 = \Omega_{\bar{\psi}} h_0^2 = 2.2 \times 10^{-11} \sqrt{g(x_f)} \mathfrak{h}(x_0, x_f) \left(\frac{T_\gamma}{2.73}\right)^3 \frac{1}{J(x_f)}. \quad (3.85)$$

Now rapid annihilation of dark matter can occur if the sum of the dark matter masses is close to the  $Z'$  pole and there is a Breit-Wigner enhancement [44–47]. Thus for the case we are considering if the mass of the  $Z'$  is close to twice the mass of the dark particle, then one can get a large annihilation cross section and correspondingly a small relic density. An analysis of the relic density arising from the annihilation of symmetric dark matter is given in Figure 3.1 and the analysis shows that the relic density arising from the symmetric component of dark matter can easily be made negligible, i.e., less than 10% of the cold dark matter density given by WMAP. In Figure 3.1 we give the analysis for the case with no asymmetry, i.e.,  $\gamma = 0$  (left panel) and the case with asymmetry (right panel) where  $\gamma = 1.3 \times 10^{-10}$ . A comparison of the left and the right panels shows that inclusion of the asymmetry has a substantial effect on the relic density. Specifically it further helps deplete the relic density of  $\bar{\psi}$  (the symmetric component of dark matter). For the case of  $g_C = 1$  the allowed upper bound of the  $Z'$  mass increases by about  $\sim 100$  GeV in the presence of an asymmetry when  $\gamma = 1.3 \times 10^{-10}$ . It is also instructive to examine the ratio of the thermal relic

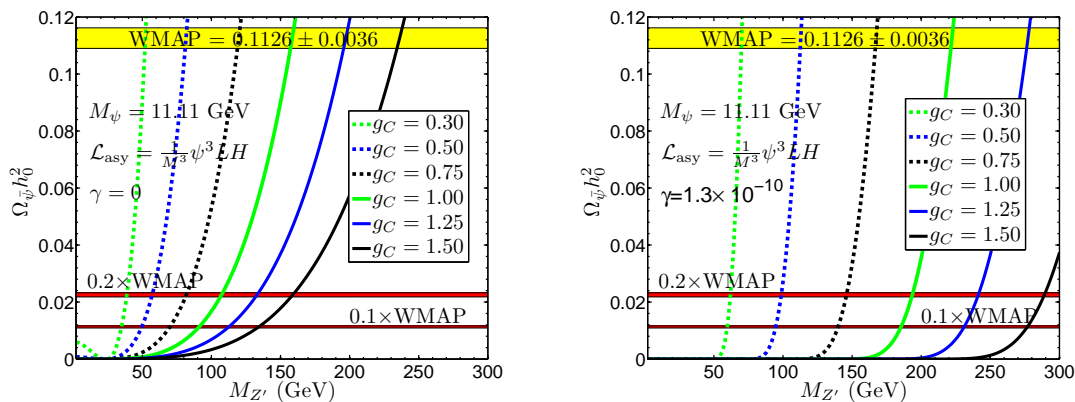


Figure 3.1: An exhibition of the thermal relic density of  $\bar{\psi}$  as a function of  $M_{Z'}$  in the model with gauged  $L_\mu - L_\tau$  for different values of the coupling constant. The left panel shows the case  $\gamma = 0$  and the right panel shows  $\gamma = 1.3 \times 10^{-10}$ . In both cases, the analysis shows that the component of dark matter that is thermally produced can be efficiently depleted by resonant annihilation via the  $Z'$  pole.

density for the cases with and without asymmetry. Here one has

$$R \equiv \frac{(\Omega_{\bar{\psi}} h_0^2)_{\gamma=\gamma_0}}{(\Omega_{\bar{\psi}} h_0^2)_{\gamma=0}} = \frac{\xi J(x_f)}{\frac{f_\psi(x_f)}{f_{\bar{\psi}}(x_f)} e^{\xi J(x_f)} - 1}. \quad (3.86)$$

As  $\xi \rightarrow 0$ ,  $\frac{f_\psi(x_f)}{f_{\bar{\psi}}(x_f)} \rightarrow 1$  and thus  $R \rightarrow 1$ . However, if we assume that the asymmetric dark matter is responsible for 5/6 of the total relic density, then for  $m_\psi \sim 10 \text{ GeV}$ , one has  $\gamma = 1.3 \times 10^{-10}$  and  $f_{\bar{\psi}}(x_f) = 6.8 \times 10^{-10}$  which gives  $\frac{f_\psi(x_f)}{f_{\bar{\psi}}(x_f)} = (1 + \gamma_0/f_{\bar{\psi}}(x_f)) \sim 1.2$ . In this circumstance one finds that  $R$  is always less than 1. Thus one finds that the inclusion of asymmetry helps deplete the symmetric component of dark matter.

# Chapter 4

## Supersymmetry

In this chapter we will do a brief overview of supersymmetry and readers seeking a more thorough knowledge of the theory are encouraged to read [48–53].

### 4.1 Minimal Supersymmetric Standard Model Overview

Supersymmetry (SUSY) extends the spacetime symmetry [49, 54–56] to a graded symmetry which includes both bosonic and fermionic generators consisting of the generators of the Poincarè group (rotations, boosts, and translations) along with fermionic generators  $Q^\alpha$ . This causes the representation of the SUSY algebra to contain both bosonic and fermionic fields.

The Minimal Supersymmetric Standard Model (MSSM) is the simplest model which extends the Standard Model to include supersymmetry. The inclusion of supersymmetry introduces a variety of new particles (such as squarks, sleptons, gauginos, and Higgsinos) which are the “superpartners” (or “sparticles”) of the Standard Model particles (quarks, leptons, gauge bosons, Higgs boson). A list of the particle

<b>CHIRAL SUPERMULTIPLER</b>								
Particle	Spin 0	Particle	Spin 1/2	$SU(3)_c$	$SU(2)_L$	$U(1)_Y$		
squark	$\begin{pmatrix} \tilde{u}_L \\ \tilde{d}_L \end{pmatrix}_i$	quark	$\begin{pmatrix} u_L \\ d_L \end{pmatrix}_i$	<b>3</b>	<b>2</b>	1/3		
				$\tilde{u}_{R,i}$	$u_{R,i}$	$\bar{\mathbf{3}}$	<b>1</b>	-1/3
				$\tilde{d}_{R,i}$	$d_{R,i}$	$\bar{\mathbf{3}}$	<b>1</b>	2/3
slepton	$\begin{pmatrix} \tilde{\nu}_L \\ \tilde{e}_L \end{pmatrix}_i$	lepton	$\begin{pmatrix} \nu_L \\ e_L \end{pmatrix}_i$	<b>1</b>	<b>2</b>	-1		
				$\tilde{e}_{R,i}$	$e_{R,i}$	<b>1</b>	<b>1</b>	1
Higgs	$\begin{pmatrix} H_u^+ \\ H_u^0 \\ H_d^0 \\ H_d^- \end{pmatrix}$	Higgsino	$\begin{pmatrix} \tilde{H}_u^+ \\ \tilde{H}_u^0 \\ \tilde{H}_d^0 \\ \tilde{H}_d^- \end{pmatrix}$	<b>1</b>	<b>2</b>	1		
				$\tilde{H}_u^0$	$\tilde{H}_d^0$	<b>1</b>	<b>2</b>	-1
				$\tilde{H}_d^0$	$\tilde{H}_d^-$	<b>1</b>	<b>2</b>	-1
<b>GAUGE SUPERMULTIPLER</b>								
Particle	Spin 1/2	Particle	Spin 1	$SU(3)_c$	$SU(2)_L$	$U(1)_Y$		
gluino	$\tilde{g}$	gluon	$g$	<b>8</b>	<b>1</b>	0		
winos	$\tilde{W}^\pm \tilde{W}^0$	W boson	$W^\pm W^0$	<b>1</b>	<b>3</b>	0		
binos	$\tilde{B}^0$	B boson	$B^0$	<b>1</b>	<b>1</b>	0		

Table 4.1: Table showing the quantum numbers for the Standard Model particles and their super-partners. Please note that the table is done using  $Q_{EM} = T_3 + \frac{1}{2}Y$ .

fields and gauge fields is given in Table 4.1 along with their Standard Model quantum numbers.

To establish supersymmetry as a valid symmetry of nature sparticles must be searched for. If supersymmetry was not a broken symmetry the sparticles would have the same mass as the Standard Model partners. This is not the case. Thus, if supersymmetry exists, it must be a broken symmetry in that the sparticles must have masses much larger than the masses of the Standard Model particles to be consistent with experimental observation. Unfortunately, the breaking of supersymmetry is a challenging task. It is possible to achieve phenomenologically viable breaking of supersymmetry within the framework of supergravity (SUGRA) [57–64]. In supergravity the breaking of supersymmetry is done in a hidden sector and communicated to the visible sector via gravitational interactions [65]. The supergravity unified models

can be viewed as the low energy limit of string models, since supergravity is the field point limit of strings. The simplest of such supergravity models is mSUGRA [65–67] which under the constraints of radiative breaking of the electroweak symmetry reduces to four and a half parameters. Thus mSUGRA is parameterized by

$$m_0, m_{1/2}, A_0, \tan \beta, \text{ and } \text{sign}(\mu) \quad (4.1)$$

where  $m_0$  is the universal scalar mass,  $m_{1/2}$  is the universal gaugino mass,  $A_0$  is the universal trilinear coupling, and  $\tan \beta = \langle H_2 \rangle / \langle H_1 \rangle$ . Here  $H_2$  gives mass to the up quarks and  $H_1$  gives mass to the down quarks and the leptons, and  $\mu$  is the Higgs mixing parameter which enters in the superpotential as  $\mu H_1 H_2$ . The mSUGRA model is the simplest of the supergravity grand unified models and is ideally suited as a benchmark for the exploration of supersymmetry at different experiments. However, mSUGRA can be extended to include non-universalities in the gaugino sector, non-universalities in the Higgs sector, and non-universalities in the third generation sector. Additionally, there are a number of interesting string based models (as well as D-brane models) that can be investigated within the supergravity framework [68].

## 4.2 *R*-Parity

In supersymmetry it is useful to introduce a new quantum number called *R*-parity defined by

$$R = (-1)^{3(B-L)+2s}, \quad (4.2)$$

where  $B$  is the baryon number,  $L$  is the lepton number, and  $s$  is the spin of the particle. This implies that for Standard Model particles  $R = 1$  and for the superpartners

$R = -1$ . If we assume that  $R$ -parity is conserved we get several interesting results. First, it implies that the lightest supersymmetric particle (LSP) must be stable and if it is neutral then it can be a dark matter candidate. Second, sparticles decay into an odd number of LSPs. Lastly, at the parton level colliders produce sparticles in pairs. Additionally, with  $R$ -parity conservation, decays of supersymmetric particles at colliders are associated with missing energy which is carried by the LSP.

# Chapter 5

## Multicomponent Dark Matter

### 5.1 Introduction

In this chapter we follow [69] and show that multicomponent dark matter [70–75] can arise from  $U(1)^n$  extensions of the Minimal Supersymmetric Standard Model with Abelian hidden sectors which include hidden sector matter. There are two main modes of detection of dark matter. One is direct detection such as via the scattering of dark matter particles from nuclei in a detector (CDMS [76, 77], XENON 100 [78–80], etc.) and the other is via annihilation where two WIMPs annihilate in the galaxy into a  $e^+e^-$  pair possibly associated with other particles (PAMELA [81–83], AMS [84], etc.). However, most models which aim to explain the PAMELA positron excess do not give a significant number of dark matter events in the direct detection experiments currently operating. Conversely, models which can give a detectable signal in direct detection experiments typically do not explain the PAMELA data without the use of enormous so-called boost factors. As will be shown here, this can be circumvented in models where the dark matter has several components. Thus, motivated in

part by the recent cosmic anomalies we develop supersymmetric models which contain minimally a hidden Abelian sector broken at the sub- TeV scale where the mass generation of the hidden states involves nontrivial mixings with the field content of the electroweak sector of the minimal supersymmetric extension of the Standard Model leading to dark matter which can have several components that can be both bosonic and fermionic.

More specifically, we go beyond the simple theoretical construction that thermal dark matter compatible with WMAP observations is composed of a single fundamental particle. There is no overriding principle that requires such a restriction, and non-baryonic dark matter (DM) may indeed be constituted of several components, so in general one has  $(\Omega h^2)_{DM} = \sum_i (\Omega h^2)_{DM_i}$ , where  $i$  refers to the various species of dark particles that can contribute to the total nonbaryonic  $(\Omega h^2)_{DM}$ . In fact we already know that neutrinos do contribute to dark matter although their contribution is relatively small. Thus we propose here a new class of multicomponent cold dark matter models in Abelian  $U(1)$  extensions of MSSM which can simultaneously provide an explanation of the PAMELA and WMAP data through a Breit-Wigner enhancement [85], while producing detectable signals for the direct searches for dark matter with CDMS/XENON and other dark matter experiments.

In this chapter we give a detailed description of two models: one of which is based on a  $U(1)_X$  extension of the MSSM where  $U(1)_X$  is a hidden sector gauge group with Dirac fermions in the hidden sector. This model allows for dark matter consisting of Dirac, Majorana, and spin-0 particles. The second model is based on a  $U(1)_X \times U(1)_C$  extension of MSSM, where  $U(1)_C$  is a gauged leptophilic symmetry and  $U(1)_X$ , as before, is the hidden sector gauge group which also contains Dirac particles in the hidden sector. This model too has Dirac, Majorana, and spin-0 parti-

cles as possible dark matter. In both cases we will primarily focus on the possibility that dark matter consists of Dirac and Majorana particles, and we will not discuss in detail the possibility of dark matter with bosonic degrees of freedom. The relic densities in the two component models will also be discussed.

## 5.2 Multicomponent Hidden Sector Models

### 5.2.1 Multicomponent $U(1)_X$ model

A  $U(1)_X$  extension of the Minimal Supersymmetric Standard Model involves the coupling of a Stueckelberg chiral multiplet  $S = (\rho + i\sigma, \chi_S, F_S)$  to vector supermultiplets  $X, B$ , where  $\rho$  is a real scalar and  $\sigma$  is an axionic pseudo-scalar. Here  $X$  is the  $U(1)_X$  vector multiplet which is neutral with respect to the Standard Model gauge group with components  $X = (X_\mu, \lambda_X, D_X)$ , and  $B$  is the  $U(1)_Y$  vector multiplet with components  $(B_\mu, \lambda_B, D_B)$ , where the components are written in the Wess-Zumino gauge. The chiral multiplet  $S$  transforms under both  $U(1)_X$  and  $U(1)_Y$  and acts as the connector sector between the visible and the hidden sectors. The total Lagrangian of the system is given by

$$\mathcal{L} = \mathcal{L}_{\text{MSSM}} + \mathcal{L}_{U(1)_X} + \mathcal{L}_{\text{St}} \quad (5.1)$$

where  $\mathcal{L}_{U(1)_X}$  is the kinetic energy piece for the  $X$  vector multiplet and  $\mathcal{L}_{\text{St}}$  is the supersymmetric Stueckelberg mixing between the  $X$  and the  $B$  vector multiplets so that [28, 29, 86, 87]

$$\mathcal{L}_{\text{St}} = \int d^2\theta d^2\bar{\theta} (M_1 X + M_2 B + S + \bar{S})^2, \quad (5.2)$$

where  $M_1$  and  $M_2$  are mass parameters. The Lagrangian of Equation (5.1) is invariant under the  $U(1)_Y$  and  $U(1)_X$  gauge transformations, i.e., under

$$\delta_X X = \zeta_X + \bar{\zeta}_X, \quad \delta_X S = -M_1 \zeta_X, \quad \delta_Y B = \zeta_Y + \bar{\zeta}_Y, \quad \delta_Y S = -M_2 \zeta_Y, \quad (5.3)$$

where  $\zeta$  is an infinitesimal transformation chiral superfield. In component form we have for the Stueckelberg sector with  $U(1)_X \times U(1)_Y$

$$\begin{aligned} \mathcal{L}_{\text{St}} = & -\frac{1}{2}(M_1 X_\mu + M_2 B_\mu + \partial_\mu \sigma)^2 - \frac{1}{2}(\partial_\mu \rho)^2 - i\chi_S \sigma^\mu \partial_\mu \bar{\chi}_S + 2|F_S|^2 \\ & + \rho(M_1 D_X + M_2 D_B) + \bar{\chi}_S(M_1 \bar{\lambda}_X + M_2 \bar{\lambda}_B) + \chi_S(M_1 \lambda_X + M_2 \lambda_B). \end{aligned} \quad (5.4)$$

In addition, one may include a supersymmetric kinetic mixing term between the  $U(1)_X$  and  $U(1)_Y$  gauge fields leading to  $\mathcal{L} = \mathcal{L}_{\text{MSSM}} + \mathcal{L}_{U(1)_X} + \mathcal{L}_{\text{KM}} + \mathcal{L}_{\text{St}}$ , where

$$\begin{aligned} \mathcal{L}_{U(1)_X} + \mathcal{L}_{\text{KM}} = & -\frac{1}{4}X^{\mu\nu}X_{\mu\nu} - i\lambda_X \sigma^\mu \partial_\mu \bar{\lambda}_X + \frac{1}{2}D_X^2 \\ & -\frac{\delta}{2}X^{\mu\nu}B_{\mu\nu} - i\delta(\lambda_X \sigma^\mu \partial_\mu \bar{\lambda}_B + \lambda_B \sigma^\mu \partial_\mu \bar{\lambda}_X) + \delta D_B D_X. \end{aligned} \quad (5.5)$$

As a consequence of the mixings, the extra gauge boson of the hidden sector couples with the Standard Model fermions and can become visible at colliders. The Lagrangian for matter interacting with the  $U(1)$  gauge fields is given by

$$\mathcal{L}_{\text{matt}} = \int d^2\theta d^2\bar{\theta} \sum_i \left[ \bar{\Phi}_i e^{2g_Y Q_Y B + 2g_X Q_X X} \Phi_i + \bar{\Phi}_{\text{hid},i} e^{2g_Y Q_Y B + 2g_X Q_X X} \Phi_{\text{hid},i} \right]. \quad (5.6)$$

where the visible sector chiral superfields are denoted by  $\Phi_i$  (quarks, squarks, leptons, sleptons, Higgs, and Higgsinos of the Minimal Supersymmetric Standard Model) and the hidden sector chiral superfields are denoted by  $\Phi_{\text{hid},i}$ . In the above,  $Q_Y$  is the hypercharge normalized so that  $Q = T_3 + Q_Y$ . As mentioned already, the Stan-

standard Model matter fields do not carry any charge under the hidden gauge group and vice versa, i.e.  $Q_X \Phi_i = 0$  and  $Q_{SM} \Phi_{\text{hid}} = 0$ . The minimal matter content of the hidden sector consists of a left chiral multiplet  $\Phi_{\text{hid}} = (\phi, f, F)$  and a charge conjugate  $\Phi_{\text{hid}}^c = (\phi', f', F')$  so that  $\Phi_{\text{hid}}$  and  $\Phi_{\text{hid}}^c$  have opposite  $U(1)_X$  charges and form an anomaly-free combination. A mass  $M_\psi$  for the Dirac field  $\psi$  arises from an additional term in the superpotential  $W_\psi = M_\psi \Phi \Phi^c$ , where  $\psi$  is composed of  $f$  and  $f'$ . The scalar fields acquire soft masses of size  $m_0$  from spontaneous breaking of supersymmetry by gravity mediation, and in addition acquire a mass from the term in the superpotential so that

$$m_\phi^2 = m_0^2 + M_\psi^2 = m_{\phi'}^2. \quad (5.7)$$

After spontaneous breaking of the electroweak symmetry there would be mixing between the vector fields  $X_\mu, B_\mu, A_{3\mu}$ , where  $A_{3\mu}$  is the third component of the  $SU(2)_L$  field  $A_{a\mu}$ , ( $a = 1, 2, 3$ ). After diagonalization  $V^T = (X, B, A_3)$  can be expressed in the terms of the mass eigenstates  $E^T = (Z', Z, \gamma)$  as follows:

$$V_i = O_{ij} E_j, \quad i, j = 1 - 3, \quad E = (Z', Z, \gamma). \quad (5.8)$$

Further, the chiral fermions in the  $S + \bar{S}$  multiplet together with the MSSM gauginos and Higgsinos will form a  $6 \times 6$  neutralino mass matrix whose eigenstates are six neutralino states  $\chi_a$ ,  $a = 1 - 6$ , where we assume that the set  $\chi_1^0 \dots \chi_4^0$  is the regular set of neutralinos and  $\chi_5^0, \chi_6^0$  are the two additional neutralinos that arise in the  $U(1)_X$  extension. From the components  $\lambda_X, \bar{\lambda}_X$  and  $\chi_S, \bar{\chi}_S$  that appear in Equation (6.16),

we can form two Majorana fields  $\Lambda_X$  and  $\psi_S$  as follows:

$$\Lambda_X = \begin{pmatrix} \lambda_{X\alpha} \\ \bar{\lambda}_{X\dot{\alpha}} \end{pmatrix}, \quad (5.9)$$

$$\psi_S = \begin{pmatrix} \chi_{\alpha,S} \\ \bar{\chi}_{S\dot{\alpha}} \end{pmatrix}. \quad (5.10)$$

$$(5.11)$$

These components combine with the MSSM gauginos and Higgsinos to form a  $6 \times 6$  neutralino mass matrix whose eigenstates are the six neutralinos  $\chi_a$ , ( $a = 1 - 6$ ). Thus  $\Lambda_X$  and  $\psi_S$  can be expanded as linear combination of  $\chi_a$ , i.e.,

$$\Lambda_X = R_{1a}\chi_a, \quad a = 1 - 6, \quad \psi_S = R_{2a}\chi_a, \quad a = 1 - 6 \quad (5.12)$$

where  $R$  is the unitary matrix which diagonalizes the  $6 \times 6$  neutralino mass matrix. Further the  $CP$ -even Higgs sector is extended by the additional state  $\rho$ . The results outlined here give the following types of interactions:

1. There are interactions of the Dirac fermion in the hidden sector with the Standard Model particles via  $Z, Z', \gamma$  interactions. Thus, the Dirac dark matter can annihilate into Standard Model particles via exchange of  $Z, Z', \gamma$  in the early universe and in the galaxy. Depending on which of the two, Dirac or Majorana, is the heavier one may have Dirac particles annihilating into Majoranas or the Majorana particles annihilating into Dirac fermions in the galaxy:

$$\bar{\psi}\psi \rightarrow \chi\chi \quad \text{or} \quad \chi\chi \rightarrow \bar{\psi}\psi. \quad (5.13)$$

2. In addition to the above we have fermion-neutralino-sfermion couplings in the hidden sector as given by Equation (5.6). Thus interactions of the type  $\bar{\psi}\chi_a\phi + \text{h.c.}$ , etc. can produce decays such as  $\phi \rightarrow \psi + \chi_a$  if they are kinematically allowed.
3. The scalar field  $\rho$  is CP even and mixes with the MSSM Higgs fields. Through these mixings  $\rho$  has couplings to the SM fermions and through these couplings it can decay into the SM fermions.

It is instructive to list all the new particles in this  $U(1)_X$  model as summarized below:

New particles of the  $U(1)_X$  model

$$\begin{aligned}
&\text{spin } 0 : \rho, \phi, \phi', \\
&\text{spin } \frac{1}{2} : \psi, \chi_5^0, \chi_6^0, \\
&\text{spin } 1 : Z'.
\end{aligned} \tag{5.14}$$

We will assume that the lightest  $R$ -parity odd particle (LSP) is the least massive neutralino ( $\chi^0 = \chi_1^0 \equiv \chi$ ) and resides in the visible sector and thus the masses of  $\chi_5^0, \chi_6^0$  are larger than the LSP  $\chi^0$  mass, and consequently  $\chi_5^0, \chi_6^0$  are unstable and decay into Standard Model particles and  $\chi^0$ . The bosons  $Z'$  and  $\rho$  are unstable and decay into Standard Model fermion pairs  $f\bar{f}$  with the decay of the  $\rho$  going dominantly through the process  $\rho \rightarrow b\bar{b}$  or  $\rho \rightarrow t\bar{t}$  if  $m_\rho > 2m_t$ . The remaining three particles  $\psi, \phi, \phi'$  are all milli-charged and, consequently, at least one of them is stable. If we assume  $m_\phi, m_{\phi'} > M_\psi$ , at least  $\psi$  is always stable and the other two may or may not be stable. These along with the LSP give rise to various possible candidates for dark matter. Thus, depending on the relative masses of the Majorana, Dirac, and spin-0 particles

there are three possibilities for the constituents of dark matter as outlined below.

### 5.2.2 Two component dark matter: Majorana + Dirac

This model arises as follows: consider the case where  $m_\phi > M_\psi + M_\chi$ . In this case the decays  $\phi, \phi' \rightarrow \psi + \chi^0$ , will occur and  $\phi, \phi'$  will be unstable. Thus  $\psi$  is stable and so is  $\chi$  under the assumption of R parity conservation. Consequently, we will have two dark matter particles; namely, one a Majorana which is the LSP in the visible sector and the other a Dirac in the hidden sector. The Majorana and Dirac particles once created will annihilate as follows:

$$\psi + \bar{\psi} \rightarrow Z, Z', \gamma \rightarrow \text{SM} + \text{SM}', \quad (5.15)$$

$$\chi + \chi \rightarrow (s : Z', Z, h, H, A, \rho), (t/u : \tilde{f}_a, \chi_i, \chi_k^\pm) \rightarrow \text{SM} + \text{SM}'. \quad (5.16)$$

where  $s$  : refers to  $s$ -channel exchanges and  $t/u$  : refers to  $t$  or  $u$  channel exchanges. In addition to Equation (5.16) there are coannihilation processes which contribute to the relic density. Since both  $\psi$  and  $\chi$  are stable, the total relic density of dark matter will be the sum of the relic densities for the two, the sum being constrained by the WMAP data.

### 5.2.3 Three component dark matter: Dirac and two spin-0 particles

Suppose the mass of  $\chi$  is larger than the sum of the masses of the Dirac plus the scalar  $\phi$ , i.e.,  $M_\chi > M_\psi + m_\phi$ . In this case the decay  $\chi \rightarrow \phi + \psi, \phi' + \psi$  will occur and, consequently,  $\chi$  is unstable. On the other hand,  $\phi, \phi'$  and  $\psi$  are stable since they cannot decay into anything else. Thus, here we have three dark matter particles: one

Dirac, and the other two spin-0. Processes that lead to the annihilation of these particles are those in Equation (5.15) for  $\psi$ , and also for  $\phi$  and  $\phi'$ , they are similar to those in Equation (5.15), i.e.,  $\phi + \phi^*, \phi' + \phi'^* \rightarrow \gamma, Z, Z' \rightarrow \text{SM} + \text{SM}'$ . In this three component dark matter model all the components reside in the hidden sector and thus their couplings to the Standard Model particles are extra weak. Consequently, they will have very small spin-independent cross sections in direct detection experiments. For this reason, this class of models is less preferred compared to the two component model.

#### 5.2.4 Four component dark matter: Majorana, Dirac, and two spin-0 particles

Finally, we consider the case when either of the following two situations occur: (i)  $M_\chi > M_\psi$  and  $m_\phi < M_\chi < M_\psi + m_\phi$ , (ii)  $M_\chi < m_\phi < M_\chi + M_\psi$ . In these cases all four particles, one Majorana, one Dirac, and two spin-0 particles, are stable and thus are possible dark matter candidates. These particles will annihilate to the SM particles as in Equation (5.15), Equation (5.16) and for  $\phi$  and  $\phi'$  via processes in the three component dark matter model as described above. This model is in many ways similar to the two component model and like the two component model this model too should lead to detectable signals in experiments for the direct detection of dark matter.

### 5.3 Multicomponent Leptophilic $U(1)_X \times U(1)_C$ model

Another model will now be discussed which contains two additional Abelian vector bosons where one of the extra bosons is leptophilic. Here we will consider a  $U(1)_X \times U(1)_C$  model where the  $U(1)_X$  as before is in the hidden sector, and  $U(1)_C$  is a leptophilic symmetry. As in the  $U(1)_X$  model, we also assume that the hidden sector has a pair of Dirac fermions  $\psi$  and  $\bar{\psi}$  which are charged under  $U(1)_X$  but are neutral under the Standard Model gauge group and under  $U(1)_C$ . Regarding  $U(1)_C$  we assume it to be  $L_e - L_\mu$ , i.e., a difference of family-lepton numbers, which is anomaly free, and can be gauged. The corresponding gauge field  $C_\mu$  couples only to  $e, \mu$  families and nothing else. The total Lagrangian in this case is

$$\mathcal{L} = \mathcal{L}_{\text{MSSM}} + \mathcal{L}_{U(1)^2} + \mathcal{L}_{\text{St}}, \quad (5.17)$$

where  $\mathcal{L}_{U(1)^2}$  is the kinetic energy for the  $X$  and  $C$  multiplets and for  $\mathcal{L}_{\text{St}}$  we assume the following form:

$$\begin{aligned} \mathcal{L}_{\text{St}} = & \int d^2\theta d^2\bar{\theta} (M_1 C + M'_2 X + M'_3 B + S + \bar{S})^2 \\ & + \int d^2\theta d^2\bar{\theta} (M'_1 C + M_2 X + M''_3 B + S' + \bar{S}')^2, \end{aligned} \quad (5.18)$$

where  $C$  is the  $U(1)_{L_e - L_\mu}$  vector multiplet with components  $(C_\mu, \lambda_C, D_C)$  and  $X$  and  $B$  are the  $U(1)_X$  and  $U(1)_Y$  multiplets as discussed before. The gauge transformations

under  $U(1)_C$ ,  $U(1)_X$ , and  $U(1)_Y$  are

$$\begin{aligned}
\delta_C C &= \zeta_C + \bar{\zeta}_C, & \delta_C S &= -M_1 \zeta_C, & \delta_C S' &= -M_1' \zeta_C \\
\delta_X X &= \zeta_X + \bar{\zeta}_X, & \delta_X S &= -M_2' \zeta_X, & \delta_X S' &= -M_2 \zeta_X, \\
\delta_Y B &= \zeta_Y + \bar{\zeta}_Y, & \delta_Y S &= -M_3' \zeta_Y, & \delta_Y S' &= -M_3'' \zeta_Y,
\end{aligned} \tag{5.19}$$

where  $\zeta_C, \zeta_X, \zeta_Y$ , etc. are the infinitesimal transformation chiral superfields. The quantities  $M_1, M_2, M_1', M_2', M_3'$ , and  $M_3''$  are the mass parameters. In the vector boson sector  $\mathcal{L}_{\text{St}}$  assumes the form

$$\mathcal{L}_{\text{St}} = -\frac{1}{2}(M_1 C_\mu + M_2' X_\mu + M_3' B_\mu + \partial_\mu \sigma)^2 - \frac{1}{2}(M_1' C_\mu + M_2 X_\mu + M_3'' B_\mu + \partial_\mu \sigma')^2. \tag{5.20}$$

The mass<sup>2</sup> matrix in the vector boson sector in the basis  $(C^\mu, X^\mu, B^\mu, A^{3\mu})$  is given by

$$\begin{pmatrix}
M_1^2 + M_1'^2 & M_1 M_2' + M_1' M_2 & M_1 M_3' + M_1' M_3'' & 0 \\
M_1 M_2' + M_1' M_2 & M_2^2 + M_2'^2 & M_2' M_3' + M_2 M_3'' & 0 \\
M_1 M_3' + M_1' M_3'' & M_2' M_3' + M_2 M_3'' & M_3'^2 + M_3''^2 + M_Y^2 & -M_Y M_W \\
0 & 0 & -M_Y M_W & M_W^2
\end{pmatrix} \tag{5.21}$$

here  $M_W = g_2 \cdot v/2$  is the  $W$  boson mass and  $M_Y = M_W \tan \theta_W = g_Y \cdot v/2$ , and where  $\theta_W$  is the weak angle. The dynamics of the model of Equation (5.21) is rather involved. Therefore, focusing on a simpler version of this more general case where we neglect the mixings with  $B_\mu$ , i.e., we set  $M_3' = M_3'' = 0$ . Inclusion of these coupling in the analysis would not drastically change the analysis or the conclusions of this work as long as we keep the mixing parameters  $M_3'/M_{1,2}, M_3''/M_{1,2}$  very small. After neglecting the mixings with  $B_\mu$ , the mass<sup>2</sup> matrix is block diagonal and so we can diagonalize the top left hand corner  $2 \times 2$  mass matrix independent of the Stan-

Standard Model sector. We are interested in the limit of small mixing between  $U(1)_X$  and  $U(1)_C$  and thus consider

$$M'_1, M'_2 \ll M_1, M_2. \quad (5.22)$$

In the above approximation the eigenvalues of this mass matrix are

$$\begin{aligned} M_{Z'}^2 &\simeq M_2^2 + M_2'^2 - \Delta_{M^2}, & M_{Z''}^2 &\simeq M_1^2 + M_1'^2 + \Delta_{M^2}, \\ \Delta_{M^2} &\simeq \frac{(M_1 M_2' + M_1' M_2)^2}{(M_1^2 + M_1'^2 - M_2^2 - M_2'^2)}. \end{aligned} \quad (5.23)$$

The corresponding mass eigenstates are  $Z'$  and  $Z''$ , where

$$\begin{aligned} C_\mu &= \cos \theta_X Z''_\mu - \sin \theta_X Z'_\mu, & X_\mu &= \sin \theta_X Z''_\mu + \cos \theta_X Z'_\mu, \\ \tan \theta_X &\simeq \frac{M_1 M_2' + M_1' M_2}{M_1^2 + M_1'^2 - M_2^2 - M_2'^2}. \end{aligned} \quad (5.24)$$

Because of Equation (5.22)  $\tan \theta_X \ll 1$ . In the above, the Dirac fermions in the hidden sector have no couplings with the photon and are electrically neutral. However, by a small mixing of  $X_\mu$  with  $B_\mu$  in Equation (5.20), we can generate a milli-charge for the Dirac particles in the hidden sector consistent with all electroweak data.

We discuss now the gaugino/chiral fermions in the extra  $U(1)$  sectors which arise from the superfields  $C, X, S + \bar{S}, S' + \bar{S}'$ . From the gaugino components  $\lambda_C, \bar{\lambda}_C, \lambda_X, \bar{\lambda}_X$ , and from the chiral fermion components in the extra  $U(1)$  sectors  $\chi_S, \bar{\chi}_S, \chi_{S'}, \bar{\chi}_{S'}$ , one can construct four component Majorana spinors two of which are exhibited in

Eq.(5.11) and the remaining two are given by

$$\Lambda_C = \begin{pmatrix} \lambda_{C\alpha} \\ \bar{\lambda}_C^{\dot{\alpha}} \end{pmatrix}, \quad (5.25)$$

$$\psi_{S'} = \begin{pmatrix} \chi_{\alpha,S'} \\ \bar{\chi}_{S'}^{\dot{\alpha}} \end{pmatrix}. \quad (5.26)$$

The neutralino mass matrix in the  $[U(1)_X \times U(1)_C] \times [SU(3)_C \times SU(2)_L \times U(1)_Y]$  model takes a block diagonal form

$$\left[ \begin{array}{c|c} U(1)_X \times U(1)_C & 0_{4 \times 4} \\ \hline \text{sector} & \\ \hline 0_{4 \times 4} & \text{MSSM} \\ & \text{sector} \end{array} \right]_{8 \times 8}. \quad (5.27)$$

Thus, the Stueckelberg mass generation produces a mass matrix in the hidden gaugino/chiral fermion sector which is decoupled from the neutralino mass matrix in the visible sector. Specifically in the 4 component notation the gaugino/chiral fermion mass matrix in the  $U(1)_X \times U(1)_C$  sector is given by

$$L_{U(1)_X \times U(1)_C}^{mass} = - \begin{pmatrix} \bar{\psi}_S \\ \bar{\psi}_{S'} \\ \bar{\Lambda}_C \\ \bar{\Lambda}_X \end{pmatrix}^T \begin{pmatrix} 0 & 0 & M_1 & M'_2 \\ 0 & 0 & M'_1 & M_2 \\ M_1 & M'_1 & 0 & 0 \\ M'_2 & M_2 & 0 & 0 \end{pmatrix} \begin{pmatrix} \psi_S \\ \psi_{S'} \\ \Lambda_C \\ \Lambda_X \end{pmatrix}. \quad (5.28)$$

In the diagonalized basis we can label the extra neutralinos by  $\chi_5^0, \chi_6^0, \chi_7^0, \chi_8^0$ . Since

the hidden sector and the neutralinos of the visible sector are decoupled, the diagonalization of the neutralinos in the visible sector, i.e., of  $\chi_i^0$ , ( $i = 1 - 4$ ) is not affected. Further, as for the case of the  $U(1)_X$  model, it is instructive to list all the new particles in this  $U(1)_X \times U(1)_C$  model as summarized below:

New particles of  $U(1)_C \times U(1)_X$  model

$$\begin{aligned}
& \text{spin } 0 : \rho, \rho', \phi, \phi', \\
& \text{spin } \frac{1}{2} : \psi, \chi_5^0, \chi_6^0, \chi_7^0, \chi_8^0, \\
& \text{spin } 1 : Z', Z''.
\end{aligned} \tag{5.29}$$

We discuss now the stability of the new particles in this model. As before we assume that the mass of  $\phi$  (and of  $\phi'$ ) is larger than the mass of  $\psi$ . Thus  $\psi$  will be stable since it cannot decay into anything. If kinematically allowed the fields  $\phi$  and  $\phi'$  can decay only via the process  $\phi, \phi' \rightarrow \psi + \chi^0$  as in the  $U(1)_X$  model. Of the remaining fields obviously  $Z'$  and  $Z''$  are unstable as they decay into  $e\bar{e}, \mu\bar{\mu}, \nu_e\bar{\nu}_e, \nu_\mu\bar{\nu}_\mu$  as well as into  $\psi\bar{\psi}$  depending on the mass of  $\psi$ . As already noted, a small milli charge can develop for the hidden sector matter via small couplings of the  $B_\mu$  and  $X_\mu$  fields. The phenomenology of such models will be very similar to the one we are discussing here.

The extra neutralinos of Equation (5.29) can also be all unstable. Thus  $\Lambda_C$  couples with leptons-sleptons ( $e, \bar{e}$  etc.) via coupling of the type  $\bar{\Lambda}_C e_L \bar{e}_L^*$ , etc. and after diagonalization of the gaugino/chiral fermion mass matrix all the  $\chi_k^0$ , ( $k = 5 - 8$ ) will have coupling with leptons-sleptons of the type indicated. Further, two of the  $\chi_k^0$  have roughly a mass of size  $M_1$  while the remaining two have roughly a mass of size  $M_2$ . Thus, if  $M_1, M_2 > m_{\chi^0}$ , which is what is assumed in this work, all the neutralinos of the hidden sector will be unstable and decay into final states of the type

$e\bar{e}\chi^0, \mu\bar{\mu}\chi^0$ , etc. Regarding the field  $\rho$ , there is an interaction of type

$$M_1 g_C \rho (\tilde{f}^* Q_C^f \tilde{f}), \quad f = e, \mu. \quad (5.30)$$

With this interaction  $\rho$  will decay as follows:  $\rho \rightarrow \tilde{f}^* \tilde{f} \rightarrow f \bar{f} \chi^0 \chi^0 (f = e, \mu)$  provided this process is kinematically allowed which we assume is the case. A similar situation occurs for the case of  $\rho'$ . Additionally, if there is a mixing with  $B_\mu$  in the Stueckelberg sector then, as in the analysis of the  $U(1)_X$  model, the fields  $\rho$  and  $\rho'$  will mix with the Higgs sector and can have decays of the type  $\rho \rightarrow b\bar{b}, \rho' \rightarrow b\bar{b}$ , etc. Thus, in the end we are left with a similar set of possibilities for dark matter as in the  $U(1)_X$  model, i.e., (i) a two component model with  $\psi$  and  $\chi^0$ , (ii) a three component model with  $\psi, \phi, \phi'$ , and (iii) a four component model with  $\psi, \phi, \phi',$  and  $\chi^0$ . However, as in the  $U(1)_X$  case we will focus on the two component model consisting of Dirac and Majorana dark particles.

We assume  $M_{Z''}^2 \gg M_{Z'}^2$ , and that the annihilation of dark matter occurs close to the  $Z'$  pole for reasons that will become apparent shortly. As a consequence, the annihilation of dark matter in the early universe and in the galaxy is controlled by the  $Z'$  pole and the effect of the  $Z''$  pole on the analysis is essentially negligible. The basic interaction of  $C_\mu$  and of  $X_\mu$  with matter is given by

$$\mathcal{L}_{int} = g_X Q_X \bar{\psi} \gamma^\mu \psi X_\mu + g_C Q_C^f \bar{f} \gamma^\mu f C_\mu \quad (5.31)$$

where  $f$  runs over  $e$  and  $\mu$  families and where  $Q_C^e = -Q_C^\mu$ . In the mass diagonal

basis the interaction of Equation (5.31) assumes the form

$$\begin{aligned}\mathcal{L}_{int} &= (g_X Q_X \bar{\psi} \gamma^\mu \psi \cos \theta_X - g_C Q_C^f \bar{f} \gamma^\mu f \sin \theta_X) Z'_\mu \\ &+ (g_X Q_X \bar{\psi} \gamma^\mu \psi \sin \theta_X + g_C Q_C^f \bar{f} \gamma^\mu f \cos \theta_X) Z''_\mu.\end{aligned}\quad (5.32)$$

The interaction of Equation (5.32) leads to the annihilation of  $\psi\bar{\psi}$  into  $e^+e^-$  and  $\mu^+\mu^-$  via the  $Z', Z''$  poles for which we assume a Breit-Wigner form. Thus, the  $\psi\bar{\psi} \rightarrow f\bar{f}$  annihilation cross section takes the form

$$\begin{aligned}\sigma_{\psi\bar{\psi} \rightarrow f\bar{f}} &= a_\psi \left| (s - M_{Z'}^2 + i\Gamma_{Z'} M_{Z'})^{-1} - (s - M_{Z''}^2 + i\Gamma_{Z''} M_{Z''})^{-1} \right|^2, \\ a_\psi &= \frac{\beta_f (g_X g_C Q_X Q_C^f \sin(2\theta_X))^2}{64\pi s \beta_\psi} \left[ s^2 \left( 1 + \frac{1}{3} \beta_f^2 \beta_\psi^2 \right) + 4M_\psi^2 (s - 2m_f^2) + 4m_f^2 (s + 2M_\psi^2) \right],\end{aligned}\quad (5.33)$$

$$(5.34)$$

where  $\beta_{f,\psi} = (1 - 4m_{f,\psi}^2/s)^{1/2}$ . The relevant partial  $Z'$  decay widths are given by

$$\Gamma(Z' \rightarrow f\bar{f}) = (g_C Q_C^f \sin \theta_X)^2 \frac{M_{Z'}}{12\pi}, \quad f = e, \mu, \quad (5.35)$$

$$\Gamma(Z' \rightarrow \psi\bar{\psi}) = (g_X Q_X \cos \theta_X)^2 \frac{M_{Z'}}{12\pi} \left( 1 + \frac{2M_\psi^2}{M_{Z'}^2} \right) \left( 1 - \frac{4M_\psi^2}{M_{Z'}^2} \right)^{1/2} \Theta(M_{Z'} - 2M_\psi), \quad (5.36)$$

and similarly for the partial decay widths of the  $Z''$  with  $M_{Z'} \rightarrow M_{Z''}$  and  $-\sin \theta_X \rightarrow \cos \theta_X$  in Equation (5.35) and  $\cos \theta_X \rightarrow \sin \theta_X$  in Equation (5.36).

A constraint on  $g_C$  comes from the contribution of the  $Z'$  and  $Z''$  to  $g_\mu - 2$ . Their exchange gives

$$\Delta(g_\mu - 2) = \frac{g_C^2 m_\mu^2}{24\pi^2} \left[ \frac{\sin^2 \theta_X}{M_{Z'}^2} + \frac{\cos^2 \theta_X}{M_{Z''}^2} \right]. \quad (5.37)$$

Using the current error [40] of  $\Delta(g_\mu - 2) = 1.2 \times 10^{-9}$  in the determination of  $g_\mu - 2$

and assuming  $\theta_X$  is small, one finds the following constraint on  $\alpha_C$ :

$$\alpha_C \lesssim 0.001 \left( \frac{M_{Z''}}{300 \text{ GeV}} \right)^2, \quad (5.38)$$

where  $\alpha_C = g_C^2/4\pi$ . We note that if the mixing angle  $\theta_X$  is small, the decay width of  $Z' \rightarrow f\bar{f}$  ( $f = e, \mu$ ) and of  $Z'' \rightarrow \psi\bar{\psi}$  will be narrow while the decay width of  $Z'' \rightarrow f\bar{f}$  ( $f = e, \mu$ ) and of  $Z' \rightarrow \psi\bar{\psi}$  will be of normal size. However, when  $M_\psi \simeq M_{Z'}/2$  the  $Z'$  decay width into  $\psi\bar{\psi}$  will also be small due to the kinematic suppression factor  $\left(1 - \left[4M_\psi^2/M_{Z'}^2\right]\right)^{1/2}$ . In this case we will have the total width of the  $Z'$  to be rather narrow. Thus for annihilation near the Breit-Wigner pole we will have a large enhancement of  $\langle\sigma v\rangle$  due to the narrowness of the  $Z'$  [85]. It was shown in the analysis of [85] that near the Breit-Wigner pole such annihilations allow one to fit the relic density as well as allow an enhancement of  $\langle\sigma v\rangle$  in the galaxy. We note that while  $Z'$  decay width is very small this is not necessarily the case for  $Z''$  which can decay into  $e\bar{e}, \mu\bar{\mu}, \nu_e\bar{\nu}_e, \nu_\mu\bar{\nu}_\mu$  with normal strength. Thus neglecting the contribution of  $Z'' \rightarrow \psi\bar{\psi}$  which is small due to the  $\sin^2\theta_X \sim \epsilon^2$  suppression, one finds the total width of  $Z''$  to be  $\Gamma_{Z''} \simeq \cos^2\theta_X\alpha_C M_{Z''}$ . Finally, the annihilation of the Dirac particles in the early universe goes by the processes

$$\psi\bar{\psi} \rightarrow Z', Z'' \rightarrow e^+e^-, \mu^+\mu^-, \nu_e\bar{\nu}_e, \nu_\mu\bar{\nu}_\mu, \quad (5.39)$$

which is to be contrasted with the processes Equation (5.15) in the  $U(1)_X$  model.

## 5.4 Relic Density in a Two Component Model

Here we discuss the relic density in models with two components. A general analysis requires solving the Boltzmann equations in a Friedmann-Robertson-Walker universe [42, 46, 88], and includes coannihilations [44] and an accurate integration over pole regions. As in the Minimal Supersymmetric Standard Model alone, one will generally encounter the  $Z$  and Higgs poles [46] and these need to be treated with care. The number changing processes include

$$\psi\bar{\psi} \leftrightarrow \text{SM SM}', \quad \psi\bar{\psi} \leftrightarrow \chi\chi, \quad \chi\chi \leftrightarrow \text{SM SM}'. \quad (5.40)$$

Note that the process  $\bar{\psi}\chi \leftrightarrow \text{SM SM}'$  is not allowed since  $\bar{\psi}\chi$  connect only to  $\phi$  and  $\phi'$ , neither of which can connect to the standard model particles. For the simplest two component model with dark matter particles  $\psi, \chi$ , with the assumption that  $M_\psi > M_\chi$  the only relevant processes in the annihilation of  $\psi\bar{\psi}$  are  $\psi\bar{\psi} \rightarrow f\bar{f}, \chi\chi$  final states. Since  $\psi$  is heavier than  $\chi$  its freeze-out occurs earlier (at a higher  $T$ ) than for  $\chi$ . Thus, the Boltzmann equations for  $n_\psi$  (which includes fermions and anti-fermions) and for  $n_\chi$  for the  $U(1)_X$  and for the  $U(1)_X \times U(1)_C$  two component models are given by

$$\frac{dn_\psi}{dt} = -3Hn_\psi - \frac{1}{2}\langle\sigma v\rangle_{\psi\bar{\psi}}(n_\psi^2 - n_{\psi,\text{eq}}^2), \quad (5.41)$$

$$\frac{dn_\chi}{dt} = -3Hn_\chi - \langle\sigma v\rangle_{\chi\chi}(n_\chi^2 - n_{\chi,\text{eq}}^2) + \frac{1}{2}\langle\sigma v\rangle_{\psi\bar{\psi}\rightarrow\chi\chi}(n_\psi^2 - n_{\psi,\text{eq}}^2). \quad (5.42)$$

Here  $\langle\sigma v\rangle_{\psi\bar{\psi}}$  refers to  $\psi\bar{\psi} \rightarrow f\bar{f}, \chi\chi$ , and  $\langle\sigma v\rangle_{\chi\chi}$  stands for  $\langle\sigma v\rangle_{\chi\chi\rightarrow\text{SM SM}'}$ . For the spin averaged cross section for the Dirac case, the extra factor of  $1/2$  is to account for the fact that we are dealing with a Dirac fermion. The number densities are  $n_\psi, n_\chi$

and  $n_{\psi,\text{eq}}, n_{\chi,\text{eq}}$  are their values at equilibrium, i.e.,

$$n_{(\psi,\chi),\text{eq}} \simeq \mathfrak{g}_{(\psi,\chi)} (M_{(\psi,\chi)} T / 2\pi)^{3/2} \exp\left(-\frac{M_{(\psi,\chi)}}{T}\right),$$

, where  $\mathfrak{g}_\psi = 4$  and  $\mathfrak{g}_\chi = 2$ . Since the two dark matter particles are sub-TeV in mass, they will freeze-out at temperatures that are not drastically different. One can solve the Boltzmann equation for  $\psi$  with the appropriate boundary conditions to compute the freeze-out temperature  $T_f^\psi$  and the relic density of  $\psi$  at the current temperatures. To compute the freeze-out temperature  $T_f^\chi$  for the particles  $\chi$ , one uses solutions for  $n_\psi$  as computed from the Boltzmann equation for  $\psi$  as input in the Boltzmann equation for  $\chi$  keeping in mind that  $n_{\psi,\text{eq}}$  in the  $\chi$  Boltzmann equation can be neglected since we are below the freeze-out temperature for  $\psi$ . It is difficult to get a closed form solution of Equation (5.42) for  $n_\chi$  and thus in general the analysis must be done numerically for  $\Omega_\chi h^2$ . However, it turns out that for both the  $U(1)_X$  and the  $U(1)_X \times U(1)_C$  models the contribution of the term proportional to  $n_\psi^2$  in Equation (5.42) is rather suppressed and it is a good approximation to neglect this term for both models. In this case, one has

$$(\Omega h^2)_{\text{WMAP}} = (\Omega_\psi h^2)_0 + (\Omega_\chi h^2)_0 \simeq \frac{C_\psi}{J_0^\psi} + \frac{C_\chi}{J_0^\chi}, \quad (5.43)$$

where

$$C_\chi \simeq \frac{1.07 \times 10^9 \text{ GeV}^{-1}}{\sqrt{\mathfrak{g}^*(\chi)} M_{\text{pl}}}, \quad C_\psi \simeq 2 \times \frac{1.07 \times 10^9 \text{ GeV}^{-1}}{\sqrt{\mathfrak{g}^*(\psi)} M_{\text{pl}}}, \quad (5.44)$$

$$J_0^\chi = \int_0^{x_f^\chi} \langle \sigma v \rangle_{\chi\chi} dx, \quad J_0^\psi = \int_0^{x_f^\psi} \langle \sigma v \rangle_{\psi\bar{\psi}} dx, \quad (5.45)$$

and where  $g^*(\psi, \chi)$  denotes the effective degrees of freedom at the freeze-out of  $\psi, \chi$  respectively. The analysis leading to Equation (5.41) and Equation (5.42) is easily extended to include coannihilations. The analysis can easily be reversed if the Majorana is heavier than the Dirac. Denoting  $\rho_{\odot, \psi}, \rho_{\odot, \chi}$  as the local density of each dark matter kind in the halo, one can assume

$$\rho_{\odot, \psi} / \rho_{\odot, \chi} \sim (\Omega_{\psi} h^2)_0 / (\Omega_{\chi} h^2)_0. \quad (5.46)$$

However, the ratios need not be the same. The local halo densities are also constrained such that  $\rho_{\odot, \psi} + \rho_{\odot, \chi} = \rho_{\odot, \text{total}} \simeq (0.35 - 0.45) \text{ GeVcm}^{-3}$ . For the calculation near the  $Z'$  pole we follow the techniques of [46]. Indeed the analytic techniques developed in [46] have been cross-checked with independent codes. For the  $U(1)_X$  model, the decay branching ratios are substantially less hadronic and more leptonic than for the annihilations via the  $Z$  boson exchange [89]. For the  $U(1)_X \times U(1)_C$  model the decays of the  $Z', Z''$  are purely leptonic. These leptophilic decay patterns for the extra  $Z'$ s help to explain the PAMELA positron excess without recourse to large *ad hoc* boost factors.

# Chapter 6

## Asymmetric Dark Matter in the MSSM

### 6.1 Introduction

In this chapter we will extend the asymmetric dark matter model of Chapter 3 to the MSSM. (The majority of this chapter comes directly from [22].) In extending the model to the MSSM the model will now have two dark matter particles, i.e. the lightest neutralino and the asymmetric dark matter. Let us quickly review asymmetric dark matter (AsyDM), which explains the cosmic coincidence, i.e., the apparent closeness of the amount of baryon asymmetry to the amount of dark matter in the Universe. The closeness of  $\Omega_{\text{DM}}h_0^2$  and  $\Omega_{\text{B}}h_0^2$  points to the possibility that the baryonic matter and dark matter may have a common origin. In the analysis within this chapter we will use a Stueckelberg  $U(1)$  extension of the minimal supersymmetric standard model (MSSM) [22, 69, 86]. Models explaining the cosmic coincidence have two main constraints in building models which is a mechanism for transferring a  $B - L$  asymmetry produced in the early universe to dark matter and a mechanism for depleting the symmetric component of dark matter generated via thermal pro-

cesses. Additionally, in the MSSM extension one needs to verify that the relic density of the lightest neutralino is also depleted.

As we did in Chapter 3, we will consider a  $U(1)_X$  extension of the Standard Model gauge group which is anomaly free and gauged under  $U(1)_X$ ,  $X = L_\mu - L_\tau$ . As is well-known, the MSSM supplemented by supergravity soft breaking gives the neutralino as the lowest supersymmetric particle and with  $R$  parity a candidate for dark matter. Thus for the AsyDM to work in the MSSM extensions it is necessary to have the neutralino as a subdominant component. This issue will be addressed. Also, when we study signatures at experiments for the direct detection of dark matter we will see that the subdominant component may still be detectable.

Much of the Standard Model analysis carried out in Section 3.2 is unchanged. The operator  $\mathcal{O}_{\text{asy}}$  in Equation (3.2) is now constructed of MSSM fields rather than just Standard Model fields. Here we will discuss two broad classes of models, i.e. the case where all of the sparticles are in the thermal bath at temperatures where the asymmetry transfer takes place and the case where the first two generations of squarks are heavy and are Boltzmann suppressed in the thermal bath. More explicitly, we will focus on the case when  $T_{\text{int}} > M_{\text{SUSY}}$  (Model E) where  $M_{\text{SUSY}}$  is the (largest) soft breaking mass. In this case all the sparticles will be in the plasma. The second case (Model F) corresponds to when the first two generations of sparticles (with mass  $M_1$ ) are heavy and drop out of the plasma (at some temperature  $T_1 < M_1$ ) while the third generation sparticles, the gauginos, the Higgses and the Higgsinos (with mass  $M_2 \ll M_1$ ) remain in the plasma. Thus for this case we have  $T_1 > T_{\text{int}} > M_2 > T_{\text{EWPT}}$ .

## 6.2 Analysis in supersymmetric framework

Since the supersymmetric case can have its own dark matter candidate, i.e., the neutralino, the relic abundance of the neutralino must be depleted. For this reason, we only consider the parameter space where relic density of the neutralino is much smaller than the WMAP value for cold dark matter (CDM) and is thus only a subdominant component. Below we discuss two regimes, one where  $T_{\text{int}} > M_{\text{SUSY}}$  and the other where  $T_1 > T_{\text{int}} > M_2 > T_{\text{EWPT}}$ .

### 6.2.1 $T > M_{\text{SUSY}}$

In this regime since the temperature is above the SUSY breaking scale all sparticle masses must be included in the  $\mu$  equations. This case is very similar to the discussion of  $T > T_{\text{EWPT}}$  in the Standard Model framework, except this time the particle spectrum includes all the Standard Model particles, the extra Higgses as well as the sparticles. For brevity we will use the same symbols for the chemical potentials, though now they stand for not only the Standard Model fields, but also their superpartners. The chemical potential equations obtained from Yukawa couplings and sphaleron processes remain the same. The only equation modified would be the hypercharge equation. The hypercharge of the Universe for the case when  $T > T_{\text{SUSY}}$  is given by

$$Y = 3 \times \left\{ 3 \times \left[ 2 \times 3 \times \frac{1}{3} \mu_q + 3 \times \frac{4}{3} \mu_u + 3 \times \left(-\frac{2}{3}\right) \mu_d + 2 \times (-1) \mu_L + (-2) \mu_e \right] + 2 \times (\mu_{H_u} - \mu_{H_d}) \right\}, \quad (6.1)$$

where the counting is similar to discussion in Chapter 3. The Higgs mixing term in the superpotential, i.e.,  $W = \mu H_u H_d$  indicates  $\mu_{H_u} + \mu_{H_d} = 0$ , and so we define  $\mu_H \equiv \mu_{H_u} = -\mu_{H_d}$ . Therefore, the hypercharge becomes

$$3\mu_q + 6\mu_u - 3\mu_d - 3\mu_L - 3\mu_e + 2\mu_H = 0. \quad (6.2)$$

Solving the chemical potential equations, we find that for Model E the total baryon and lepton numbers are given by

$$B_E = 3 \times 3 \times [2\mu_q + (\mu_u + \mu_d)] = -12\mu_L, \quad (6.3)$$

$$L_E = 3 \times 3 \times (2\mu_L + \mu_e) = \frac{153}{7}\mu_L, \quad (6.4)$$

so that  $(B - L)_E = -\frac{237}{7}\mu_L$ . Note that in the above equations, the extra factor of  $3 = 1 + 2$  (compare to the Standard Model case) takes into account the contributions of both fermions and bosons from the superfields, c.f. Equation (3.5).

### 6.2.2 $T_1 > T > M_2 > T_{\text{EWPT}}$

Here we consider two soft breaking mass scales  $M_1$  and  $M_2$  where  $M_1 \gg M_2$ . When temperature drops below  $T_1$ , all the sparticles with masses greater than  $M_1$  would drop out of the thermal bath. We assume that this is the case for the first two generations of squarks and sleptons. Similar to Model C, we simply assume here that these sparticles would drop out of the thermal bath at  $M_1 > T_1 > M_2$ . Thus the only sparticles remaining in the thermal bath are from the third generation, the gauginos, the Higgses and the Higgsinos. We make the approximation that these particles are relativistic at  $T_1 > T > M_2$ . This case is labeled Model F. Following the analysis of

Equation (6.2) we find that the vanishing of the hypercharge for Model F gives

$$5\mu_q + 10\mu_u - 5\mu_d - 5\mu_L - 5\mu_e + 6\mu_H = 0. \quad (6.5)$$

Solving the  $\mu$ -equations, we obtain

$$B_F = (3 \times 1 + 2) \times [2\mu_q + (\mu_u + \mu_d)] = -\frac{20}{3}\mu_L, \quad (6.6)$$

$$L_F = (3 \times 1 + 2) \times (2\mu_L + \mu_e) = \frac{485}{39}\mu_L, \quad (6.7)$$

and  $(B - L)_F = -\frac{745}{39}\mu_L$ .

### 6.2.3 The AsyDM mass: SUSY case

The supersymmetric interactions which transfer  $B - L$  asymmetry typically have a different form than the ones in the non-supersymmetric case. The most general interaction that transfers  $B - L$  to the dark sector for the MSSM case is

$$W_{\text{asy}} = \frac{1}{M_{\text{asy}}^n} X^k \mathcal{O}_{\text{asy}}^{\text{MSSM}}, \quad (6.8)$$

where the dark matter superfield  $X = (\phi_X, \psi_X)$  with  $\phi_X$  as the bosonic and  $\psi_X$  as the fermionic component. Now the following possibilities arise in terms of dark matter. First, after soft breaking if  $\phi_X$  and  $\psi_X$  have a similar mass, both of them are stable, and could be dark matter candidates. Next, consider the case where one of the components has a much larger mass than the other and would decay into the lighter one. In this case we have two possibilities: either  $\phi_X$  is heavier than  $\psi_X$  so that  $\phi_X \rightarrow \psi_X + \tilde{\chi}^{\text{St}}$  (where  $\tilde{\chi}^{\text{St}}$  is a Stueckelberg neutralino) in which case  $\psi_X$  is the dark matter candidate, or  $\psi_X$  is heavier than  $\phi_X$  so that  $\psi_X \rightarrow \phi_X + \tilde{\chi}^{\text{St}}$  in which

case  $\phi_X$  is the dark matter candidate (The possibility that either  $\tilde{\chi}^{\text{St}}$  or the MSSM neutralino is a dark matter candidate is discussed later in the chapter). For either of these three cases, when computing the total dark particle number from Equation (3.5), we need to multiply by an additional factor of 3, since both bosonic and fermionic components of the dark matter superfield would contribute. But for concreteness in our analysis we will assume that  $\psi_X$  is lighter than  $\phi_X$  and thus would be the asymmetric dark matter.

Applying the same method we used in Section 3.3.3, we find

$$m_{\text{DM}}^{\text{E}} \approx -\frac{11.11 \text{ GeV}}{Q_{B-L}^{\mathcal{O}^{\text{MSSM}}}}, \quad m_{\text{DM}}^{\text{F}} \approx -\frac{6.51 \text{ GeV}}{Q_{B-L}^{\mathcal{O}^{\text{MSSM}}}}. \quad (6.9)$$

Thus for the  $B - L$  transfer interactions with  $Q_{B-L}^{\mathcal{O}^{\text{MSSM}}} = -1$ , where  $\mathcal{O}_{\text{asy}}^{\text{MSSM}}$  can be  $LH_u$ ,  $LLe^c$ ,  $Lqd^c$ , or  $u^c d^c d^c$ , the dark particle masses are

$$m_X = 11.11 \text{ GeV} \quad \text{Model E}; \quad m_X = 6.51 \text{ GeV} \quad \text{Model F}. \quad (6.10)$$

For the case  $W_{\text{asy}} = \frac{1}{M_{\text{asy}}^3} X^2 (LH_u)^2$  with  $Q_{B-L}^{\mathcal{O}^{\text{MSSM}}} = -2$ , which we will discuss in Section 6.3, the dark particle masses are

$$m_X = 5.55 \text{ GeV} \quad \text{Model E}; \quad m_X = 3.25 \text{ GeV} \quad \text{Model F}, \quad (6.11)$$

and using Equation (3.3) one finds

$$M_{\text{asy}}^{\text{E}} \gtrsim 3.7 \times 10^5 \text{ GeV}. \quad (6.12)$$

### 6.3 Asymmetric dark matter in a Stueckelberg extension of the MSSM

The analysis of dark matter in the MSSM extension is more complex in that there are now three contributions to the dark matter relic density, i.e., from the asymmetric and symmetric components as in Equation (3.57) and from the neutralino. Thus here one has

$$\Omega_{\text{DM}} = \Omega_{\text{DM}}^{\text{asy}} + \Omega_{\text{DM}}^{\text{sym}} + \Omega_{\tilde{\chi}^0}, \quad (6.13)$$

where  $\Omega_{\tilde{\chi}^0}$  is the relic density from the neutralino. In this case for the asymmetric dark matter to work, one must significantly deplete not only the symmetric component of dark matter but also the contribution from the neutralino. Thus here we take the criterion that  $\Omega_{\text{DM}}^{\text{sym}} / \Omega_{\text{DM}} < 0.1$ , and  $\Omega_{\tilde{\chi}^0} / \Omega_{\text{DM}} < 0.1$ . For the analysis of AsyDM in extensions of MSSM we consider the interaction (in the superpotential)

$$W_{\text{asy}} = \frac{1}{M_{\text{asy}}^3} X^2 (LH_u)^2. \quad (6.14)$$

Here we note that the choice  $W_{\text{asy}} \sim X^2 LH_u$  would have allowed the decay  $\tilde{\chi}^0 \rightarrow XX\nu \dots$  and would have required the constraint  $m_{\tilde{\chi}^0} < 2m_X$  for the neutralino to be stable. Further, while the choices  $W_{\text{asy}} \sim X^2 LLe^c, X^2 Lqd^c$  do not allow the neutralino decay at the tree-level, such a decay can occur at the loop level since it is not forbidden by a symmetry. Additionally  $W_{\text{asy}} \sim X^3 LH_u, X^3 LLe^c, X^3 Lqd^c$  can also preserve the stability of the neutralino. Here and elsewhere we are assuming that the Stueckelberg neutralinos are heavier than the lightest neutralino in the MSSM sector. Returning to Equation (6.14), the corresponding dark particle masses are computed to be 5.55 GeV (Model E) and 3.25 GeV (Model F). Now the Stueckelberg extension

of MSSM, is more complex than the SM extension. We exhibit the relevant parts of this extension below.

For the Stueckelberg Lagrangian of the supersymmetric case we choose [29, 86]

$$\mathcal{L}_{\text{St}} = \int d\theta^2 d\bar{\theta}^2 [MC + S + \bar{S}]^2, \quad (6.15)$$

where  $C$  is the  $U(1)_C$  vector multiplet,  $S$  and  $\bar{S}$  are chiral multiplets, and  $M$  is a mass parameter. We define  $C$  in the Wess-Zumino gauge as  $C = -\theta\sigma^\mu\bar{\theta}C_\mu + i\theta\theta\bar{\theta}\bar{\lambda}_C - i\bar{\theta}\bar{\theta}\theta\lambda_C + \frac{1}{2}\theta\theta\bar{\theta}\bar{\theta}D_C$ , while  $S = \frac{1}{2}(\rho + ia) + \theta\chi + i\theta\sigma^\mu\bar{\theta}\frac{1}{2}(\partial_\mu\rho + i\partial_\mu a) + \theta\theta F + \frac{i}{2}\theta\theta\bar{\theta}\bar{\theta}\partial_\mu\chi + \frac{1}{8}\theta\theta\bar{\theta}\bar{\theta}(\square\rho + i\square a)$ . Its complex scalar component contains the axionic pseudo-scalar  $a$ , which is the analogue of the real pseudo-scalar that appears in the non-supersymmetric version in [28, 29, 86]. We write  $\mathcal{L}_{\text{St}}$  in component notation as

$$\mathcal{L}_{\text{St}} = -\frac{1}{2}(MC_\mu + \partial_\mu a)^2 - \frac{1}{2}(\partial_\mu\rho)^2 - i\chi\sigma^\mu\partial_\mu\bar{\chi} + 2|F|^2 + M\rho D_C + M\bar{\chi}\bar{\lambda}_C + M\chi\lambda_C. \quad (6.16)$$

For the gauge fields we add the kinetic terms

$$\mathcal{L}_{\text{gkin}} = -\frac{1}{4}C_{\mu\nu}C^{\mu\nu} - i\lambda_C\sigma^\mu\partial_\mu\bar{\lambda}_C + \frac{1}{2}D_C^2, \quad (6.17)$$

with  $C_{\mu\nu} \equiv \partial_\mu C_\nu - \partial_\nu C_\mu$ . For the matter fields (quarks, leptons, Higgs scalars, plus hidden sector matter) chiral superfields with components  $(f_i, z_i, F_i)$  are introduced and the matter Lagrangian is given by

$$\mathcal{L}_{\text{matt}} = -|D_\mu z_i|^2 - if_i\sigma^\mu D_\mu\bar{f}_i - \left(i\sqrt{2}g_C Q_C z_i \bar{f}_i \bar{\lambda}_C + \text{h.c.}\right) + g_C D_C(\bar{z}_i Q_C z_i) + |F_i|^2, \quad (6.18)$$

where  $(Q_C, g_C)$  are the charge operator and coupling constant of  $U(1)_C$ , and  $D_\mu = \partial_\mu + ig_C Q_C C_\mu$  is the gauge covariant derivative. It is convenient to replace the two-

component Weyl-spinors  $(\chi, \bar{\chi}), (\lambda_C, \bar{\lambda}_C)$  by four-component Majorana spinors, which we label as  $\psi_S = (\chi_\alpha, \bar{\chi}^{\dot{\alpha}})^T$ , and  $\lambda_C = (\lambda_{C\alpha}, \bar{\lambda}_C^{\dot{\alpha}})$ . The total Lagrangian of the MSSM then takes the form

$$\mathcal{L}_{\text{StMSSM}} = \mathcal{L}_{\text{MSSM}} + \mathcal{L}_{U(1)} + \Delta\mathcal{L}_{\text{St}}, \quad (6.19)$$

with

$$\begin{aligned} \Delta\mathcal{L}_{\text{St}} = & -\frac{1}{2}(MC_\mu + \partial_\mu a)^2 - \frac{1}{2}(\partial_\mu \rho)^2 - \frac{1}{2}M^2\rho^2 \\ & -\frac{i}{2}\bar{\psi}_S\gamma^\mu\partial_\mu\psi_S - \frac{1}{4}C_{\mu\nu}C^{\mu\nu} - \frac{i}{2}\bar{\lambda}_C\gamma^\mu\partial_\mu\lambda_C + M\bar{\psi}_S\lambda_C \\ & -\sum_i \left[ |D_\mu z_i|^2 - |D_\mu z_i|_{C_\mu=0}^2 + \rho g_C M(\bar{z}_i Q_C z_i) \right. \\ & \left. + \frac{1}{2}g_C C_\mu \bar{f}_i \gamma^\mu Q_C f_i + \sqrt{2}g_C (iz_i Q_C \bar{f}_i \lambda_C + \text{h.c.}) \right] \\ & -\frac{1}{2} \left[ g_C \sum_i \bar{z}_i Q_C z_i \right]^2. \end{aligned} \quad (6.20)$$

As in the SM case we assume that the  $U(1)_C$  is a gauged  $L_\mu - L_\tau$ . Further, we assume that all hidden sector fields while charged under  $U(1)_C$  are neutral under the MSSM gauge group and some of the MSSM particles, i.e., the second and the third generation leptons, are charged under  $U(1)_C$ . As discussed already an essential ingredient to explain the cosmic coincidence is that the symmetric component of dark matter produced in thermal processes is significantly depleted. For the MSSM Stueckelberg extension the analysis of annihilation is essentially identical to the case of the Stueckelberg extension of the Standard Model and we do not discuss it further.

We now discuss what happens to the extra particles that arise in the  $U(1)_C$  Stueckelberg extension of MSSM. This extension involves the following set of particles:  $Z', \rho, \psi, \phi, \psi_S, \lambda_C$ . The decay of the  $Z'$  has already been discussed (see Chapter 3). Next we consider the  $\rho$ . Equation (6.20) gives the interaction of the  $\rho$  with the sfermions.

Specifically its couplings to the mass diagonal sfermions are given by

$$\mathcal{L}_{\rho\tilde{f}^\dagger\tilde{f}} = -g_\rho M_\rho \left[ \cos(2\theta_{\tilde{f}_i}) \left( \tilde{f}_{1i}^\dagger \tilde{f}_{1i} - \tilde{f}_{2i}^\dagger \tilde{f}_{2i} \right) + \sin(2\theta_{\tilde{f}_i}) \left( \tilde{f}_{1i}^\dagger \tilde{f}_{2i} + \tilde{f}_{2i}^\dagger \tilde{f}_{1i} \right) \right], \quad (6.21)$$

where  $f_i$  refer to  $\mu, \nu_\mu, \tau, \nu_\tau$ . Thus the  $\rho$  will decay via second and third generation slepton loops into  $\mu^+ \mu^-, \nu_\mu \bar{\nu}_\mu, \tau^+ \tau^-, \nu_\tau, \bar{\nu}_\tau$  and disappear in the thermal bath quickly (see Section 6.4). Next we discuss the neutralino sector. Here in the  $U(1)_C$  Stueckelberg extension of MSSM the neutralino sector is enlarged in that one has two more fields, i.e., the gaugino, and the higgsino fields ( $\Psi_S, \Lambda_C$ ) as mentioned earlier. In this case the neutralino mass matrix of the  $U(1)_C$  extension of MSSM is given by

$$\mathcal{M}_{\text{neutralino}} = \left( \begin{array}{c|c} \mathcal{M}_{st} & 0_{2 \times 4} \\ \hline 0_{4 \times 2} & \mathcal{M}_{\text{MSSM}} \end{array} \right), \quad \mathcal{M}_{st} = \begin{pmatrix} 0 & M \\ M & \tilde{M} \end{pmatrix}, \quad (6.22)$$

where  $M_{st}$  is in the basis ( $\Psi_S, \Lambda_C$ ),  $M$  is the Stueckelberg mass and  $\tilde{M}$  is the soft mass. The neutralino mass eigenstates arising from Equation (6.22) can be labeled  $\tilde{\chi}_1^{\text{St}}, \tilde{\chi}_2^{\text{St}}$ . We consider the possibility that the Stueckelberg neutralinos are heavier than the LSP of the MSSM ( $\tilde{\chi}_1^0$ ) and decay into the MSSM neutralino which is assumed to be stable. In this case one will have more than one dark matter particle, i.e., the  $\psi$  from the Stueckelberg sector and  $\tilde{\chi}_1^0$  from the MSSM sector. Again in the case of AsyDM the relic density of  $\tilde{\chi}_1^0$  must be much smaller than the WMAP relic density for CDM. To this end we carry out an explicit analysis of the relic density within supergravity (SUGRA) grand unification [48, 65]. As shown in Figure 6.1 the relic density of  $\tilde{\chi}_1^0$  can be very small, which allows the dominant component of the dark matter observed today to be the asymmetric dark matter.

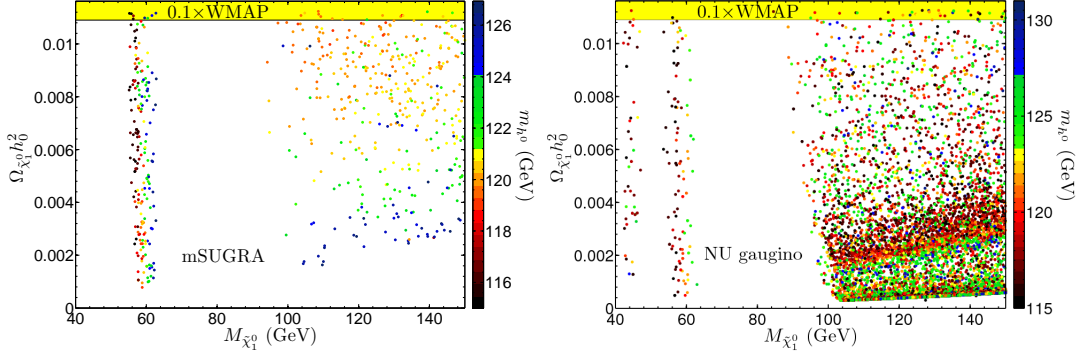


Figure 6.1: An exhibition of the depletion of the MSSM neutralino dark matter below 10% of the WMAP relic density for cold dark matter. Parameter points are displayed by their light CP even Higgs mass and the yellow band corresponds to 10% of the WMAP-7 observed limit. The left panel shows the parameter points of mSUGRA and the right panel shows the non-universal gaugino parameter points. All parameter points shown pass the general constraints.

## 6.4 Decay of the $\rho$

Here we compute the decay of the  $\rho$ . From Equation (6.21) one finds that  $\rho$  couples to smuons, staus, muon sneutrino, and tau sneutrino. This means that the  $\rho$  decay has  $\mu^+\mu^-$ ,  $\nu_\mu\bar{\nu}_\mu$ ,  $\tau^+\tau^-$ ,  $\nu_\tau\bar{\nu}_\tau$  final states which arise via the exchange of neutralinos and charginos in the loops (a generic diagram is shown in Figure 6.2). The amplitude of the generic diagram reads,

$$i\mathcal{M} = -ig_{\rho ij}C_{ki}C_{kj}^* \int \frac{d^4k}{(2\pi)^4} \bar{u}(p') \frac{(\not{k} - \not{p}) + m_{\tilde{\chi}_k}}{(k^2 - m_i^2)(k'^2 - m_j^2)((k-p)^2 - m_{\tilde{\chi}_k}^2)} v(p), \quad (6.23)$$

where  $k' = q - k$ ,  $m_i, m_j$  are the masses of the sleptons, and  $m_{\tilde{\chi}_k}$  is the mass of the neutralino or of the chargino in the loop, while  $g_{\rho ij}, C_{ki}$  are the couplings. Here we are only interested in estimating the size of the lifetime. Therefore, it is sufficient to estimate the contribution for one set of diagrams. Thus we consider the decay of the  $\rho$  to final states  $\mu^+\mu^-$  via the exchange of neutralinos. In this case we will

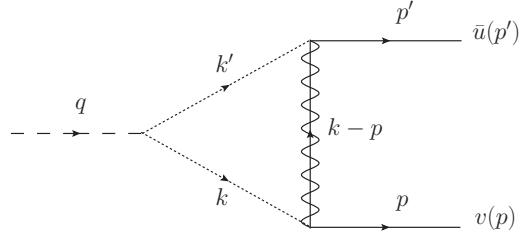


Figure 6.2: A generic diagram showing the decay of the  $\rho$  to one of the final states which could be  $\mu^+\mu^-$ ,  $\nu_\mu\bar{\nu}_\mu$ ,  $\tau^+\tau^-$ ,  $\nu_\tau\bar{\nu}_\tau$  via exchange of sleptons, charginos and neutralinos at one loop.

have the exchange of smuons and neutralinos in the loop. Further, we will ignore the mixing between the left and the right chiral smuons so that the mixing angle  $\theta_{\tilde{f}_i}$  in Equation (6.21) can be set to zero. In this circumstance the off-diagonal term involving two smuons in the loop does not contribute and the relevant loop integral takes the form

$$\frac{1}{(k^2 - m_i^2)(k'^2 - m_j^2)((k-p)^2 - m_{\tilde{\chi}_k}^2)} = \int_0^1 dx dy dz \delta(x+y+z-1) \frac{2}{D_{ik}^3}, \quad (6.24)$$

where  $D_{ik} = l^2 - \Delta_{ik} + i\epsilon$  in which  $l \equiv k - (yq + zp)$  and

$$\Delta_{ik} = (1-z)m_i^2 - xym_\rho^2 + zm_{\tilde{\chi}_k}^2 + (z^2 - z)m_\mu^2. \quad (6.25)$$

The masses in the loops are much larger than the muon mass and thus the muon mass can be ignored. The integration on  $l$  gives

$$i\mathcal{M} = \frac{-ig_{\rho ij}C_{ki}C_{ki}^*}{(4\pi)^2} \int_0^1 dx dy dz \delta(x+y+z-1) \frac{\bar{u}(p')m_{\tilde{\chi}_k}v(p)}{\Delta_{ik}}. \quad (6.26)$$

Further, an approximate evaluation of integration on the Feynman parameters gives

$$i\mathcal{M} = \frac{-ig_{\rho ii}C_{ki}C_{ki}^*}{(4\pi)^2}\bar{u}(p')\frac{m_{\tilde{\chi}_k}}{m_i^2}v(p), \quad (6.27)$$

under the assumption  $m_{\tilde{\chi}_k}^2/m_i^2 \ll 1$  and  $m_\rho^2/m_i^2 \ll 1$ . The decay width of  $\rho \rightarrow \mu^+\mu^-$  is then given by

$$d\Gamma = \frac{1}{2m_\rho} \int \frac{d^3\vec{p}}{(2\pi)^3 2E_{\mu^+}} \int \frac{d^3\vec{p}'}{(2\pi)^3 2E_{\mu^-}} |\sum i\mathcal{M}|^2 (2\pi)^4 \delta^{(4)}(q - p - p') = \frac{|\sum i\mathcal{M}|^2}{8\pi m_\rho}. \quad (6.28)$$

Next, note that  $g_{\rho 11} = -g_{\rho 22} = g_C Q_C m_\rho$  and thus

$$|\sum i\mathcal{M}|^2 \simeq \frac{(g_C Q_C)^2 m_\rho^4}{16\pi^4} \left| \sum_{k=1}^6 \sum_{i=1}^2 (-1)^{i+1} \frac{C_{ki}C_{ki}^*}{m_i^2} \right|^2. \quad (6.29)$$

A numerical estimate using Equation (6.28) and Equation (6.29) and the inputs  $m_1 = 1 \text{ TeV}$ ,  $m_2 \gg m_1$ ,  $m_\rho = 100 \text{ GeV}$ , the lightest neutralino mass of  $50 \text{ GeV}$  gives  $\tau_\rho = \hbar/\Gamma \sim 10^{-14 \pm 1} \text{ s}$ . Thus the decay of the  $\rho$  is very rapid.

# Chapter 7

## Early Search for SUSY at the LHC

### 7.1 Introduction

In this chapter we go over the early search potential for supersymmetry at the Large Hadron Collider. We start by studying the Standard Model background, then we explore the early reach potential of the LHC, and finally these results are compared to what ATLAS and CMS observed at  $\sqrt{s} = 7 \text{ TeV}$  and  $35 \text{ pb}^{-1}$  of data. The work for this chapter comes directly from [90, 91].

### 7.2 Standard Model Backgrounds at $\sqrt{s} = 7 \text{ TeV}$

One of the most important aspects to the discovery of new physics at the LHC is the understanding of the Standard Model (SM). The SM processes act as background in the channels used to search for new physics. Throughout the remainder of the analysis we will use the Standard Model background that was generated in [90]. This background was generated using MADGRAPH 4.4 [92] for parton level processes,

PYTHIA 6.4 [93] for hadronization, and PGS-4 for detector simulation [94]. Additionally, a MLM matching with a  $k_T$  jet clustering scheme was used to prevent double counting of final states. The result of our analysis is presented in Table 7.1 with parton level cuts as specified Equation (7.1) and in the caption of Table 7.1. The generation of the background implemented the CTEQ6L1 [95] parton distribution functions for the SM background, and a basic cut was applied such that all final state partons (except the top quarks) are required to have  $p_T > 40$  GeV.

$$\begin{aligned} \text{Cuts1} &= 40 \text{ GeV} < E_T(j_1) < 100 \text{ GeV}, \quad \text{Cuts2} = 100 \text{ GeV} < E_T(j_1) < 200 \text{ GeV}, \\ \text{Cuts3} &= 200 \text{ GeV} < E_T(j_1) < 500 \text{ GeV}, \quad \text{Cuts4} = 500 \text{ GeV} < E_T(j_1) < 3000 \text{ GeV} \\ &\text{Parton level cuts.} \end{aligned} \tag{7.1}$$

An important note for the Standard Model backgrounds, is an issue of double counting. When studying  $W + \bar{t}b$  ( $t\bar{b}$ ) processes there is a potential to double count such final states if one also considers  $t\bar{t}$  production processes. To prevent this double counting we have eliminated all diagrams involving a top quark from the set of diagrams that lead to  $W + \bar{t}b$  final states, with an analogous requirement for  $W + t\bar{b}$  production.

### 7.3 Sparticle production cross sections at $\sqrt{s} = 7$ TeV

Before studying the reach of the LHC it is beneficial to first look at the sparticle cross sections. As discussed earlier in mSUGRA, one has just four parameters and the sign of the Higgs mixing parameter  $\mu$ ; i.e., one has

$$m_0, m_{1/2}, A_0, \tan \beta, \text{sign}(\mu), \tag{7.2}$$

**A display of the processes analyzed and their Standard Model backgrounds at  
 $\sqrt{s} = 7 \text{ TeV}$**

SM process	Cross section (fb)	Number of events	Luminosity ( $\text{fb}^{-1}$ )
QCD 2,3,4 jets (Cuts1)	$2.0 \times 10^{10}$	74M	$3.7 \times 10^{-3}$
QCD 2,3,4 jets (Cuts2)	$7.0 \times 10^8$	98M	0.14
QCD 2,3,4 jets (Cuts3)	$4.6 \times 10^7$	40M	0.88
QCD 2,3,4 jets (Cuts4)	$3.9 \times 10^5$	1.7M	4.4
$t\bar{t} + 0,1,2$ jets	$1.6 \times 10^5$	4.8M	30
$b\bar{b} + 0,1,2$ jets	$9.5 \times 10^7$	95M	1.0
$Z/\gamma (\rightarrow \ell\bar{\ell}, \nu\bar{\nu}) + 0,1,2,3$ jets	$6.2 \times 10^6$	6.2M	1.0
$W^\pm (\rightarrow \ell\nu) + 0,1,2,3$ jets	$1.9 \times 10^7$	21M	1.1
$Z/\gamma (\rightarrow \ell\bar{\ell}, \nu\bar{\nu}) + t\bar{t} + 0,1,2$ jets	56	1.0M	$1.7 \times 10^4$
$Z/\gamma (\rightarrow \ell\bar{\ell}, \nu\bar{\nu}) + b\bar{b} + 0,1,2$ jets	$2.8 \times 10^3$	0.1M	36
$W^\pm (\rightarrow \ell\nu) + b\bar{b} + 0,1,2$ jets	$3.2 \times 10^3$	0.6M	$1.8 \times 10^2$
$W^\pm (\rightarrow \ell\nu) + t\bar{t} + 0,1,2$ jets	70	4.6M	$6.5 \times 10^4$
$W^\pm (\rightarrow \ell\nu) + t\bar{b} (\bar{t}b) + 0,1,2$ jets	$2.4 \times 10^2$	2.1M	$8.7 \times 10^3$
$t\bar{t}t\bar{t}$	0.5	0.09M	$1.8 \times 10^5$
$t\bar{t}b\bar{b}$	$1.2 \times 10^2$	0.32M	$2.7 \times 10^3$
$b\bar{b}b\bar{b}$	$2.2 \times 10^4$	0.22M	1.0
$W^\pm (\rightarrow \ell\nu) + W^\pm (\rightarrow \ell\nu)$	$2.0 \times 10^3$	0.05M	25
$W^\pm (\rightarrow \ell\nu) + Z (\rightarrow \text{all})$	$1.1 \times 10^3$	1.3M	$1.1 \times 10^3$
$Z (\rightarrow \text{all}) + Z (\rightarrow \text{all})$	$7.3 \times 10^2$	2.6M	$3.6 \times 10^3$
$\gamma + 1,2,3$ jets	$1.5 \times 10^7$	16M	1.1

Table 7.1: An exhibition of the Standard Model backgrounds computed in this work at  $\sqrt{s} = 7 \text{ TeV}$ . All processes were generated using MADGRAPH 4.4. Our notation here is that  $\ell = e, \mu, \tau$ , and  $\text{all} = \ell, \nu, \text{jets}$ . Cuts1-Cuts4 indicated in the table are defined in (7.1). In the background analysis we eliminate double counting between the process  $W^\pm + t\bar{b} (\bar{t}b)$  and  $t\bar{t}$  by subtracting out double resonant diagrams of  $t\bar{t}$  when calculating  $W^\pm + t\bar{b} (\bar{t}b)$ .

where  $m_0$  is the universal scalar mass,  $m_{1/2}$  is the universal gaugino mass,  $A_0$  is the coefficient of the trilinear coupling, and  $\tan \beta$  is the ratio of two Higgs vacuum expectation values in the MSSM.

In this framework, we choose parameter points that successfully impose REWSB, particle mass limits from LEP and the Tevatron, relic density constraints from WMAP [2],

the  $g_\mu - 2$  constraint [40], and flavor changing neutral current (FCNC) constraints from  $B_s \rightarrow \mu^+ \mu^-$  and  $b \rightarrow s + \gamma$ . For the analysis of just mSUGRA, we will only take into account a single component of dark matter, i.e. coming from the lightest neutralino. Additionally, we will take into account the errors in the theoretical computations and possible variations in the computation of the relic density using different codes, by taking a  $4\sigma$  range around the mean. In the literature there is some debate on the  $g_\mu - 2$  constraint, however the hadronic corrections [96] indicate a significant deviation ( $3.9\sigma$ ) between the Standard Model prediction and the experimentally measured value. Such a contribution can arise from supersymmetry [97] or a  $Z'$ .

For most of the analysis throughout this chapter and later chapters we will use the following constraints some of which have been updated since the original analysis has been done. For the FCNC process  $B_s \rightarrow \mu^+ \mu^-$  we take the constraint to be  $\mathcal{BR}(B_s \rightarrow \mu^+ \mu^-) < 5.8 \times 10^{-8}$  [39, 98] and for the branching ratio of the process  $b \rightarrow s\gamma$  we take the constraint to be  $\mathcal{BR}(b \rightarrow s\gamma) = (352 \pm 34) \times 10^{-6}$  [99, 100]. In addition to the above, LEP and Tevatron mass constraints on the sparticle masses and on the Higgs masses are applied. These are  $m_A > 85 \text{ GeV}$ ,  $m_{H^\pm} > 79.3 \text{ GeV}$ ,  $m_{\tilde{\tau}_1} > 101.5 \text{ GeV}$ , and  $m_{\tilde{\tau}_1} > 98.8 \text{ GeV}$  where  $A$  is the  $CP$ -odd Higgs and  $H^\pm$  is the charged Higgs. Further, we impose the lightest  $CP$ -even Higgs mass constraint [101]

$$m_h > \left( 93.5 + 15x + 54.3x^2 - 48.4x^3 - 25.7x^4 + 24.8x^5 - 0.5 \right) \text{ GeV} \quad (7.3)$$

where  $x = \sin^2(\beta - \alpha)$  and  $\alpha$  is the Higgs mixing angle. The final term in the bound represents a theoretical error of 0.5 GeV in the calculation of  $M_h$  and  $M_A$  assumed by the authors of Ref. [101]. Additionally we use the constraints  $m_{\chi_1^\pm} > 104.5 \text{ GeV}$  if  $|m_{\chi_1^\pm} - m_{\chi_1^0}| > 3 \text{ GeV}$  for the chargino mass and  $m_{\tilde{g}} > 309 \text{ GeV}$  for the gluino mass

### Sparticle Production Cross Sections of mSUGRA at $\sqrt{s} = 7 \text{ TeV}$

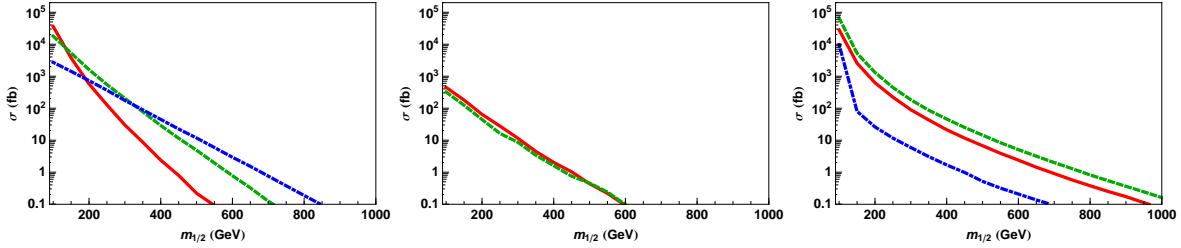


Figure 7.1: An exhibition of the sparticle production cross sections at the LHC at  $\sqrt{s} = 7 \text{ TeV}$  for mSUGRA as a function of the universal gaugino mass  $m_{1/2}$  at the GUT scale when  $m_0 = 500 \text{ GeV}$ ,  $A_0 = 0$ ,  $\tan \beta = 20$  and  $\text{sign}(\mu) = +1$ . Left panel: production cross sections of  $\tilde{g}\tilde{g}$ ,  $\tilde{g}\tilde{q}$ ,  $\tilde{q}\tilde{q}$  (solid red, dashed green, dashed blue lines). Middle panel: production cross sections for  $\tilde{g}\chi^\pm$ ,  $\tilde{g}\chi^0$  (solid red, dashed green lines). Right panel: production cross sections for  $\chi^\pm\chi^\pm$ ,  $\chi^\pm\chi^0$ ,  $\chi^0\chi^0$  (solid red, dashed green, dashed blue lines).

[39]. In the analysis we use a top (pole) mass of  $m_t = 173.1 \text{ GeV}$ .

The next question that is of interest is how large do we expect the sparticle cross sections to be at the LHC with  $\sqrt{s} = 7 \text{ TeV}$ . To do this we generate parameter points using MICRMEGAs [102] and SUSPECT [103] and apply the above mentioned constraints. These (successful) parameter points are then simulated in PYTHIA to determine their cross section at the LHC with  $\sqrt{s} = 7 \text{ TeV}$ . The cross sections for sparticle production processes in mSUGRA are shown in Figure 7.1. The figures were made by generating 5K events for multiple  $m_{1/2}$  values where the other parameters are taken to be  $m_0 = 500 \text{ GeV}$ ,  $A_0 = 0$ ,  $\tan \beta = 20$ , and  $\mu > 0$ . The left panel gives the cross sections for the production of  $\tilde{g}\tilde{g}$  (solid red line),  $\tilde{g}\tilde{q}$  (dashed green line),  $\tilde{q}\tilde{q}$  (dashed blue line) as a function of  $m_{1/2}$ . The middle panel gives the cross sections for the production of  $\tilde{g}\chi^\pm$  (solid red line),  $\tilde{g}\chi^0$  (dashed green line), and the right panel gives the production cross section for  $\chi^\pm\chi^\pm$  (solid red line),  $\chi^\pm\chi^0$  (dashed green line),  $\chi^0\chi^0$  (dashed blue line). The analysis of Figure 7.1 shows that these cross sections to be significant, indicating that at low mass scales as many as  $10^4$  or more SUSY events

will be generated with  $1 \text{ fb}^{-1}$  of integrated luminosity at the LHC. With the LHC finding a Higgs of  $\sim 126 \text{ GeV}$  [4–8] this above scenario with  $m_0$  low and  $A_0 = 0$  has been ruled out.

This analysis can also be extended to the case of non-universalities in the gaugino mass sector and this case is given in Figure 7.2, where contour plots are given in the  $m_{\tilde{g}} - m_{\chi^\pm}$  mass plane with other parameters as stated in the caption of the figure. The plots display contours of constant  $\log(\sigma_{\text{SUSY}}/\text{fb})$  in the range 1 – 3.5. These plots indicate that a chargino mass up to about 500 GeV and a gluino mass up to roughly 1 TeV would give up to  $10^3$  or more events with  $1 \text{ fb}^{-1}$  of integrated luminosity.

## 7.4 Signature Analysis and SUSY Discovery Reach at

$$\sqrt{s} = 7 \text{ TeV and } 1 \text{ fb}^{-1}$$

The next question to consider is in the first round of data what is expected for the LHC to exclude at  $\sqrt{s} = 7 \text{ TeV}$ . To do this we simulate models at the LHC in a detector simulation with no trigger imposed (L0). Once the models have been simulated we run them through the cuts given in [90]. These cuts are on the combination of multi-jets,  $b$ -tagged jets, multi-leptons, jets and leptons, and photons. The cuts were chosen to reduce the Standard Model background and enhance the SUSY signal with and without missing energy. Figure 7.3 gives the reach of the LHC for its early runs at  $\sqrt{s} = 7 \text{ TeV}$  for mSUGRA in the  $m_{1/2} - m_0$  plane. To rule out models we use the criteria that a signal,  $S$  would be observables if  $S > \max(5\sqrt{B}, 10)$  where  $B$  is the events comings from the Standard Model background. The reach shows that the LHC can probe mSUGRA models up to about 400 GeV for  $m_{1/2}$  at low values of  $m_0$  and up to about 2 TeV for  $m_0$  for low values of  $m_{1/2}$  with  $1 \text{ fb}^{-1}$  of integrated lumi-

## Contours of $\sigma_{SUSY}$ in the $m_{\tilde{g}} - m_{\tilde{\chi}^\pm}$ mass plane at $\sqrt{s} = 7$ TeV

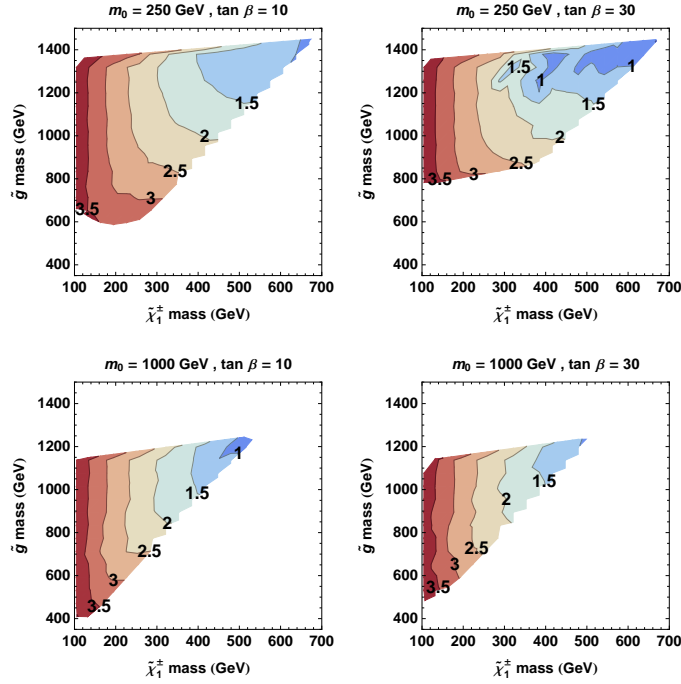


Figure 7.2: Contour plots with constant values of  $\log(\sigma_{SUSY}/\text{fb})$  for  $\sigma_{SUSY}$  in  $m_{\tilde{g}} - m_{\tilde{\chi}^\pm}$  mass plane for the case with nonuniversalities in the gaugino sector. Gaugino masses  $m_1, m_2,$  and  $m_3$  vary up to 1 TeV. First panel from left:  $m_0 = 250$  GeV,  $\tan \beta = 10$  while  $A_0 = 0, \text{sign}(\mu)=+1$ ; second panel from left:  $m_0 = 250$  GeV,  $\tan \beta = 30$ ; third panel from left:  $m_0 = 1000$  GeV,  $\tan \beta = 10$ ; fourth panel from left:  $m_0 = 1000$  GeV,  $\tan \beta = 30$ .

osity, and up to about 450 GeV for  $2 \text{ fb}^{-1}$  of data, and for  $m_0$  the reach can extend up to 1.9 (2) TeV for 1 (2)  $\text{fb}^{-1}$  of integrated luminosity.

## 7.5 LHC Reach with $35 \text{ pb}^{-1}$ of Data

During the time of this graduate work, the ATLAS collaboration released two analyses, one with 1 lepton [104] and the other with 0 leptons [105]. For the 1 lepton analysis we follow the selection requirements that ATLAS reports in [104], which include

Reach Plot at  $\sqrt{s} = 7 \text{ TeV}$  up to  $2 \text{ fb}^{-1}$  of Integrated Luminosity.

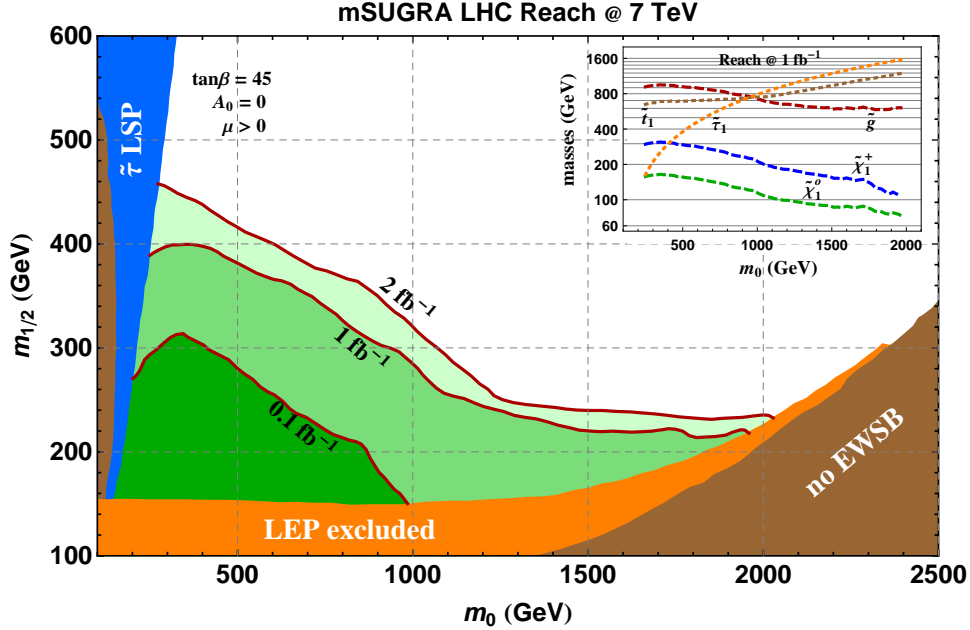


Figure 7.3: A reach plot for mSUGRA using the Standard Model backgrounds given in Table 7.1 at the LHC with  $\sqrt{s} = 7 \text{ TeV}$  with  $1 \text{ fb}^{-1}$  of integrated luminosity. The mSUGRA parameters used are  $A_0 = 0$ ,  $\tan \beta = 45$ ,  $\text{sign}(\mu) = 1$ . The condition used for a signal to be observable is  $S > \max(5\sqrt{B}, 10)$  where  $B$  stands for the Standard Model background. Early LHC reaches at  $1 \text{ fb}^{-1}$  for the gluino ( $\tilde{g}$ ), the chargino ( $\tilde{\chi}_1^\pm$ ), the neutralino ( $\tilde{\chi}_1^0$ ), the stau ( $\tilde{\tau}_1$ ), and the stop ( $\tilde{t}_1$ ) are exhibited in the inset where the  $y$ -axis is plotted on a logarithmic scale.

the preselection requirements for events having a jet with  $p_T > 20 \text{ GeV}$  and  $|\eta| < 2.5$ , electrons having  $p_T > 20 \text{ GeV}$  and  $|\eta| < 2.47$  and muons having  $p_T > 20 \text{ GeV}$  and  $|\eta| < 2.4$ . Further, we veto the “medium” electrons<sup>1</sup> in the electromagnetic calorimeter transition region,  $1.37 < |\eta| < 1.52$ . An event is considered if it has a single lepton with  $p_T > 20 \text{ GeV}$  and its three hardest jets have  $p_T > 30 \text{ GeV}$ , with the leading jet having  $p_T > 60 \text{ GeV}$ . The distance,  $\Delta R = \sqrt{(\Delta\eta)^2 + (\Delta\phi)^2}$ , between each jet with the lepton must satisfy  $\Delta R(j_i, \ell) > 0.4$ , and events are rejected if the reconstructed missing energy,  $\cancel{E}_T$ , points in the direction of any of the three leading jets,

<sup>1</sup>See [106] for a definition of “loose”, “medium” and “tight” electrons

$\Delta\phi(j_i, \cancel{E}_T) > 0.2$ . Events are then classified into 2 channels, depending on whether the lepton is a muon or an electron. These are then further classified into four regions based on the missing energy and  $m_T$  cuts, where we reconstruct the missing transverse momentum using the selected lepton plus jets with  $p_T > 20 \text{ GeV}$  and  $|\eta| < 4.9$  following ATLAS analysis, and  $m_T = \sqrt{2p_T(\ell) \cancel{E}_T (1 - \cos(\Delta\phi(\ell, \cancel{E}_T)))}$  is the transverse mass between the lepton and the missing transverse momentum vector. The four regions alluded to above are labeled the “signal region”, the “top region”, the “W region” and the “QCD region”. For the “signal region” events were required to pass the additional cuts of  $m_T > 100 \text{ GeV}$ ,  $\cancel{E}_T > 125 \text{ GeV}$ ,  $\cancel{E}_T > 0.25m_{\text{eff}}$  and  $m_{\text{eff}} > 500 \text{ GeV}$ . Here the effective mass,  $m_{\text{eff}}$ , is the scalar sum of the missing energy with the  $p_T$ 's of the selected visible objects (in this case the lepton and the 3 jets). The number of events were then compared to the 95% CL upper bounds that ATLAS found ( $N_e < 2.2$  events and  $N_\mu < 2.5$  events) [104]. The “top region” and “W region” are defined by events with  $30 \text{ GeV} < \cancel{E}_T < 80 \text{ GeV}$  and  $40 \text{ GeV} < m_T < 80 \text{ GeV}$ , where the “top region” requires at least one of the three hardest jets to be  $b$ -tagged and the “W region” requires none of the three hardest jets to be  $b$ -tagged. The “QCD region” was required to have  $m_T, \cancel{E}_T < 40 \text{ GeV}$  and was purely data driven. For our analysis events were rejected if they contaminated the three control regions. Using the Standard Model background from [90] we reproduced the ATLAS results.

For the 0 lepton analysis we follow the selection requirements that ATLAS reports in [105] where the preselection is the same as for the 1 lepton case except that leptons are identified to have  $p_T > 10 \text{ GeV}$ . Here the events are classified into 4 regions “A”, “B”, “C” and “D”; where regions A and B have at least 2 jets and regions C and D have at least 3 jets. When referring to different cuts in these regions we define cuts on the “selected” jets to mean that the minimum number of jets in this region must satisfy the following requirement: For regions A and B “selected” jets mean that they are

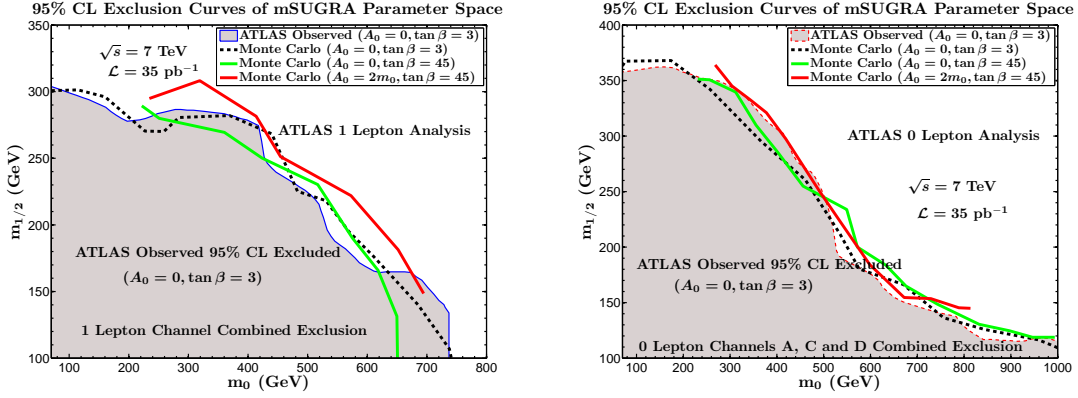


Figure 7.4: Left: Reach plot with  $35 \text{ pb}^{-1}$  of integrated luminosity using the ATLAS cuts discussed in the text with different  $\tan \beta$  and  $A_0$ :  $A_0 = 0$  and  $\tan \beta = 3$  (dashed line);  $A_0 = 0$  and  $\tan \beta = 45$  (solid green line);  $A_0 = 2m_0$  and  $\tan \beta = 45$  (solid red line). For comparison we give the ATLAS observed limit ( $A_0 = 0$  and  $\tan \beta = 3$ ) (solid blue line). Right: Reach plot with  $35 \text{ pb}^{-1}$  of integrated luminosity of data using the ATLAS 0 lepton cuts. For comparison we give the ATLAS observed limit (red dashed line).

the first two hardest jets and for regions C and D “selected” jets mean that they are the three hardest jets. Events are required to have  $\cancel{E}_T > 100 \text{ GeV}$  and the selected jets must each have  $p_T > 40 \text{ GeV}$  with the leading jet  $p_T > 120 \text{ GeV}$ . As in the case with 1 lepton, events are rejected if the missing energy points in the direction of any of the selected jets,  $\Delta\phi(j_i, \cancel{E}_T) > 0.4$ , where  $i$  is over the selected jets. Region A requires events to have  $\cancel{E}_T > 0.3m_{\text{eff}}$  and  $m_{\text{eff}} > 500 \text{ GeV}$  and regions C and D require events to have  $\cancel{E}_T > 0.25m_{\text{eff}}$  with region C requiring  $m_{\text{eff}} > 500 \text{ GeV}$  and region D requiring  $m_{\text{eff}} > 1 \text{ TeV}$ . In this case  $m_{\text{eff}}$  is defined in terms of selected jets, i.e. for regions A and B it is the scalar sum of the first two hardest jets and for regions C and D it is the scalar sum of the first three hardest jets. For the analysis here we do not apply the cut for region B, i.e.  $m_{T2} > 300 \text{ GeV}$ , since the models excluded in this region are already excluded in region D (see online webpage for [105]).

Following the framework of the ATLAS Collaboration [104] a set of three parameter sweeps in the  $m_0 - m_{1/2}$  plane taking  $m_{1/2} \leq 500 \text{ GeV}$  and  $m_0 \leq 1 \text{ TeV}$  was

carried out. Two of the parameter sweeps were a  $10 \text{ GeV} \times 10 \text{ GeV}$  grid scan in the  $m_0 - m_{1/2}$  plane having a fixed universal trilinear parameter,  $A_0 = 0$ , and fixed  $\tan \beta$ ; one set with  $\tan \beta = 3$  and the other with  $\tan \beta = 45$ . A third parameter scan was done with  $A_0 = 2m_0$  and  $\tan \beta = 45$ . Throughout the analysis we take  $\mu > 0$  and  $m_{\text{top}}^{\text{pole}} = 173.1 \text{ GeV}$ . A comparison of our reach to the reach done by the ATLAS Collaboration is shown in Figure 7.4.

Figure 7.5 exhibits the number of signal events for electrons in the  $m_0 - m_{1/2}$  plane where the reach plot from ATLAS is also exhibited and where the ATLAS reach plot corresponds to the number of observed events and those that have a larger number predicted by the model. For the 1 lepton analysis, we first present the models excluded by the muon channel, colored by  $N_{\text{events}}^{\mu}$  (indicated by squares). Next, the remaining models are overlaid with those that have been excluded by the electron channel, and colored by  $N_{\text{events}}^e$  (indicated by diamonds). Similarly for the 0 lepton analysis, we begin with models excluded by channel A, colored by  $N_{\text{events}}^A$  (indicated by squares); overlay models excluded by C (but not A) and colored by  $N_{\text{events}}^C$  (indicated by diamonds). Next, models excluded by channel D alone are overlaid in a single color (stars), as  $N_{\text{events}}^D$  are not comparable with  $N_{\text{events}}^A$  or  $N_{\text{events}}^C$ . Also shown are the number of signal events for electrons in the  $m_{\tilde{g}} - m_{\tilde{q}}$  plane. An ATLAS reach curve is also exhibited.

The upper left panel of Figure 7.5) gives a more quantitative description of the electron and muon channels in putting constraints on the  $m_0 - m_{1/2}$  parameter space with  $35 \text{ pb}^{-1}$  of data. As expected the largest number of single  $e$  and  $\mu$  events arise at low mass scales, i.e., for low values of  $m_0$  and of  $m_{1/2}$  and the number of signal events decrease and we approach the boundary after which they fall below 2 for the 1 lepton ATLAS analysis. It is also instructive to examine the signal events in the

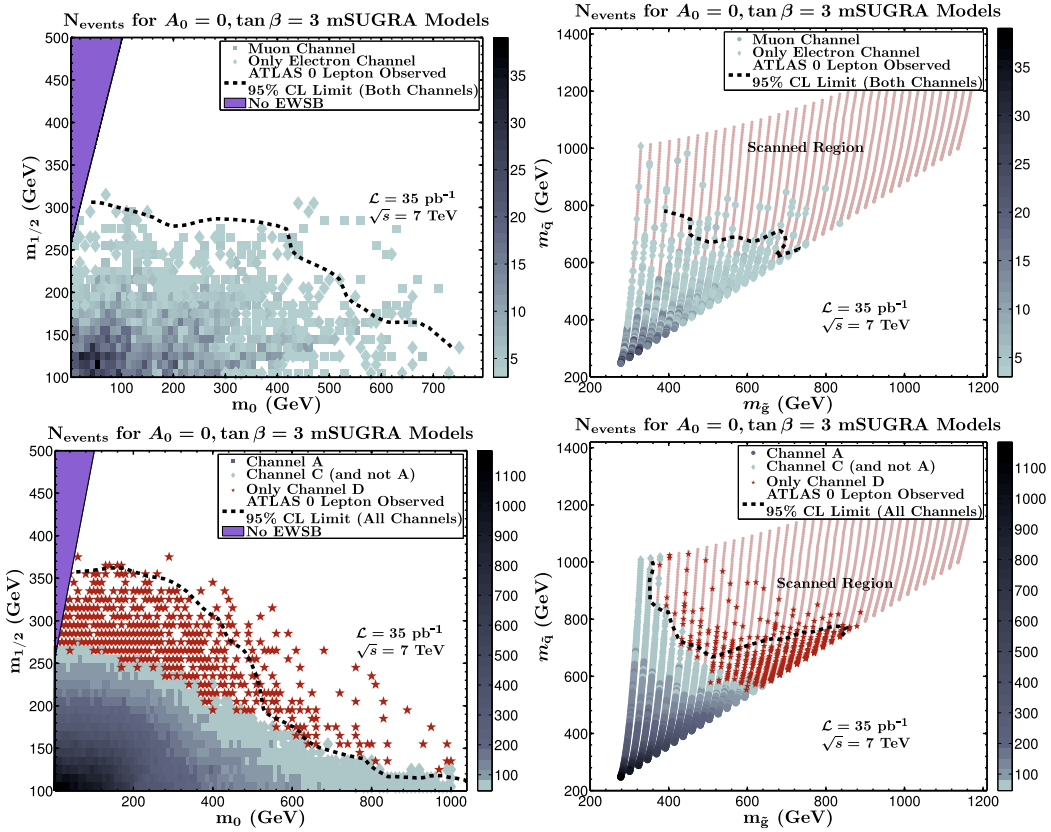


Figure 7.5: Top left panel: Number of signal events in the  $m_0 - m_{1/2}$  plane for the case  $A_0 = 0, \tan \beta = 3$  using the 1 lepton ATLAS cuts in the  $m_0 - m_{1/2}$  plane. The dark areas correspond to number of events greater than 2 with the actual numbers indicated along the vertical line to the right while the white areas are filled with models but have number of events smaller than 2. Top right panel: Same as the left panel except that the plot is  $m_{\tilde{g}}$  (gluino) –  $m_{\tilde{q}}$  (squark) mass plane for the lightest squark of the first 2 generations. The square region in the left panel becomes squeezed into the polygon-like region in the physical mass plane in the right panel. One may note that the ATLAS constraints do not rule out a low mass gluino on the scale of order 400 GeV for heavy squarks. Bottom left panel: The same as the top left panel except that the analysis is done using 0 lepton ATLAS cuts. Bottom right panel: Same as the top right panel except that the analysis is done using the 0 lepton ATLAS cuts. The (red) stars correspond to channel D. In channel D we find maximally 51 events over the space scanned after a requirement that the number of events be at least 15 before cuts. However, when only considering models not already excluded by channels A and C, the number of events in channel D is maximally 18.

gluino-squark mass plane where the squark mass corresponds to the average first two generation squark mass. This is done in the upper right panel of Figure 7.5. Here

the polygon shape of the region is a simple mapping of the allowed parameter in the  $m_0 - m_{1/2}$  plane of the upper left panel. The plot is useful as it directly correlates squark and gluino model points that are either excluded or allowed by the 1 lepton ATLAS analysis. The 0 lepton analysis of the lower panels in Figure 7.5 is very similar to the analysis of the upper panels except for different array of cuts. There is a general consistency in the analysis of the 1 lepton and the 0 lepton analysis, although the 0 lepton cuts appear more constraining as they appear to exclude a somewhat larger region of the parameter space. Together the analysis of the upper and lower panels of Figure 7.5 gives a more analytical understanding of the relative strengths of the 1 lepton and 0 lepton cuts.

## 7.6 Implications of The Early LHC Constraints

In the analysis of the ATLAS and CMS reach plots experimental constraints were not imposed beyond those that arise from the ATLAS analyses. What if these constraints were included? For this portion of the analysis all four parameters ( $m_0, m_{1/2}, A_0, \tan \beta$ ) are allowed to vary. In doing so, various constraints from searches on the sparticle mass limits, B-physics and from  $g_\mu - 2$  are applied. Next the constraint from upper bound on the relic density from WMAP only are explored, and then with combination of all of the above is considered. These constraints are done as discussed earlier. In the upper left panel of Figure 7.6 the following "collider/ flavor constraints" [39] are applied  $m_h > 93.5 \text{ GeV}$ ,  $m_{\tilde{\tau}_1} > 81.9 \text{ GeV}$ ,  $m_{\tilde{\chi}_1^\pm} > 103.5 \text{ GeV}$ , and  $m_{\tilde{t}_1} > 100 \text{ GeV}$ , along with  $(-11.4 \times 10^{-10}) \leq \delta(g_\mu - 2) \leq (9.4 \times 10^{-9})$ , see [40],  $Br(B_s \rightarrow \mu^+ \mu^-) \leq 4.7 \times 10^{-8}$  (90 % C.L.) [99], and  $(2.77 \times 10^{-4}) \leq Br(b \rightarrow s\gamma) \leq (4.27 \times 10^{-4})$  [98]. These collider/ flavor constraints by themselves have an effect, but the effect is quite small in terms of reducing the density of models that are al-

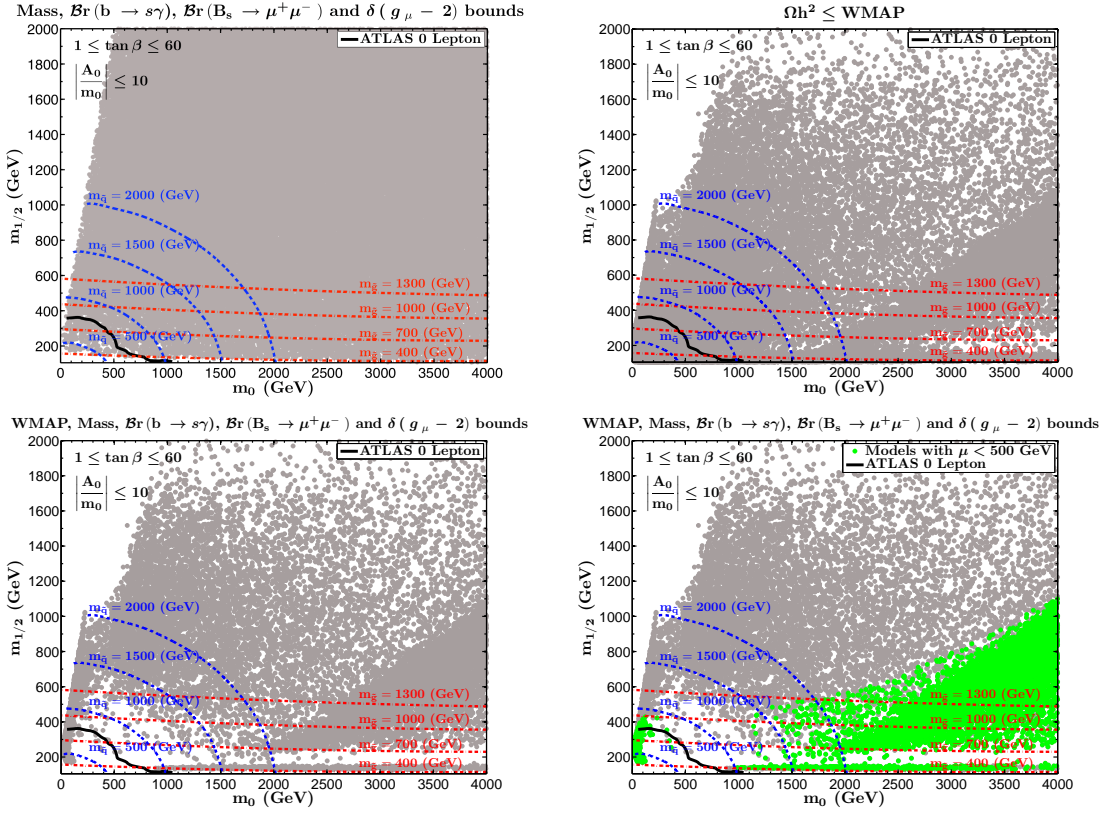


Figure 7.6: Upper left panel: An exhibition of the allowed models indicated by grey (dark) dots in the  $m_0 - m_{1/2}$  plane when only flavor and collider constraints are imposed. The region excluded by ATLAS (as well as CMS) lies below the thick black curve in the left hand corner. Upper right panel: same as the left upper panel except that only an upper bound on relic density of  $\Omega h^2 \leq 0.14$  is imposed. Lower left panel: Same as the upper left panel except that the relic density constraint as in the upper right panel is also applied. This panel exhibits that most of the parameter space excluded by ATLAS is already excluded by the collider/ flavor and relic density constraints. The dark region below the ATLAS curve is the extra region excluded by ATLAS which was not previously excluded by the indirect constraints. Lower right panel: The analysis of this figure is similar to the lower left panel except that models with  $|\mu| < 500$  GeV are exhibited in green.

ready constrained by the ATLAS results.

It is important to note that our scans of the parameter are very dense with  $10^6$  models after EWSB alone. In the  $m_0 - m_{1/2}$  plane the collider/ flavor cuts eliminate 12% of the models. However because  $A_0$  and  $\tan \beta$  are not fixed to specific values, but

are allowed to run over their full natural ranges, a model point which is eliminated for say, large  $\tan \beta$  by  $b \rightarrow s\gamma$  or  $B_s \rightarrow \mu^+\mu^-$  at a specific point in the  $m_0 - m_{1/2}$  plane can correspond to a model point with a smaller value of  $\tan \beta$  for the same  $(m_0, m_{1/2})$  which is not eliminated. Thus the  $m_0 - m_{1/2}$  plane appears densely filled. This is contrary to what one would observe for fixed values of  $(A_0, \tan \beta)$ . For example, for  $(A_0, \tan \beta) = (0, 45)$  the  $b \rightarrow s\gamma$  constraint would remove models at large  $m_0$  up to close to 2 TeV and  $m_{1/2}$  up to about 750 GeV. As another example, for  $(A_0, \tan \beta) = (0, 3)$  (the space looked at by ATLAS, and in the previous section) a strict limit of  $m_h < 102$  GeV for light CP even Higgs removes all model points below the ATLAS limits. However because one is varying  $(A_0, \tan \beta)$  the area below the ATLAS limit is filled in this case.

Next consider the “cosmological constraint” in the upper right panel of Figure 7.6 where we apply only an upper bound on the relic density of the thermally produced neutralino dark matter of  $\Omega h^2$  below the  $4\sigma$  upperbound. The WMAP upper bound constraint removes 96.5% of the models alone, thus this cosmological constraint is very severe eliminating a large fraction of models, but again the ATLAS constraints remain quite strong.

Next consider the “combined collider/ flavor and cosmological constraints” and notice that together these constraints are generally much more severe than the ATLAS constraints. This is shown in the lower left panel of Figure 7.6. Here models that were separately allowed by previously known collider/ flavor constraints, and models that were separately allowed by just the upper bound from WMAP, are now eliminated under the imposition of the combined constraints. There is, however, a new region that ATLAS appears to exclude above and beyond what the indirect constraints exclude and this region is a region for low  $m_0$  and for  $m_{1/2}$  around 350 GeV.

Thus it would require a larger integrated luminosity to move past the barren region, which is above the ATLAS bound, to get into the fertile region of the parameter space, where the fertile region is the area above the white patch in the lower panel of Figure 7.6.

Finally exhibited in the lower right panel of Figure 7.6 is the value of  $\mu$  (at the electroweak symmetry breaking scale) in the  $m_{1/2} - m_0$  plane where  $\mu$  is the Higgsino mass parameter that enters in the Higgs bilinear term in the superpotential. The analysis is given under the “combined constraints” discussed in the lower left panel of Figure 7.6. It is important to note that essentially all of the natural region of the parameter space corresponding to small  $\mu$ , most of which lies close to the hyperbolic branch (Focus point) (HB/FP) [107–112] of radiative breaking of the electroweak symmetry or near the vicinity of the light  $CP$ -even Higgs pole region [46] remains untouched by the CMS and LHC exclusion limits as illustrated in the lower right panel of Figure 7.6 and remains to be explored. Further, as pointed out in [113], low mass gluinos as low as even 420 GeV in mSUGRA are allowed for the region for large  $m_0$  where relic density can be satisfied on the light  $CP$ -even Higgs pole [46]. This can be seen from Figure 7.6 as the gluino and squark masses are exhibited in the plots. Along the Higgs pole region, electroweak symmetry breaking can also be natural, i.e., one has a small  $\mu$ . It is also seen that this region is not constrained by CMS and ATLAS since their limits taper off at large  $m_0$  as  $m_{\text{squark}}$  gets heavy and the jets from squark production are depleted (see [113]).

# Chapter 8

## Signatures

In this chapter we will consider signatures and discoverable modes of the earlier discussed topics.

### 8.1 Asymmetric Dark Matter Signatures at Colliders

Much of this section comes directly from [22]. The AsyDM models discussed in the earlier chapters can produce a dramatic signature at a muon collider, see Figure 8.1, which will be discussed now. This signature arises from a  $Z'$  resonance. It is worth noting that the  $Z'$  boson has no couplings with the first generation leptons and thus a process such as  $e^+e^- \rightarrow Z' \rightarrow \mu^+\mu^-, \tau^+\tau^-$  is absent at the tree-level. This process can only arise at the loop level which, however, is suppressed relative to the tree. This explains why such a resonance has not been observed yet at an  $e^+e^-$  collider (see Section 8.1.1). However, dramatic signals will arise at a muon collider where we

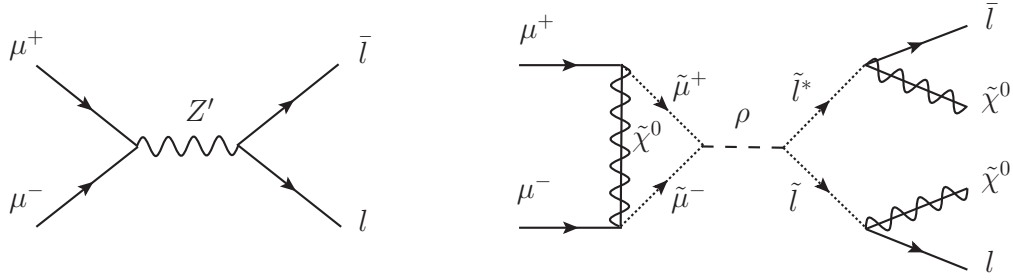


Figure 8.1: Left: Leptonic final states in a  $\mu^+\mu^-$  collider where the  $\mu^+\mu^- \rightarrow \bar{l}l$ , with  $l = \mu, \nu_\mu, \tau, \nu_\tau$ , final state arising from direct channel poles involving  $Z'$ . The  $Z'$  pole does not allow for a  $e^+e^-$  final state and thus the relative production cross section for  $\mu^+\mu^- \rightarrow \tau^+\tau^-$  vs  $\mu^+\mu^- \rightarrow e^+e^-$  can be used to detect the existence of a  $L_\mu - L_\tau$  gauged boson. Right: A similar analysis is possible for  $\rho$  but its production is suppressed relative to  $Z'$  since it must be produced at the loop level.

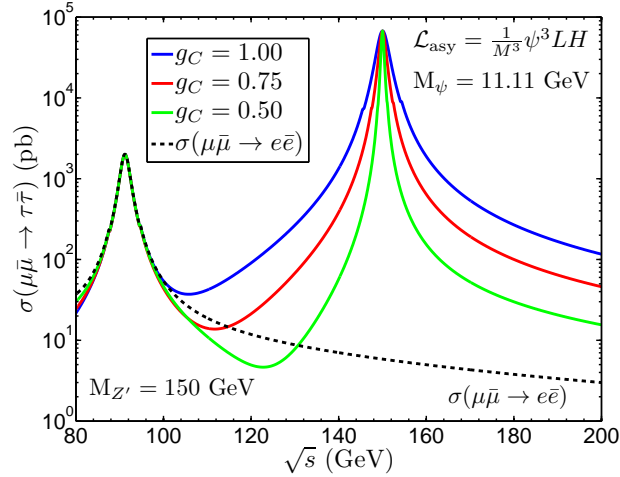


Figure 8.2: An exhibition of the relative strength of the  $\tau^+\tau^-$  vs  $e^+e^-$  signal at a muon collider. The presence of a detectable  $Z'$  resonance in the  $\mu^+\mu^- \rightarrow \tau^+\tau^-$  channel provides a smoking gun signature for the gauged  $L_\mu - L_\tau$  AsyDM model. A similar resonance is also present in the  $\mu^+\mu^- \rightarrow \mu^+\mu^-$  channel while  $\mu^+\mu^- \rightarrow e^+e^-$  cross section shows no such enhancement in the  $Z'$  region.

will have processes of the type

$$\mu^+\mu^- \rightarrow Z' \rightarrow \mu^+\mu^-, \nu_\mu\bar{\nu}_\mu, \tau^+\tau^-, \nu_\tau\bar{\nu}_\tau.$$

Since the final states contain no  $e^+e^-$  this would provide a smoking gun signature for the model. In Figure 8.2 the cross section  $\sigma(\mu^+\mu^- \rightarrow \tau^+\tau^-)$  for various values of  $g_C$  is exhibited when the AsyDM mass is taken to be 11.11 GeV and the  $Z'$  mass is 150 GeV. For comparison  $\sigma(\mu^+\mu^- \rightarrow e^+e^-)$  is also plotted. One finds that the  $\sigma(\mu^+\mu^- \rightarrow \tau^+\tau^-)$  exhibits a detectable  $Z'$  resonance and the cross section varies dramatically as a function of  $\sqrt{s}$  relative to  $\sigma(\mu^+\mu^- \rightarrow e^+e^-)$  which is a rather smoothly falling function beyond the  $Z$  boson pole. In Section 8.1.1 it is shown that the loop contribution to  $\mu^+\mu^- \rightarrow e^+e^-$  is suppressed and the  $Z'$  resonance is not discernible in this channel at a  $\mu^+\mu^-$  collider. There is a second overlapping resonance from a spin-0  $\rho$  state where  $\mu^+\mu^- \rightarrow \rho \rightarrow \tilde{\mu}^*\tilde{\mu} \rightarrow \mu^+\mu^- 2\tilde{\chi}^0$ . However, the  $\rho$  resonance can only proceed at the loop level and is suppressed relative to the  $Z'$  pole.

### 8.1.1 $Z'$ exchange contribution to $\mu^+\mu^- \rightarrow e^+e^-$ at loop level

At a muon collider,  $e^+e^-$  final states can be created via photon exchange and via a  $Z$  boson exchange. Since the  $Z'$  has no direct coupling with the first generation leptons, there is no tree-level  $Z'$  exchange contribution to  $e^+e^-$  final states. However, at the loop level a  $Z'$  exchange can make a contribution where the second and third generation leptons are exchanged in the loop as shown in Figure 8.3. We now compute this contribution to determine its size. Thus we consider a  $\mu^+\mu^- \rightarrow e^+e^-$  process with a  $Z'$  exchange via the second and third generation leptons loops as shown in

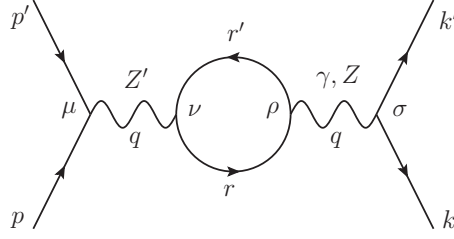


Figure 8.3:  $Z' - \gamma$  and  $Z' - Z$  exchange via  $\mu^+\mu^-$ ,  $\nu_\mu\bar{\nu}_\mu$ ,  $\tau^+\tau^-$ ,  $\nu_\tau\bar{\nu}_\tau$  loops.

Figure 8.3. In this case the contribution to the scattering amplitude is

$$\begin{aligned}
\sum i\mathcal{M} &= i\mathcal{M}_{\gamma Z'} + i\mathcal{M}_{ZZ'} \\
&= \bar{v}(p') \left( \frac{i}{2} g_C Q_\mu \gamma^\mu \right) u(p) \frac{-i(g_{\mu\nu} - q_\mu q_\nu / m_{Z'}^2)}{q^2 - m_{Z'}^2} (i\Pi_{\gamma Z'}^{\nu\rho}) \frac{-ig_{\rho\sigma}}{q^2} \bar{u}(k) (-ie\gamma^\sigma) v(k') \\
&+ \bar{v}(p') \left( \frac{i}{2} g_C Q_\mu \gamma^\mu \right) u(p) \frac{-i(g_{\mu\nu} - q_\mu q_\nu / m_{Z'}^2)}{q^2 - m_{Z'}^2} (i\Pi_{ZZ'}^{\nu\rho}) \\
&\quad \times \frac{-i(g_{\rho\sigma} - q_\rho q_\sigma / m_Z^2)}{q^2 - m_Z^2} \bar{u}(k) \frac{-ig\gamma^\sigma}{\cos\theta_W} (g_V + g_A\gamma^5) v(k'),
\end{aligned} \tag{8.1}$$

where  $Q_\mu$  is the  $U(1)_{L_\mu - L_\tau}$  charge for muon,  $g_V = \frac{1}{2}(T_3)_L + \sin^2\theta_W$ ,  $g_A = -\frac{1}{2}(T_3)_L$ , and the vacuum polarization tensors  $i\Pi_{\gamma Z'}^{\nu\rho}$  and  $i\Pi_{ZZ'}^{\nu\rho}$  are the sums of the contributions from  $\mu^+\mu^-$ ,  $\nu_\mu\bar{\nu}_\mu$ ,  $\tau^+\tau^-$ ,  $\nu_\tau\bar{\nu}_\tau$  loops

$$i\Pi^{\nu\rho} = i\Pi_\mu^{\nu\rho} + i\Pi_{\nu_\mu}^{\nu\rho} + i\Pi_\tau^{\nu\rho} + i\Pi_{\nu_\tau}^{\nu\rho}. \tag{8.2}$$

First let us focus on  $i\Pi_{\gamma Z',\mu}^{\nu\rho}$  which is the muon loop contribution to the  $Z' - \gamma$  exchange. It reads

$$\begin{aligned}
i\Pi_{\gamma Z',\mu}^{\nu\rho} &= -\left(\frac{i}{2}g_C Q_\mu\right)(-ie) \int \frac{d^4 r}{(2\pi)^4} \text{tr} \left[ \gamma^\nu \frac{i(\not{r} + m_\mu)}{(r^2 - m_\mu^2)} \gamma^\rho \frac{i(\not{r}' + m_\mu)}{(r'^2 - m_\mu^2)} \right] \\
&= \frac{4ieg_C Q_\mu}{(4\pi)^2} (q^2 g^{\nu\rho} - q^\nu q^\rho) \int_0^1 dx x(1-x) \frac{\Gamma(2 - \frac{d}{2})}{\Delta_\mu^{2 - \frac{d}{2}}} \\
&= \frac{4ieg_C Q_\mu}{(4\pi)^2} (q^2 g^{\nu\rho} - q^\nu q^\rho) \int_0^1 dx x(1-x) \left( \frac{2}{\epsilon} - \log \Delta_\mu - \gamma + \log(4\pi) + \mathcal{O}(\epsilon) \right),
\end{aligned} \tag{8.3}$$

where  $\Delta_\mu = m_\mu^2 - x(1-x)q^2$ , and in the last step we use the dimensional regularization. The expression of  $i\Sigma_{\gamma Z',\tau}^{\nu\rho}$  differs from  $i\Sigma_{\gamma Z',\mu}^{\nu\rho}$  by only the  $Q_\tau$  factor, and it takes the form

$$i\Pi_{\gamma Z',\tau}^{\nu\rho} = \frac{4ieg_C Q_\tau}{(4\pi)^2} (q^2 g^{\nu\rho} - q^\nu q^\rho) \int_0^1 dx x(1-x) \left( \frac{2}{\epsilon} - \log \Delta_\mu - \gamma + \log(4\pi) + \mathcal{O}(\epsilon) \right). \tag{8.4}$$

Summing over these two terms, we find a dramatic cancellation of the divergence in the loop due to  $Q_\mu = -Q_\tau = 1$ , making the loop finite so that

$$i\Pi_{\gamma Z',\mu}^{\nu\rho} + i\Pi_{\gamma Z',\tau}^{\nu\rho} = \frac{4ieg_C}{(4\pi)^2} (q^2 g^{\nu\rho} - q^\nu q^\rho) \times I, \tag{8.5}$$

where

$$I = \int_0^1 dx x(1-x) \log \frac{\Delta_\tau}{\Delta_\mu} = \int_0^1 dx x(1-x) \log \frac{m_\tau^2 - x(1-x)q^2}{m_\mu^2 - x(1-x)q^2}. \tag{8.6}$$

One can also obtain the neutrino exchange contributions from the above by setting the fermion masses to zero in the equation above (assuming neutrinos to be massless) which gives a vanishing contribution.

Now we want to compare the contribution of the  $Z' - \gamma$  exchange loop diagram with the tree-level process  $\mu^+\mu^- \rightarrow \gamma \rightarrow e^+e^-$ , whose amplitude reads

$$i\mathcal{M}_\gamma = \bar{v}(p')(-ie\gamma^\mu)u(p)\frac{-ig^{\mu\nu}}{q^2}\bar{u}(k)(-ie\gamma^\nu)v(k'). \quad (8.7)$$

With some manipulation we find

$$i\mathcal{M}_{\gamma Z'} = -\frac{2g_c^2 I}{(4\pi)^2} \cdot \frac{q^2}{q^2 - m_{Z'}^2} \times i\mathcal{M}_\gamma \equiv f \times i\mathcal{M}_\gamma. \quad (8.8)$$

Thus, the total squared amplitudes involving a photon can be written as

$$\begin{aligned} |i\mathcal{M}_\gamma + i\mathcal{M}_{\gamma Z'}|^2 &= |1 + f|^2 \times |i\mathcal{M}_\gamma|^2 \\ &= (1 + f + f^* + ff^*) \times |i\mathcal{M}_\gamma|^2. \end{aligned} \quad (8.9)$$

Our numerical analysis shows that  $(f + f^* + ff^*)$  is smaller than  $\sim 10^{-3}$  and thus the loop makes only a tiny contribution to the total cross section in this case. The analysis of  $Z' - Z$  exchange is similar and gives a very small value. Thus we conclude that a  $Z'$  peak will not be visible in the  $\mu^+\mu^- \rightarrow e^+e^-$  process at a muon collider. The above analysis also exhibits why a  $Z'$  in this model would not be visible in an  $e^+e^-$  machine.

## 8.2 The Predictive Higgs Pole Model

In this section we follow [113] and study a particular region of the unified supersymmetric parameter space which satisfies all the existing experimental and astrophysical bounds and was testable to the LHC in its early runs. We focus on the region

where the neutralino has a mass in the range  $\sim (50 - 65)$  GeV. We will refer to the collective region of the parameter space, with  $|m_{\tilde{\chi}_1^0} - m_h/2|_{\max} \lesssim O(5)$  GeV as the ‘‘Higgs-pole region’’. This region is actually very predictive. For the models surveyed in this section we require

$$\left| m_{\tilde{\chi}_1^0} - \frac{1}{2} m_h \right|_{\max} \leq 7 \text{ GeV}, \quad (8.10)$$

with most models being within about 4 GeV or less. As shown in [113] this then relates the lightest neutralino to the following masses

$$\begin{aligned} m_h &= \alpha_h m_{\tilde{\chi}_1^0}, & 1.78 &\leq \alpha_h \leq 2.25 \\ m_{\tilde{\chi}_1^\pm} &= \alpha_{\tilde{\chi}_1^\pm} m_{\tilde{\chi}_1^0}, & 1.65 &\leq \alpha_{\tilde{\chi}_1^\pm} \leq 2.07 \\ m_{\tilde{\chi}_2^0} &= \alpha_{\tilde{\chi}_2^0} m_{\tilde{\chi}_1^0}, & 1.70 &\leq \alpha_{\tilde{\chi}_2^0} \leq 2.07 \\ m_{\tilde{g}} &= \alpha_{\tilde{g}} m_{\tilde{\chi}_1^0}, & 7.34 &\leq \alpha_{\tilde{g}} \leq 9.25, \end{aligned} \quad (8.11)$$

and the normal mSUGRA scaling relations can be replaced by the more quantitative relations

$$\begin{aligned} m_h &= \alpha_{\tilde{\chi}_1^0} m_{\tilde{\chi}_1^0} = \beta_{\tilde{\chi}_1^\pm} m_{\tilde{\chi}_1^\pm} (\simeq \beta_{\tilde{\chi}_2^0} m_{\tilde{\chi}_2^0}) = \beta_{\tilde{g}} m_{\tilde{g}} \\ 0.92 &\leq \beta_{\tilde{\chi}_1^\pm} \leq 1.17, & 0.22 &\leq \beta_{\tilde{g}} \leq 0.29. \end{aligned} \quad (8.12)$$

The distribution of gluino masses for the models is well approximated by a Gaussian with a remarkably small width. As shown in [113] the distribution in the dimensionless ratio  $\alpha_{\tilde{g}} = m_{\tilde{g}}/m_{\tilde{\chi}_1^0}$  from Eq. (8.11). In general the model produce a gluino mass of

$$m_{\tilde{g}} = (451 \pm 20) \text{ GeV} \quad (1 \sigma). \quad (8.13)$$

Predictions for the Sparticle Masses and LSP Eigencontent	
Mass Predictions ( GeV)	Eigencontent of the LSP
$110 \leq m_h \leq 126$	$0.888 \leq n_{11} \leq 0.996$ ( $\tilde{B}$ )
$52 \leq m_{\tilde{\chi}_1^0} \leq 67$	$-0.163 \leq n_{12} \leq -0.016$ ( $\tilde{W}$ )
$104 \leq m_{\tilde{\chi}_1^\pm} \leq 131$	$0.019 \leq n_{13} \leq 0.396$ ( $\tilde{H}_1$ )
$396 \leq m_{\tilde{g}} \leq 575$	$-0.167 \leq n_{14} \leq -0.006$ ( $\tilde{H}_2$ )

Table 8.1: General predictions for the sparticle masses for the models with  $m_0 \leq 10$  TeV satisfying all phenomenological constraints discussed in the text. It is further found that  $m_0 \geq 1.05$  TeV, and the scalar masses are bounded as :  $m_{\tilde{t}_1} \geq 323$  GeV,  $m_{\tilde{b}_1} \geq 706$  GeV,  $m_{\tilde{\tau}_1} \geq 484$  GeV,  $m_{\tilde{q}} \geq 1070$  GeV,  $m_{\tilde{\ell}} \geq 1050$  GeV, and  $m_A \geq 187$  GeV.

Thus consistent with scaling relations one finds

$$m_{\tilde{g}}/m_{\tilde{\chi}_1^0} = 7.86 \pm 0.21 \quad (1 \sigma). \quad (8.14)$$

In Table 8.1 the general ranges given in Equation (8.11) are expanded.

## 8.2.1 Signatures of the Higgs-pole region at the LHC

To study the signatures of the low mass gaugino models at LHC-7 we simulate events at  $\sqrt{s} = 7$  TeV for a sample of 700 model points from the larger set discussed in the previous section. The standard model (SM) backgrounds considered are the same from earlier chapters. The total R parity-odd SUSY production cross section ( $\sigma_{\text{total}}$ ) for the low mass gaugino models are composed, to a first approximation, of only three contributions: production of chargino and the second lightest neutralino (i.e.  $\sigma_{\tilde{\chi}_1^\pm \tilde{\chi}_2^0}/\sigma_{\text{total}}$ ;  $47\% \pm 3\%$ ); gluino pair production (i.e.  $\sigma_{\tilde{g}\tilde{g}}/\sigma_{\text{total}}$ ;  $28\% \pm 3\%$ ); and chargino pair production (i.e.  $\sigma_{\tilde{\chi}_1^\pm \tilde{\chi}_1^\mp}/\sigma_{\text{total}}$ ;  $23\% \pm 1\%$ ). The three sparticles produced with the largest production modes, namely  $\tilde{g}$ ,  $\tilde{\chi}_1^\pm$ , and  $\tilde{\chi}_2^0$ , then decay with the dominant branching ratios shown in Table 8.2. The ranges shown are for the

## Branching Ratios of the Low Mass Gaugino models in the Higgs-pole region

Br( $\tilde{g} \rightarrow X$ )	%	Br( $\tilde{\chi}_2^0 \rightarrow X$ )	%	Br( $\tilde{\chi}_1^\pm \rightarrow X$ )	%
$u_i \bar{u}_i \tilde{\chi}_2^0$	$2 \times (5.1 \pm 0.4)$	$u_i \bar{u}_i \tilde{\chi}_1^0$	$2 \times (12.5 \pm 0.6)$	$u_i \bar{d}_i \tilde{\chi}_1^0$	$2 \times (33.5 \pm 0.1)$
$d_i \bar{d}_i \tilde{\chi}_2^0$	$2 \times (5.0 \pm 0.3)$	$d_i \bar{d}_i \tilde{\chi}_1^0$	$2 \times (16.3 \pm 0.9)$	$l \nu_l \tilde{\chi}_1^0$	$3 \times (11.0 \pm 0.1)$
$b \bar{b} \tilde{\chi}_2^0$	$15.1 \pm 2.5$	$b \bar{b} \tilde{\chi}_1^0$	$16.1 \pm 1.9$		
$u_i \bar{d}_i \tilde{\chi}_1^- + \text{h.c.}$	$4 \times (10.1 \pm 0.8)$	$l^+ l^- \tilde{\chi}_1^0$	$3 \times (2.9 \pm 0.5)$		
$t \bar{b} \tilde{\chi}_1^- + \text{h.c.}$	$2 \times (5.5 \pm 1.2)$	$\nu_1 \bar{\nu}_l \tilde{\chi}_1^0$	$3 \times (5.7 \pm 1.1)$		

Table 8.2: Typical size of dominant branching ratios of the sparticles with the largest production modes emerging from proton-proton collision at the LHC over a subset of 700 models. Here  $u, d$  includes the first 2 generations of quarks and  $l$  includes all 3 generations of leptons (hence the factors of 2 and 3 in the Table). The factor of 4 includes  $u, d$  and the conjugate modes for the charginos. In addition to the three dominant sparticles arising from proton-proton collisions (the three cases considered in the Table), a small subset of models are found to produce light stops ( $m_{\tilde{t}_1} \sim 350$  GeV) at the LHC which decay via  $\tilde{t}_1 \rightarrow (t \tilde{\chi}_1^0, b \tilde{\chi}_1^-, t \tilde{\chi}_2^0)$  respectively, depending on the particular model point.

subset of 700 models. The total SUSY production cross section is relatively large for this class of models given the relatively light gluino, charginos and neutralinos ( $\sigma_{\text{total}} = 9.65 \text{ pb} \pm 1.43 \text{ pb}$ ) over the set of 700 models.

There is a relationship between the effective mass peak and the minimum mass of the gluino and the first two generation squark masses. Since in the low mass gaugino models that lie in the Higgs-pole region, the first and the second generation squark masses are always heavier than the gluino mass, the peak of the effective mass gives a relationship to the gluino mass. Analyzing the effective mass peak for all 700 simulated models under the cuts mentioned in [113] we find in general

$$m_{\text{eff}}^{\text{peak}} \simeq 1.5 m_{\tilde{g}}, \quad (8.15)$$

with the precise range being  $m_{\text{eff}}^{\text{peak}}/m_{\tilde{g}} = 1.57 \pm 0.085$ , as can be seen from the distribution in the left panel of Figure 8.4. Thus a measurement of  $m_{\text{eff}}^{\text{peak}}$  provides an

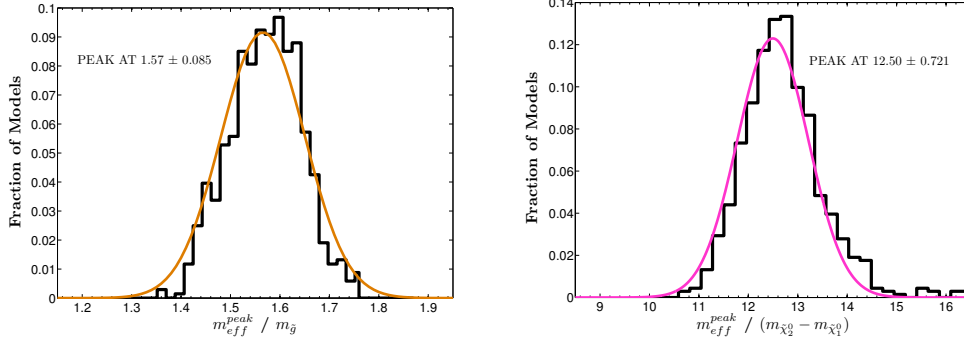


Figure 8.4: Left: Distribution of the ratio of the effective mass peak to the gluino mass. The models plotted here are the 700 model subset and the peak is found after adding the SM background and applying a cut as discussed in the text. We find the peak to be at  $1.57 \pm 0.085$ . Right: Distribution of the ratio of effective mass peak to the mass difference between the two lightest neutralinos under the same cut. The mass difference between the two lightest neutralinos corresponds to the upper bound of the edge in the OSSF dilepton invariant mass plot. We find the peak to be at  $12.50 \pm 0.721$ .

important early clue to the size of the gluino mass. Next, defining

$$\Delta m \equiv m_{\tilde{\chi}_2^0} - m_{\tilde{\chi}_1^0} = (\alpha_{\tilde{\chi}_2^0} - 1) m_{\tilde{\chi}_1^0} , \quad (8.16)$$

the mass relations found in Eq. (8.11) or Eq. (8.12) suggest that the peak in the effective mass distribution will be proportional to  $\Delta m$

$$\frac{m_{\text{eff}}^{\text{peak}}}{\Delta m} \simeq 1.5 \times \frac{m_{\tilde{g}}}{(\alpha_{\tilde{\chi}_2^0} - 1) m_{\tilde{\chi}_1^0}} = 1.5 \times \frac{\alpha_{\tilde{g}}}{(\alpha_{\tilde{\chi}_2^0} - 1)} . \quad (8.17)$$

The distribution of  $m_{\text{eff}}^{\text{peak}} / \Delta m$  is shown to be peaked in the right panel of Figure 8.4, a result which follows from the left panel of Figure 8.4 and from the distribution in  $\alpha_{\tilde{g}}$  as discussed earlier.

Additional mass parameters can be measured for this model as shown in [113]. However, we will not go more into detail on this model since it has been ruled out

by the LHC already.

## 8.3 Higgs discovery implications

This work comes from [114]. The recent search at the LHC [4–8] for the Higgs boson with the combined 7 TeV and 8 TeV data indicated a signal for the Higgs boson with mass  $125.3 \pm 0.4$  (stat.)  $\pm 0.5$  (syst.) GeV for CMS and with mass  $126.0 \pm 0.4$  (stat.)  $\pm 0.4$  (syst.) GeV for ATLAS. As is well known the Higgs boson mass at the tree level lies below the  $Z^0$  boson mass, but it can be made larger by inclusion of loop corrections. However, in supergravity grand unification there is another upper limit, i.e., of about 130 GeV due to the constraint of radiative breaking of the electroweak symmetry (for a review see [114] and references within). Let us now consider the implications of these values on the mSUGRA space.

### 8.3.1 Implications for mSUGRA

In the analysis we use the Higgs boson mass constraint within the Bayesian statistical framework to estimate the soft parameters of mSUGRA. The model's parameter set is defined by,  $\theta = \{m_0, m_{1/2}, A_0, \tan \beta\}$ , and additionally we consider a set of the most sensitive standard model nuisance parameters,  $\psi = \{m_t, m_b(m_b)^{\overline{\text{MS}}}, \alpha_s(m_Z)^{\overline{\text{MS}}}, \alpha_{\text{EM}}(m_Z)^{\overline{\text{MS}}}\}$ . These together form the basis parameter set:  $\Theta = \{\theta, \psi\}$ . Using Bayes's theorem, the posterior probability density function (PDF) for the theory described by  $\Theta$ , which may be mapped to observables,  $\zeta(\Theta)$  to be compared against experimental data,  $d$  is given by:

$$p(\Theta|d) = \frac{p(d|\zeta(\Theta))\pi(\Theta)}{p(d)}, \quad (8.18)$$

where  $\mathcal{L} \equiv p(d|\zeta(\Theta))$  is the likelihood function—the terms of which are described in [114],  $\pi(\Theta)$  is the distribution in  $\Theta$  prior to considering experimental results, and  $\mathcal{Z} \equiv p(d)$  is the Bayesian evidence which can be used in model selection. However, in our goal of parameter estimation, it serves only as a normalization factor. Results are obtained by considering both the 2D marginalized posterior PDF (where the full N-dimensional posterior PDF of Equation (8.18) has been integrated over the other parameters), as well as the profile likelihoods (where the confidence levels are determined by comparison to the global best-fit point). (For a more detailed description see [115].) For more details on how the analysis was done and what packages were used please see [114].

For the analysis, the prior knowledge of the parameters were taken to be either flat linear distributions or flat logarithmic distributions, with  $m_0 \in (0.05, 8)$  TeV (log),  $m_{1/2} \in (0.05, 5)$  TeV (log),  $A_0 \in (-30, 30)$  TeV (linear), and  $\tan \beta \in (3, 60)$  (linear). We have fixed  $\text{sign}(\mu)$  to be positive. The Standard Model nuisance parameters were allowed to vary in  $2\sigma$  windows of their central values. Our MULTINEST sampling parameters, as defined in [115], were  $n_{\text{live}} = 20,000$  and  $\text{tol} = 0.0001$ . It has been shown in [116] and in [115] that these parameters are not only sufficient to provide a map of the posterior PDF, but also to find the true best-fit point which is essential for the profile likelihood analysis.

In the likelihood analysis we use the CMS result since that result was available earlier. The fits to the data are reported, including the Higgs mass, in Figure 8.5 in the form of 2D posterior PDF maps (left panels) as well as the profile likelihood maps (right panels). The posterior mean is marked with a large dot and the global best-fit is marked with a circled 'X'. (Note that while the best-fit point is crucial in Frequentist likelihood-ratio tests, it has no significance in the Bayesian framework.)

The top panels exhibit the constraint in the  $m_0 - m_{1/2}$  plane and show that  $m_0$  is typically a TeV or larger, while  $m_{1/2}$  can lie below 500 GeV. The middle panels exhibit the constraint in the  $A_0/m_0 - \tan \beta$  plane, and here one finds that most of the allowed parameter space lies in the narrow strip  $|A_0/m_0| \leq 1$  with a small strip in the range  $|A_0/m_0| \in (-2, -6)$ . The bottom panels exhibit the constraint in the  $m_A - \tan \beta$  plane, and here one finds that the majority of the allowed range of  $m_A$  lies above 1 TeV. Thus  $m_A \gg m_{h^0}$  for the majority of the parameter space and thus we are in the so-called decoupling limit.

It was pointed out in [112] that most of the experimentally consistent parameter space of mSUGRA lies on the Hyperbolic Branch of radiative breaking of the electroweak symmetry under the LHC-7 constraints. The HB region has sub-regions which we may label as Focal Point (HB/FP), Focal Curves (HB/FC $_i$ ,  $i=1,2$ ), and Focal Surfaces (HB/FS). It was shown in [112, 117] that the HB/FP is mostly depleted while the remaining parameter space lies on HB/FC $_i$  or HB/FS. Specifically we note here that the right edge of  $A_0/m_0$  in Figure 8.5 is  $\sim 1$ .

In Figure 8.6 we present the 2D posterior PDF's (left panels) and the profile likelihoods (right panels) in the planes of the phenomenologically important sparticle masses. The top panels present the results in the gluino–squark mass plane, and indicate that the gluino can be below a TeV. The second row is plotted in the squark–chargino mass plane and demonstrates that the chargino masses are only bounded from below by the direct searches at LEP. The next row exhibits our fit in the stau–stop mass plane. Here one finds that the stau and stop masses are typically large except for a small strip where the stop mass can lie below a TeV. This is largely to be expected as a heavy stop is relied upon to provide a sizable loop correction to the Higgs mass. The bottom panels show the analysis in the  $\mu - m_{\tilde{g}}$  plane. One finds

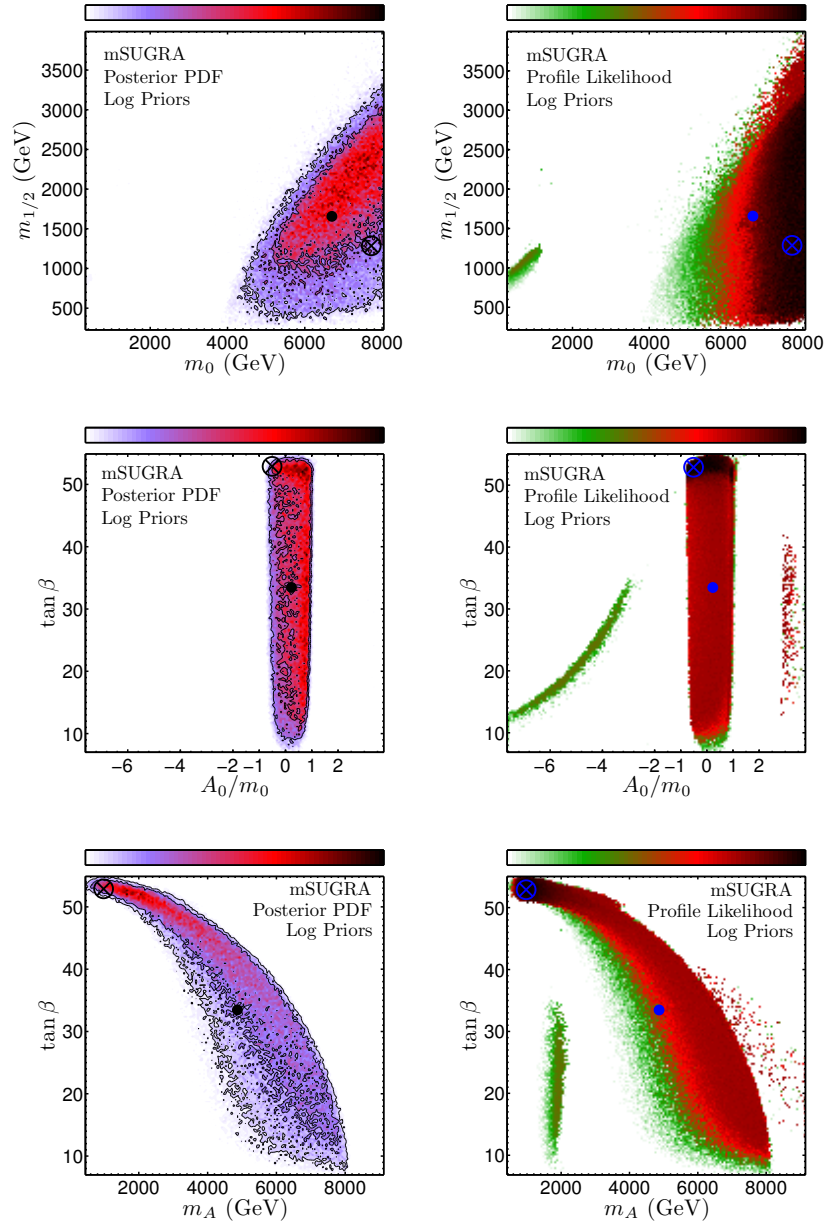


Figure 8.5: Left panels: plots of the 2D posterior probability densities,  $1\sigma$  and  $2\sigma$  contours are also drawn. Right panels: plots of the profile likelihoods. Top: in the  $m_0 - m_{1/2}$  plane. Middle: in the  $A_0/m_0 - \tan \beta$  plane. Bottom: in the  $m_A - \tan \beta$  plane. The posterior mean is marked by a large dot while the best-fit point is shown by a circled 'X'. The color bar above the top panel gives the relative likelihood which increases left-to-right.

that  $\mu$  is typically quite light, i.e.,  $\mu$  can be significantly below 500 GeV.

Using the marginalized 1D posterior PDF we are able to set lower limits on the sparticle masses from the  $2\sigma$  credible regions. We present those limits here:  $m_{\tilde{g}} > 1.39 \text{ TeV}$ ,  $m_{\tilde{\chi}_1^\pm} > 196 \text{ GeV}$ ,  $m_{A_0} \sim m_{H_0} \sim m_{H^\pm} > 1.3 \text{ TeV}$ ,  $m_{\tilde{t}_1} > 3.1 \text{ TeV}$ ,  $m_{\tilde{\tau}_1} > 3.1 \text{ TeV}$ ,  $m_{\tilde{q}} > 5 \text{ TeV}$ , and  $m_{\tilde{\ell}} > 4.8 \text{ TeV}$ . The profile likelihood analysis yields different results. Here, we find the 95% CL sparticle lower limits to be  $m_{\tilde{g}} > 690 \text{ GeV}$ ,  $m_{\tilde{\chi}_1^\pm} > 95 \text{ GeV}$ ,  $m_{A_0 \sim H_0 \sim H^\pm} > 540 \text{ GeV}$ ,  $m_{\tilde{t}_1} > 580 \text{ GeV}$ ,  $m_{\tilde{\tau}_1} > 310 \text{ GeV}$ ,  $m_{\tilde{q}} > 1.5 \text{ TeV}$ , and  $m_{\tilde{\ell}} > 580 \text{ GeV}$ . We note that as expected the lower limits given by the profile likelihood analysis lie lower than the limits given by the PDF analysis. The analysis thus indicates that the light particles in mSUGRA in view of the Higgs mass measurement are the neutralino, the chargino, the gluino, the stau and the stop. Among these the most likely candidates for discovery in the next phase of CERN experiment are the gluino, the chargino and the stop.

### 8.3.2 125 GeV Higgs boson and dark matter

Neutralino-proton spin independent cross section  $\sigma_{\tilde{\chi}_1^0 p}^{\text{SI}}$  depends sensitively on the Higgs boson mass (for a discussion see [117]). Thus considering the  $\sim 125 \text{ GeV}$  Higgs mass leads to a more constrained prediction for dark matter. In Figure 8.7 we give a plot of  $\mathcal{R} \times \sigma_{\tilde{\chi}_1^0 p}^{\text{SI}}$  as a function of the lightest neutralino mass  $m_{\tilde{\chi}_1^0}$  where the factor  $\mathcal{R}$  is defined by  $\mathcal{R} \equiv (\Omega h^2) / (\Omega h^2)_{\text{WMAP}}$ , and  $(\Omega h^2)_{\text{WMAP}}$  is the central value of the WMAP-7 data. By only applying a likelihood penalty for points that are above the WMAP-7 limit, we have taken into account the possibility that there may be additional components of dark matter beyond the neutralino [69]. Quite remarkably, the bulk of the credible region of mSUGRA falls essentially exclusively between the current limits on dark matter by XENON-100 and the projected sensitivity of SuperCDMS and XENON-1T [114].

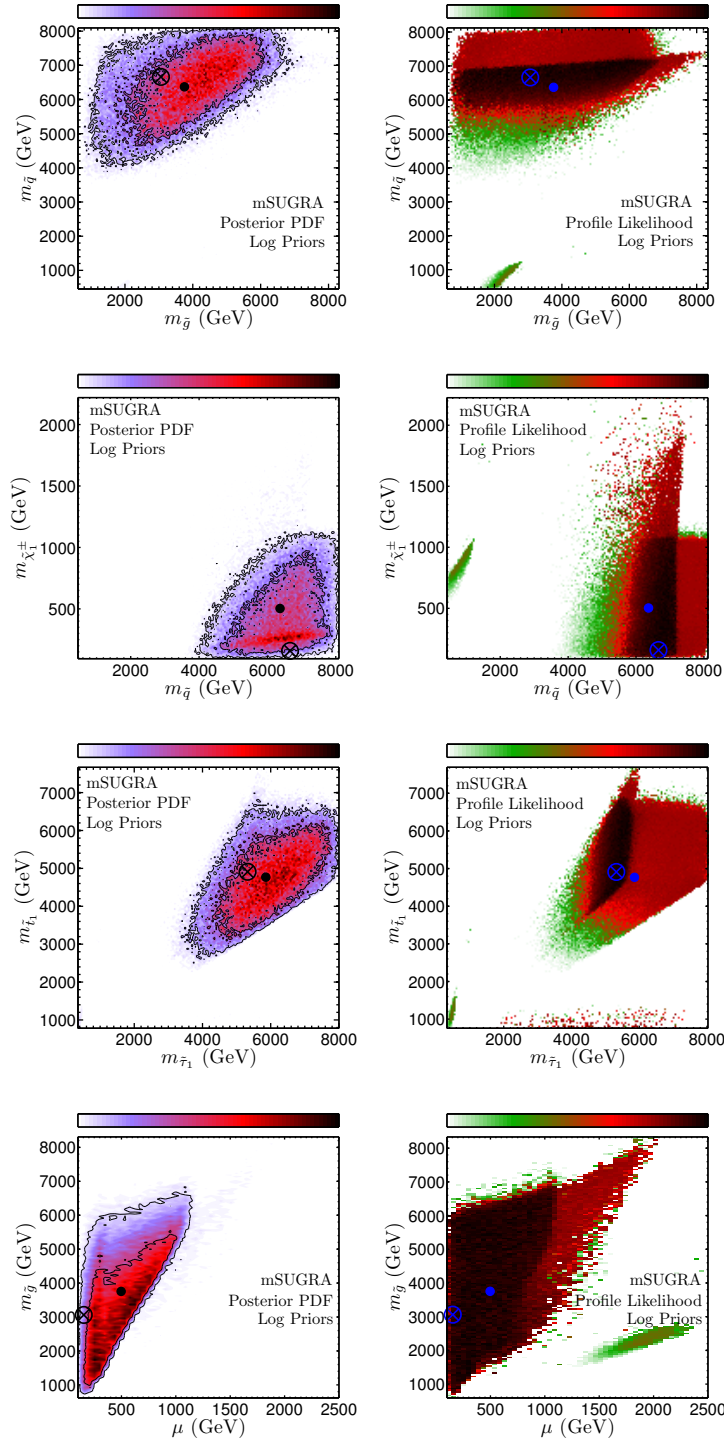


Figure 8.6: Left panels: plots of the 2D posterior probability densities,  $1\sigma$  and  $2\sigma$  contours are also drawn. Right panels: plots of the profile likelihoods. Top: in the  $m_{\tilde{g}}-m_{\tilde{q}}$  plane. Upper-middle: in the  $m_{\tilde{q}}-m_{\tilde{\chi}_{1\pm}}$  plane. Lower-middle: in the  $m_{\tilde{\tau}_1} - m_{\tilde{\tau}_1}$  plane. Bottom: in the  $\mu - m_{\tilde{g}}$  plane. The posterior mean is marked by a large dot while the best-fit point is shown by a circled 'X'. The color bar above the top panel gives the relative likelihood which increases left-to-right.

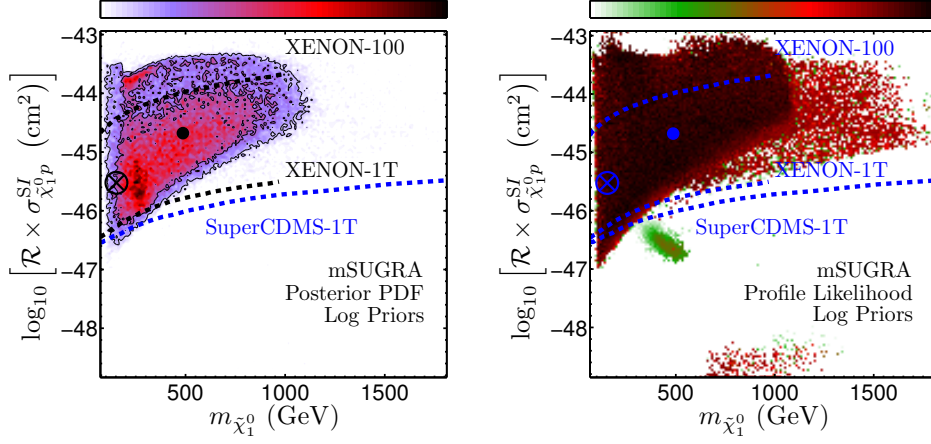


Figure 8.7: Plots of  $\mathcal{R} \equiv (\Omega h^2) / (\Omega h^2)_{\text{WMAP}}$  vs the neutralino mass  $m_{\tilde{\chi}_1^0}$ . The left panel presents the 2D posterior PDF, and the right panel presents the profile likelihood. The analysis shows that virtually all of credible region of mSUGRA will be probed by the SuperCDMS and XENON-1T experiments. The color bar above the panels gives the relative likelihood which increases left-to-right.

We discuss now the constraint from  $g_\mu - 2$ . In supersymmetric theories, sparticle loops make significant contributions to the anomalous magnetic moment of the muon if the relevant sparticles (charginos, neutralinos, smuons, sneutrinos) entering the loops are relatively light. The experimental determination of  $\delta a_\mu = a_\mu^{\text{exp}} - a_\mu^{\text{SM}}$  where  $a_\mu = (g_\mu - 2)/2$ , depends sensitively on the hadronic correction to the Standard Model value. There are two main procedures for the estimation of the hadronic correction, which are either using the  $e^+e^-$  annihilation cross section or from  $\tau$  decay. The result using the  $e^+e^-$  annihilation gives  $\delta a_\mu = (28.7 \pm 8.0) \times 10^{-10}$  ( $3.6\sigma$ ) while for  $\tau$ -based hadronic contributions one has  $\delta a_\mu = (19.5 \pm 8.3) \times 10^{-10}$  ( $2.4\sigma$ ) [118]. In any case, within the universal soft SUSY-breaking paradigm there would be tension between the  $g_\mu - 2$  result (specifically the one using  $e^+e^-$  annihilation cross section) and the 125 GeV Higgs boson mass since the  $m_0$  scale is rather high. If the  $g_\mu - 2$  results stay, then there are at least two avenues open to make compatible the  $g_\mu - 2$  results and the Higgs boson mass. The first possibility is that we stay within the universal soft breaking paradigm and additional contributions to the Higgs mass

arise due to the presence of extra matter which can generate new loop corrections to the Higgs mass, or from extra gauge groups under which the Higgs is charged yielding corrections to the Higgs mass through  $D$ -terms.

# Chapter 9

## Conclusions

During the completion of this thesis the Large Hadron Collider (LHC) accumulated a substantial amount of integrated luminosity [1], dark matter direct detection experiments collected data [2], and the Planck satellite released its observations [3]. This data enriched era was a very exciting time in particle physics. The field recently surpassed a milestone with the July 2012 announcement of a  $5\sigma$  detection of a boson around 125 GeV, with preliminary results indicating a Higgs boson [4–8]. My research was directly tied to the new wave of data that came forth from the LHC and dark matter related experiments. Thus, my work involved Supersymmetry [48, 49], Stueckelberg extensions to the Standard Model [28] as well as to the Minimal Supersymmetric Standard Model [86], multicomponent dark matter [75], and asymmetric dark matter [27], which all have direct bearing on data from colliders and dark matter experiments.

## 9.1 Multicomponent Dark Matter

The majority of current studies on dark matter consider only the case where one fundamental particle contributes to cold dark matter, but there is no overriding principle that requires such a restriction. Thus, dark matter may in fact be composed of several components. A branch of my research has been to investigate such a possibility. In Chapter 5, we have proposed extending the Minimal Supersymmetric Standard Model by a  $U(1)^n$  hidden sector that includes both fermionic and baryonic stable particles as dark matter candidates. These models were required to be consistent with the current cold dark matter relic density observed by WMAP and are found to successfully explain the excess seen in the PAMELA experiment while still being consistent with direct detection experiments. More specifically, an exploration of the case when the dark matter consists of Dirac and Majorana particles shows that the Dirac component can fit the PAMELA data via its annihilation close to a Breit-Wigner pole while the Majorana component of dark matter remained the dominant component and can be detected in direct detection dark matter experiments. Additionally, we show that in the multicomponent picture it is possible to generate events that can be tested by XENON-100 and other ongoing direct detection experiments. Further, allowing a leptophilic gauge symmetry in the model can produce a discoverable  $Z''$  vector boson with signatures in the  $e^+e^-$  and  $\mu^+\mu^-$  final states.

## 9.2 Asymmetric Dark Matter

It is intriguing to investigate whether there is some underlining principle behind the ratio of the dark matter relic density to baryonic relic density being  $\sim 5$ , i.e. the cosmic coincidence. In Chapters 3 and 6, we extend the Standard Model as well as the Mini-

mal Supersymmetric Standard Model using the Stueckelberg mechanism to explain the cosmic coincidence by assuming a generation of  $B - L$  in the visible sector in the early universe which can generate asymmetric dark matter carrying non-vanishing  $B - L$ . We discuss several candidate models for asymmetric dark matter using a variety of operators constructed from Standard Model fields with a non-vanishing  $B - L$  quantum number, which is transferred to the dark matter sector at thermal equilibrium in the early universe. The Stueckelberg extension provides us with a mechanism to deplete the symmetric component of dark matter produced by thermal processes. To accomplish this, the dark matter annihilates through a massive boson ( $Z'$ ) from a  $L_\mu - L_\tau$  gauge symmetry via a Breit-Wigner pole. In the Minimal Supersymmetric Standard Model extension with the conservation of  $R$  parity, the model has two dark matter candidates with the additional one being the stable neutralino. For a broad class of supersymmetric models we found that the neutralino could be the subdominant component of dark matter and still be consistent with experimental SUSY constraints (including a  $\sim 125$  GeV Higgs). Additionally, these models are also accessible at future direct detection experiments and can produce clear excesses at a muon collider in  $\mu$  and  $\tau$  channels compared to the  $e$  channel.

### 9.3 Early Discovery Potential of the LHC

During the initial data taking stage of the LHC, my research focused on the potential to discover new physics in the early runs as well as models with multicomponent dark matter. Such studies included the crucial understanding and proper simulation of background processes [90] using MADGRAPH [92] for parton level processes, PYTHIA [93] for hadronization, and PGS-4 [94] for the detector simulation. In the same work, these Standard Model processes were then used to investigate the LHC's

reach potential in mSUGRA/CMSSM, which is in excellent agreement with their present reach. During this period, I began to develop a computer program to efficiently analyze signal models to compare to the large generated background. This led to the investigation of light gaugino models, i.e. parameter points with gluino mass below 750 GeV, at the LHC [119]. Parameter points with varying sparticle spectra were analyzed to find the most encouraging modes of discovery. These parameter points were also investigated at indirect and direct detection dark matter experiments and were found to be testable at multiple experiments. I later explored parameter points where the mass of the lightest neutralino was roughly half the mass of the light  $CP$  even Higgs, i.e. Higgs pole models [113]. Such parameter points have very predictable spectra and give distinct signatures on several experiments. We successfully showed how using potential results from a variety of experiments one can reconstruct the gaugino sector of the model by measuring the peak of the effective mass distribution, the edge of the dilepton invariant mass distribution, and the spin independent neutralino-proton cross section.

## 9.4 LHC SUSY Searches

In the beginning of 2011 the CMS and ATLAS Collaborations started to release their early 7 TeV analysis on beyond the Standard Model physics. The limits they found in the mSUGRA/CMSSM parameter space surpassed those from the Tevatron. Colleagues and I began to study how their results could be extended to other regions of the parameter space, i.e. different  $A_0$  and  $\tan \beta$ . We also compared the reach of CMS and ATLAS with the indirect SUSY constraints, e.g. from flavor physics. Specifically, it was found that a significant portion of the parameter space excluded by the LHC was essentially already excluded by the indirect constraints and the majority

of parameter space was yet to be probed. Additionally, we explored the implications that these results had on direct detection dark matter experiments. It was found that within supergravity models the LHC had excluded a large region of the signature space at direct detection experiments. The analysis was then extended to supergravity models with nonuniversal soft breaking in the gaugino sector. In this case we found that a part of the dark matter excluded region became repopulated and thus a signature to observe nonuniversality [91, 120].

## 9.5 Higgs Discovery at the LHC

Following the evidence of the Standard Model Higgs boson at the LHC in December of 2011, which indicated a signal in the range 115 GeV to 131 GeV, I worked on the implications of this result within Supersymmetry and multicomponent dark matter extensions. As is well known in SUSY, if one is to raise the Higgs mass significantly above  $M_Z$  one needs a large loop correction to the tree value ( $m_{h^0}$ ), which satisfies the constraint  $m_{h^0} < M_Z$ . The analysis done in the framework of SUSY with gravity mediation showed that one needed a large scalar mass ( $m_0$ ) and a large trilinear coupling ( $A_0$ ) so that  $A_0/m_0$  is sizable in order to generate a loop correction that could boost the Higgs boson mass to the allowed range. We further explored the implications of the new constraint on SUSY searches at the LHC as well as dark matter experiments (This material can be found in [117, 120] and was done during the time of the thesis, but was omitted in the thesis write up). Once the LHC's data confirmed the discovery of the (Higgs) boson with a mass near 125 GeV, collaborators and I carried out a Bayesian analysis to identify more precisely the regions of the parameter space that were consistent with the measurement of the boson mass. Our findings showed that the universal gaugino mass ( $m_{1/2}$ ) could be in the sub-TeV region, the

scalar mass was typically a TeV or larger, and the ratio of  $A_0/m_0$  was confined to a narrow strip with  $|A_0/m_0| \leq 1$ . Further, we used our Bayesian analysis to set 95% confidence level lower bounds on sparticle masses. Additionally, we observed that the spin independent neutralino-proton cross section lies just beyond the reach of the current sensitivity.

## 9.6 Further Research

Currently there are many possible extensions one can do based on the work discussed in this thesis. One project focuses on the investigations of naturalness with nonuniversal soft breaking. A common feature of such models is that some of the sparticle masses can be low such as the electroweak gauginos and sleptons while squarks could be heavy to provide the desired loop correction to the Higgs boson mass. To this end, one would need to analyze parameter points that produce light staus, but still agree with experimental constraints including the branching ratio of the light  $CP$ -even Higgs boson into diphotons. On the dark matter front, one could pursue the phenomenology at the LHC of multicomponent dark matter models. Such a study would look at signatures in missing energy and expand on current analyses with inclusion of  $m_{T2}$  and its variances. Additionally, one could use machine learning techniques, e.g. support vector machines, or artificial neural networks to determine clear and decisive ways to distinguish a multicomponent dark matter model from a single component dark matter model. These same techniques could be applied to the study and detection of extra dimensions, among many other models of new physics.

# Bibliography

- [1] “LHC Performance and Statistics”,  
<https://lhc-statistics.web.cern.ch/LHC-Statistics/>.
- [2] WMAP Collaboration, “Nine-Year Wilkinson Microwave Anisotropy Probe (WMAP) Observations: Cosmological Parameter Results”,  
[arXiv:1212.5226](https://arxiv.org/abs/1212.5226).
- [3] Planck Collaboration, “Planck 2013 results. I. Overview of products and scientific results”, [arXiv:1303.5062](https://arxiv.org/abs/1303.5062).
- [4] CMS Collaboration, “A new boson with a mass of 125 GeV observed with the CMS experiment at the Large Hadron Collider”, *Science* **338** (2012) 1569–1575, [doi:10.1126/science.1230816](https://doi.org/10.1126/science.1230816).
- [5] CMS Collaboration, “Observation of a new boson with mass near 125 GeV in pp collisions at  $\sqrt{s} = 7$  and 8 TeV”, [arXiv:1303.4571](https://arxiv.org/abs/1303.4571).
- [6] CMS Collaboration, “Observation of a new boson at a mass of 125 GeV with the CMS experiment at the LHC”, *Phys. Lett. B* **716** (2012) 30–61, [doi:10.1016/j.physletb.2012.08.021](https://doi.org/10.1016/j.physletb.2012.08.021), [arXiv:1207.7235](https://arxiv.org/abs/1207.7235).
- [7] ATLAS Collaboration, “Observation of a new particle in the search for the Standard Model Higgs boson with the ATLAS detector at the LHC”, *Phys. Lett. B* **716** (2012) 1–29, [doi:10.1016/j.physletb.2012.08.020](https://doi.org/10.1016/j.physletb.2012.08.020), [arXiv:1207.7214](https://arxiv.org/abs/1207.7214).
- [8] ATLAS Collaboration, “A particle consistent with the Higgs Boson observed with the ATLAS Detector at the Large Hadron Collider”, *Science* **338** (2012) 1576–1582, [doi:10.1126/science.1232005](https://doi.org/10.1126/science.1232005).
- [9] S. Glashow, “Partial Symmetries of Weak Interactions”, *Nucl.Phys.* **22** (1961) 579–588, [doi:10.1016/0029-5582\(61\)90469-2](https://doi.org/10.1016/0029-5582(61)90469-2).
- [10] S. Weinberg, “A Model of Leptons”, *Phys.Rev.Lett.* **19** (1967) 1264–1266, [doi:10.1103/PhysRevLett.19.1264](https://doi.org/10.1103/PhysRevLett.19.1264).

- [11] A. Salam, “Weak and Electromagnetic Interactions”, in *Elementary Particle Theory*, N. Svartholm, ed., p. 367. Almquist & Wiksell, Stockholm, 1968.
- [12] G. 't Hooft, “Renormalization of Massless Yang-Mills Fields”, *Nucl. Phys. B* **33** (1971) 173–199, [doi:10.1016/0550-3213\(71\)90395-6](https://doi.org/10.1016/0550-3213(71)90395-6).
- [13] D. Gross and F. Wilczek, “Ultraviolet Behavior of Nonabelian Gauge Theories”, *Phys.Rev.Lett.* **30** (1973) 1343–1346, [doi:10.1103/PhysRevLett.30.1343](https://doi.org/10.1103/PhysRevLett.30.1343).
- [14] H. D. Politzer, “Reliable Perturbative Results for Strong Interactions?”, *Phys.Rev.Lett.* **30** (1973) 1346–1349, [doi:10.1103/PhysRevLett.30.1346](https://doi.org/10.1103/PhysRevLett.30.1346).
- [15] S. Novaes, “Standard model: An Introduction”, [arXiv:hep-ph/0001283](https://arxiv.org/abs/hep-ph/0001283).
- [16] C. Burgess and G. Moore, “The standard model: A primer”,.
- [17] F. Englert and R. Brout, “Broken Symmetry and the Mass of Gauge Vector Mesons”, *Phys.Rev.Lett.* **13** (1964) 321–323, [doi:10.1103/PhysRevLett.13.321](https://doi.org/10.1103/PhysRevLett.13.321).
- [18] P. W. Higgs, “Broken symmetries, massless particles and gauge fields”, *Phys.Lett.* **12** (1964) 132–133, [doi:10.1016/0031-9163\(64\)91136-9](https://doi.org/10.1016/0031-9163(64)91136-9).
- [19] P. W. Higgs, “Broken Symmetries and the Masses of Gauge Bosons”, *Phys.Rev.Lett.* **13** (1964) 508–509, [doi:10.1103/PhysRevLett.13.508](https://doi.org/10.1103/PhysRevLett.13.508).
- [20] G. Guralnik, C. Hagen, and T. Kibble, “Global Conservation Laws and Massless Particles”, *Phys.Rev.Lett.* **13** (1964) 585–587, [doi:10.1103/PhysRevLett.13.585](https://doi.org/10.1103/PhysRevLett.13.585).
- [21] A. Salam, “Weak and Electromagnetic Interactions”, *Conf.Proc.* **C680519** (1968) 367–377.
- [22] W.-Z. Feng, P. Nath, and G. Peim, “Cosmic Coincidence and Asymmetric Dark Matter in a Stueckelberg Extension”, *Phys.Rev.* **D85** (2012) 115016, [doi:10.1103/PhysRevD.85.115016](https://doi.org/10.1103/PhysRevD.85.115016), [arXiv:1204.5752](https://arxiv.org/abs/1204.5752).
- [23] S. Nussinov, “TECHNOCOSMOLOGY: COULD A TECHNIBARYON EXCESS PROVIDE A ‘NATURAL’ MISSING MASS CANDIDATE?”, *Phys.Lett.* **B165** (1985) 55, [doi:10.1016/0370-2693\(85\)90689-6](https://doi.org/10.1016/0370-2693(85)90689-6).
- [24] K. Griest and D. Seckel, “Cosmic Asymmetry, Neutrinos and the Sun”, *Nucl.Phys.* **B283** (1987) 681, [doi:10.1016/0550-3213\(87\)90293-8](https://doi.org/10.1016/0550-3213(87)90293-8).
- [25] R. S. Chivukula and T. P. Walker, “TECHNICOLOR COSMOLOGY”, *Nucl.Phys.* **B329** (1990) 445, [doi:10.1016/0550-3213\(90\)90151-3](https://doi.org/10.1016/0550-3213(90)90151-3).

- [26] S. Dodelson, B. R. Greene, and L. M. Widrow, “Baryogenesis, dark matter and the width of the Z”, *Nucl.Phys.* **B372** (1992) 467–493, [doi:10.1016/0550-3213\(92\)90328-9](https://doi.org/10.1016/0550-3213(92)90328-9).
- [27] D. B. Kaplan, “A Single explanation for both the baryon and dark matter densities”, *Phys.Rev.Lett.* **68** (1992) 741–743, [doi:10.1103/PhysRevLett.68.741](https://doi.org/10.1103/PhysRevLett.68.741).
- [28] B. Kors and P. Nath, “A Stueckelberg extension of the standard model”, *Phys.Lett.* **B586** (2004) 366–372, [doi:10.1016/j.physletb.2004.02.051](https://doi.org/10.1016/j.physletb.2004.02.051), [arXiv:hep-ph/0402047](https://arxiv.org/abs/hep-ph/0402047).
- [29] B. Kors and P. Nath, “Aspects of the Stueckelberg extension”, *JHEP* **0507** (2005) 069, [doi:10.1088/1126-6708/2005/07/069](https://doi.org/10.1088/1126-6708/2005/07/069), [arXiv:hep-ph/0503208](https://arxiv.org/abs/hep-ph/0503208).
- [30] H. Davoudiasl and R. N. Mohapatra, “On Relating the Genesis of Cosmic Baryons and Dark Matter”, *New J.Phys.* **14** (2012) 095011, [doi:10.1088/1367-2630/14/9/095011](https://doi.org/10.1088/1367-2630/14/9/095011), [arXiv:1203.1247](https://arxiv.org/abs/1203.1247).
- [31] X. He, G. C. Joshi, H. Lew et al., “NEW Z-prime PHENOMENOLOGY”, *Phys.Rev.* **D43** (1991) 22–24, [doi:10.1103/PhysRevD.43.22](https://doi.org/10.1103/PhysRevD.43.22).
- [32] X.-G. He, G. C. Joshi, H. Lew et al., “Simplest Z-prime model”, *Phys.Rev.* **D44** (1991) 2118–2132, [doi:10.1103/PhysRevD.44.2118](https://doi.org/10.1103/PhysRevD.44.2118).
- [33] W. Buchmuller, R. Peccei, and T. Yanagida, “Leptogenesis as the origin of matter”, *Ann.Rev.Nucl.Part.Sci.* **55** (2005) 311–355, [doi:10.1146/annurev.nucl.55.090704.151558](https://doi.org/10.1146/annurev.nucl.55.090704.151558), [arXiv:hep-ph/0502169](https://arxiv.org/abs/hep-ph/0502169).
- [34] D. E. Kaplan, M. A. Luty, and K. M. Zurek, “Asymmetric Dark Matter”, *Phys.Rev.* **D79** (2009) 115016, [doi:10.1103/PhysRevD.79.115016](https://doi.org/10.1103/PhysRevD.79.115016), [arXiv:0901.4117](https://arxiv.org/abs/0901.4117).
- [35] J. A. Harvey and M. S. Turner, “Cosmological baryon and lepton number in the presence of electroweak fermion number violation”, *Phys.Rev.* **D42** (1990) 3344–3349, [doi:10.1103/PhysRevD.42.3344](https://doi.org/10.1103/PhysRevD.42.3344).
- [36] E. Kolb and M. Turner, “The Early Universe”. Addison-Wesley Pub. Company, 1989.
- [37] D. Aristizabal Sierra, J. F. Kamenik, and M. Nemevsek, “Implications of Flavor Dynamics for Fermion Triplet Leptogenesis”, *JHEP* **1010** (2010) 036, [doi:10.1007/JHEP10\(2010\)036](https://doi.org/10.1007/JHEP10(2010)036), [arXiv:1007.1907](https://arxiv.org/abs/1007.1907).
- [38] M. Ibe, S. Matsumoto, and T. T. Yanagida, “The GeV-scale dark matter with B-L asymmetry”, *Phys.Lett.* **B708** (2012) 112–118, [doi:10.1016/j.physletb.2012.01.032](https://doi.org/10.1016/j.physletb.2012.01.032), [arXiv:1110.5452](https://arxiv.org/abs/1110.5452).

- [39] Particle Data Group, “Review of Particle Physics (RPP)”, *Phys. Rev. D* **86** (2012) 010001, [doi:10.1103/PhysRevD.86.010001](https://doi.org/10.1103/PhysRevD.86.010001).
- [40] J. P. Miller, E. de Rafael, and B. L. Roberts, “Muon (g-2): Experiment and theory”, *Rept.Prog.Phys.* **70** (2007) 795, [doi:10.1088/0034-4885/70/5/R03](https://doi.org/10.1088/0034-4885/70/5/R03), [arXiv:hep-ph/0703049](https://arxiv.org/abs/hep-ph/0703049).
- [41] K. A. Olive, D. N. Schramm, and G. Steigman, “Limits on New Superweakly Interacting Particles from Primordial Nucleosynthesis”, *Nucl.Phys.* **B180** (1981) 497, [doi:10.1016/0550-3213\(81\)90065-1](https://doi.org/10.1016/0550-3213(81)90065-1).
- [42] B. W. Lee and S. Weinberg, “Cosmological Lower Bound on Heavy Neutrino Masses”, *Phys.Rev.Lett.* **39** (1977) 165–168, [doi:10.1103/PhysRevLett.39.165](https://doi.org/10.1103/PhysRevLett.39.165).
- [43] R. J. Scherrer and M. S. Turner, “On the Relic, Cosmic Abundance of Stable Weakly Interacting Massive Particles”, *Phys.Rev.* **D33** (1986) 1585, [doi:10.1103/PhysRevD.33.1585](https://doi.org/10.1103/PhysRevD.33.1585), [10.1103/PhysRevD.34.3263](https://doi.org/10.1103/PhysRevD.34.3263).
- [44] K. Griest and D. Seckel, “Three exceptions in the calculation of relic abundances”, *Phys.Rev.* **D43** (1991) 3191–3203, [doi:10.1103/PhysRevD.43.3191](https://doi.org/10.1103/PhysRevD.43.3191).
- [45] P. Gondolo and G. Gelmini, “Cosmic abundances of stable particles: Improved analysis”, *Nucl.Phys.* **B360** (1991) 145–179, [doi:10.1016/0550-3213\(91\)90438-4](https://doi.org/10.1016/0550-3213(91)90438-4).
- [46] P. Nath and R. L. Arnowitt, “Predictions in SU(5) supergravity grand unification with proton stability and relic density constraints”, *Phys.Rev.Lett.* **70** (1993) 3696–3699, [doi:10.1103/PhysRevLett.70.3696](https://doi.org/10.1103/PhysRevLett.70.3696), [arXiv:hep-ph/9302318](https://arxiv.org/abs/hep-ph/9302318).
- [47] R. L. Arnowitt and P. Nath, “Cosmological constraints and SU(5) supergravity grand unification”, *Phys.Lett.* **B299** (1993) 58–63, [doi:10.1016/0370-2693\(93\)90883-J](https://doi.org/10.1016/0370-2693(93)90883-J), [arXiv:hep-ph/9302317](https://arxiv.org/abs/hep-ph/9302317).
- [48] R. L. Arnowitt and P. Nath, “Supersymmetry and Supergravity: Phenomenology and Grand Unification”, [arXiv:hep-ph/9309277](https://arxiv.org/abs/hep-ph/9309277).
- [49] S. P. Martin, “A Supersymmetry primer”, [arXiv:hep-ph/9709356](https://arxiv.org/abs/hep-ph/9709356).
- [50] I. J. Aitchison, “Supersymmetry and the MSSM: An Elementary introduction”, [arXiv:hep-ph/0505105](https://arxiv.org/abs/hep-ph/0505105).
- [51] M. Drees, R. Godbole, and P. Roy, “Theory and phenomenology of sparticles: An account of four-dimensional N=1 supersymmetry in high energy physics”,.

- [52] S. P. Martin, “TASI 2011 lectures notes: two-component fermion notation and supersymmetry”, [arXiv:1205.4076](https://arxiv.org/abs/1205.4076).
- [53] Y. Shirman, “TASI 2008 Lectures: Introduction to Supersymmetry and Supersymmetry Breaking”, [arXiv:0907.0039](https://arxiv.org/abs/0907.0039).
- [54] Y. A. Golfand and E. P. Likhtman, “Extension of the Algebra of Poincare Group Generators and Violation of p Invariance”, *JETP Lett.* **13** (1971) 323–326.
- [55] D. Volkov and V. Akulov, “Is the Neutrino a Goldstone Particle?”, *Phys. Lett. B* **46** (1973) 109–110, [doi:10.1016/0370-2693\(73\)90490-5](https://doi.org/10.1016/0370-2693(73)90490-5).
- [56] J. Wess and B. Zumino, “Supergauge Transformations in Four-Dimensions”, *Nucl. Phys. B* **70** (1974) 39–50, [doi:10.1016/0550-3213\(74\)90355-1](https://doi.org/10.1016/0550-3213(74)90355-1).
- [57] P. Nath and R. L. Arnowitt, “Generalized Supergauge Symmetry as a New Framework for Unified Gauge Theories”, *Phys. Lett. B* **56** (1975) 177, [doi:10.1016/0370-2693\(75\)90297-X](https://doi.org/10.1016/0370-2693(75)90297-X).
- [58] R. L. Arnowitt, P. Nath, and B. Zumino, “Superfield Densities and Action Principle in Curved Superspace”, *Phys.Lett.* **B56** (1975) 81, [doi:10.1016/0370-2693\(75\)90504-3](https://doi.org/10.1016/0370-2693(75)90504-3).
- [59] D. Z. Freedman, P. van Nieuwenhuizen, and S. Ferrara, “Progress Toward a Theory of Supergravity”, *Phys.Rev.* **D13** (1976) 3214–3218, [doi:10.1103/PhysRevD.13.3214](https://doi.org/10.1103/PhysRevD.13.3214).
- [60] S. Deser and B. Zumino, “Consistent Supergravity”, *Phys. Lett. B* **62** (1976) 335, [doi:10.1016/0370-2693\(76\)90089-7](https://doi.org/10.1016/0370-2693(76)90089-7).
- [61] P. Nath and R. L. Arnowitt, “Supergravity and Gauge Supersymmetry”, *Phys. Lett. B* **65** (1976) 73, [doi:10.1016/0370-2693\(76\)90537-2](https://doi.org/10.1016/0370-2693(76)90537-2).
- [62] P. Van Nieuwenhuizen, “Supergravity”, *Phys. Rept.* **68** (1981) 189–398, [doi:10.1016/0370-1573\(81\)90157-5](https://doi.org/10.1016/0370-1573(81)90157-5).
- [63] J. Wess and J. Bagger, “Supersymmetry and Supergravity”. Princeton University Press, 1992.
- [64] D. Z. Freedman and A. Van Proeyen, “Supergravity”. Cambridge University Press, 2012.
- [65] A. H. Chamseddine, R. L. Arnowitt, and P. Nath, “Locally Supersymmetric Grand Unification”, *Phys.Rev.Lett.* **49** (1982) 970, [doi:10.1103/PhysRevLett.49.970](https://doi.org/10.1103/PhysRevLett.49.970).

- [66] P. Nath, R. L. Arnowitt, and A. H. Chamseddine, “Gauge Hierarchy in Supergravity Guts”, *Nucl. Phys. B* **227** (1983) 121, [doi:10.1016/0550-3213\(83\)90145-1](https://doi.org/10.1016/0550-3213(83)90145-1).
- [67] L. J. Hall, J. D. Lykken, and S. Weinberg, “Supergravity as the Messenger of Supersymmetry Breaking”, *Phys. Rev. D* **27** (1983) 2359–2378, [doi:10.1103/PhysRevD.27.2359](https://doi.org/10.1103/PhysRevD.27.2359).
- [68] P. Nath, B. D. Nelson, H. Davoudiasl et al., “The Hunt for New Physics at the Large Hadron Collider”, *Nucl.Phys.Proc.Suppl.* **200-202** (2010) 185–417, [doi:10.1016/j.nuclphysbps.2010.03.001](https://doi.org/10.1016/j.nuclphysbps.2010.03.001), [arXiv:1001.2693](https://arxiv.org/abs/1001.2693).
- [69] D. Feldman, Z. Liu, P. Nath et al., “Multicomponent Dark Matter in Supersymmetric Hidden Sector Extensions”, *Phys.Rev.* **D81** (2010) 095017, [doi:10.1103/PhysRevD.81.095017](https://doi.org/10.1103/PhysRevD.81.095017), [arXiv:1004.0649](https://arxiv.org/abs/1004.0649).
- [70] H. S. Cheon, S. K. Kang, and C. Kim, “Doubly Coexisting Dark Matter Candidates in an Extended Seesaw Model”, *Phys.Lett.* **B675** (2009) 203–209, [doi:10.1016/j.physletb.2009.03.083](https://doi.org/10.1016/j.physletb.2009.03.083), [10.1016/j.physletb.2011.03.031](https://doi.org/10.1016/j.physletb.2011.03.031), [arXiv:0807.0981](https://arxiv.org/abs/0807.0981).
- [71] J.-H. Huh, J. E. Kim, and B. Kyae, “Two dark matter components in dark matter extension of the minimal supersymmetric standard model and the high energy positron spectrum in PAMELA/HEAT data”, *Phys.Rev.* **D79** (2009) 063529, [doi:10.1103/PhysRevD.79.063529](https://doi.org/10.1103/PhysRevD.79.063529), [arXiv:0809.2601](https://arxiv.org/abs/0809.2601).
- [72] K. M. Zurek, “Multi-Component Dark Matter”, *Phys.Rev.* **D79** (2009) 115002, [doi:10.1103/PhysRevD.79.115002](https://doi.org/10.1103/PhysRevD.79.115002), [arXiv:0811.4429](https://arxiv.org/abs/0811.4429).
- [73] S. Profumo, K. Sigurdson, and L. Ubaldi, “Can we discover multi-component WIMP dark matter?”, *JCAP* **0912** (2009) 016, [doi:10.1088/1475-7516/2009/12/016](https://doi.org/10.1088/1475-7516/2009/12/016), [arXiv:0907.4374](https://arxiv.org/abs/0907.4374).
- [74] F. Chen, J. M. Cline, and A. R. Frey, “Nonabelian dark matter: Models and constraints”, *Phys.Rev.* **D80** (2009) 083516, [doi:10.1103/PhysRevD.80.083516](https://doi.org/10.1103/PhysRevD.80.083516), [arXiv:0907.4746](https://arxiv.org/abs/0907.4746).
- [75] F. D’Eramo and J. Thaler, “Semi-annihilation of Dark Matter”, *JHEP* **1006** (2010) 109, [doi:10.1007/JHEP06\(2010\)109](https://doi.org/10.1007/JHEP06(2010)109), [arXiv:1003.5912](https://arxiv.org/abs/1003.5912).
- [76] CDMS-II Collaboration, “Dark Matter Search Results from the CDMS II Experiment”, *Science* **327** (2010) 1619–1621, [doi:10.1126/science.1186112](https://doi.org/10.1126/science.1186112), [arXiv:0912.3592](https://arxiv.org/abs/0912.3592).
- [77] CDMS Collaboration, “Search for Weakly Interacting Massive Particles with the First Five-Tower Data from the Cryogenic Dark Matter Search at the

- Soudan Underground Laboratory”, *Phys.Rev.Lett.* **102** (2009) 011301, [doi:10.1103/PhysRevLett.102.011301](https://doi.org/10.1103/PhysRevLett.102.011301), [arXiv:0802.3530](https://arxiv.org/abs/0802.3530).
- [78] XENON100 Collaboration, “First Dark Matter Results from the XENON100 Experiment”, *Phys.Rev.Lett.* **105** (2010) 131302, [doi:10.1103/PhysRevLett.105.131302](https://doi.org/10.1103/PhysRevLett.105.131302), [arXiv:1005.0380](https://arxiv.org/abs/1005.0380).
- [79] XENON100 Collaboration, “Likelihood Approach to the First Dark Matter Results from XENON100”, *Phys.Rev.* **D84** (2011) 052003, [doi:10.1103/PhysRevD.84.052003](https://doi.org/10.1103/PhysRevD.84.052003), [arXiv:1103.0303](https://arxiv.org/abs/1103.0303).
- [80] XENON100 Collaboration, “Dark Matter Results from 100 Live Days of XENON100 Data”, *Phys.Rev.Lett.* **107** (2011) 131302, [doi:10.1103/PhysRevLett.107.131302](https://doi.org/10.1103/PhysRevLett.107.131302), [arXiv:1104.2549](https://arxiv.org/abs/1104.2549).
- [81] O. Adriani, G. Barbarino, G. Bazilevskaya et al., “A new measurement of the antiproton-to-proton flux ratio up to 100 GeV in the cosmic radiation”, *Phys.Rev.Lett.* **102** (2009) 051101, [doi:10.1103/PhysRevLett.102.051101](https://doi.org/10.1103/PhysRevLett.102.051101), [arXiv:0810.4994](https://arxiv.org/abs/0810.4994).
- [82] PAMELA Collaboration, “An anomalous positron abundance in cosmic rays with energies 1.5-100 GeV”, *Nature* **458** (2009) 607–609, [doi:10.1038/nature07942](https://doi.org/10.1038/nature07942), [arXiv:0810.4995](https://arxiv.org/abs/0810.4995).
- [83] O. Adriani, G. Barbarino, G. Bazilevskaya et al., “A statistical procedure for the identification of positrons in the PAMELA experiment”, *Astropart.Phys.* **34** (2010) 1–11, [doi:10.1016/j.astropartphys.2010.04.007](https://doi.org/10.1016/j.astropartphys.2010.04.007), [arXiv:1001.3522](https://arxiv.org/abs/1001.3522).
- [84] AMS-01 Collaboration, “Cosmic-ray positron fraction measurement from 1 to 30-GeV with AMS-01”, *Phys.Lett.* **B646** (2007) 145–154, [doi:10.1016/j.physletb.2007.01.024](https://doi.org/10.1016/j.physletb.2007.01.024), [arXiv:astro-ph/0703154](https://arxiv.org/abs/astro-ph/0703154).
- [85] D. Feldman, Z. Liu, and P. Nath, “PAMELA Positron Excess as a Signal from the Hidden Sector”, *Phys.Rev.* **D79** (2009) 063509, [doi:10.1103/PhysRevD.79.063509](https://doi.org/10.1103/PhysRevD.79.063509), [arXiv:0810.5762](https://arxiv.org/abs/0810.5762).
- [86] B. Kors and P. Nath, “A Supersymmetric Stueckelberg U(1) extension of the MSSM”, *JHEP* **0412** (2004) 005, [doi:10.1088/1126-6708/2004/12/005](https://doi.org/10.1088/1126-6708/2004/12/005), [arXiv:hep-ph/0406167](https://arxiv.org/abs/hep-ph/0406167).
- [87] D. Feldman, B. Kors, and P. Nath, “Extra-weakly Interacting Dark Matter”, *Phys.Rev.* **D75** (2007) 023503, [doi:10.1103/PhysRevD.75.023503](https://doi.org/10.1103/PhysRevD.75.023503), [arXiv:hep-ph/0610133](https://arxiv.org/abs/hep-ph/0610133).
- [88] H. Goldberg, “Constraint on the Photino Mass from Cosmology”, *Phys.Rev.Lett.* **50** (1983) 1419, [doi:10.1103/PhysRevLett.50.1419](https://doi.org/10.1103/PhysRevLett.50.1419).

- [89] D. Feldman, Z. Liu, and P. Nath, “The Stueckelberg Z Prime at the LHC: Discovery Potential, Signature Spaces and Model Discrimination”, *JHEP* **0611** (2006) 007, doi:[10.1088/1126-6708/2006/11/007](https://doi.org/10.1088/1126-6708/2006/11/007), [arXiv:hep-ph/0606294](https://arxiv.org/abs/hep-ph/0606294).
- [90] B. Altunkaynak, M. Holmes, P. Nath et al., “SUSY Discovery Potential and Benchmarks for Early Runs at  $\sqrt{s} = 7$  TeV at the LHC”, *Phys.Rev.* **D82** (2010) 115001, doi:[10.1103/PhysRevD.82.115001](https://doi.org/10.1103/PhysRevD.82.115001), [arXiv:1008.3423](https://arxiv.org/abs/1008.3423).
- [91] S. Akula, N. Chen, D. Feldman et al., “Interpreting the First CMS and ATLAS SUSY Results”, *Phys.Lett.* **B699** (2011) 377–382, doi:[10.1016/j.physletb.2011.04.041](https://doi.org/10.1016/j.physletb.2011.04.041), [arXiv:1103.1197](https://arxiv.org/abs/1103.1197).
- [92] J. Alwall, P. Demin, S. de Visscher et al., “MadGraph/MadEvent v4: the new web Generation”, *JHEP* **0709** (2007) 028, doi:[10.1088/1126-6708/2007/09/028](https://doi.org/10.1088/1126-6708/2007/09/028), [arXiv:0706.2334](https://arxiv.org/abs/0706.2334).
- [93] T. Sjostrand, S. Mrenna, and P. Z. Skands, “PYTHIA 6.4 physics and manual”, *JHEP* **0605** (2006) 026, doi:[10.1088/1126-6708/2006/05/026](https://doi.org/10.1088/1126-6708/2006/05/026), [arXiv:hep-ph/0603175](https://arxiv.org/abs/hep-ph/0603175).
- [94] J. Conway, “PGS 4: pretty good simulation of high energy collisions”, <http://physics.ucdavis.edu/~conway/research/software/pgs/pgs4-general.htm>.
- [95] J. Pumplin, D. Stump, J. Huston et al., “New generation of parton distributions with uncertainties from global QCD analysis”, *JHEP* **0207** (2002) 012, [arXiv:hep-ph/0201195](https://arxiv.org/abs/hep-ph/0201195).
- [96] M. Davier, A. Hoecker, B. Malaescu et al., “Reevaluation of the hadronic contribution to the muon magnetic anomaly using new  $e^+e^- \rightarrow \pi^+\pi^-$  cross section data from BABAR”, *Eur.Phys.J.* **C66** (2010) 1–9, doi:[10.1140/epjc/s10052-010-1246-1](https://doi.org/10.1140/epjc/s10052-010-1246-1), [arXiv:0908.4300](https://arxiv.org/abs/0908.4300).
- [97] T. Yuan, R. L. Arnowitt, A. H. Chamseddine et al., “Supersymmetric Electroweak Effects on G-2 (mu)”, *Z.Phys.* **C26** (1984) 407, doi:[10.1007/BF01452567](https://doi.org/10.1007/BF01452567).
- [98] CDF Collaboration, “Search for  $B_s^0 \rightarrow \mu^+\mu^-$  and  $B_d^0 \rightarrow \mu^+\mu^-$  decays with  $2fb^{-1}$  of  $p\bar{p}$  collisions”, *Phys.Rev.Lett.* **100** (2008) 101802, doi:[10.1103/PhysRevLett.100.101802](https://doi.org/10.1103/PhysRevLett.100.101802), [arXiv:0712.1708](https://arxiv.org/abs/0712.1708).
- [99] Heavy Flavor Averaging Group, “Averages of  $b$ -hadron and  $c$ -hadron Properties at the End of 2007”, [arXiv:0808.1297](https://arxiv.org/abs/0808.1297).

- [100] M. Misiak, H. Asatrian, K. Bieri et al., “Estimate of  $B(\bar{B} \rightarrow X(s)\gamma)$  at  $O(\alpha(s)^2)$ ”, *Phys.Rev.Lett.* **98** (2007) 022002, [doi:10.1103/PhysRevLett.98.022002](https://doi.org/10.1103/PhysRevLett.98.022002), [arXiv:hep-ph/0609232](https://arxiv.org/abs/hep-ph/0609232).
- [101] A. Djouadi, M. Drees, and J. Kneur, “Constraints on the minimal supergravity model and prospects for SUSY particle production at future linear  $e^+e^-$  colliders”, *JHEP* **0108** (2001) 055, [arXiv:hep-ph/0107316](https://arxiv.org/abs/hep-ph/0107316).
- [102] G. Belanger, F. Boudjema, P. Brun et al., “Indirect search for dark matter with micrOMEGAs2.4”, *Comput.Phys.Commun.* **182** (2011) 842–856, [doi:10.1016/j.cpc.2010.11.033](https://doi.org/10.1016/j.cpc.2010.11.033), [arXiv:1004.1092](https://arxiv.org/abs/1004.1092).
- [103] A. Djouadi, J.-L. Kneur, and G. Moultaka, “SuSpect: A Fortran code for the supersymmetric and Higgs particle spectrum in the MSSM”, *Comput.Phys.Commun.* **176** (2007) 426–455, [doi:10.1016/j.cpc.2006.11.009](https://doi.org/10.1016/j.cpc.2006.11.009), [arXiv:hep-ph/0211331](https://arxiv.org/abs/hep-ph/0211331).
- [104] ATLAS Collaboration, “Search for supersymmetry using final states with one lepton, jets, and missing transverse momentum with the ATLAS detector in  $\sqrt{s} = 7$  TeV  $pp$ ”, *Phys.Rev.Lett.* **106** (2011) 131802, [doi:10.1103/PhysRevLett.106.131802](https://doi.org/10.1103/PhysRevLett.106.131802), [arXiv:1102.2357](https://arxiv.org/abs/1102.2357).
- [105] ATLAS Collaboration, “Search for squarks and gluinos using final states with jets and missing transverse momentum with the ATLAS detector in  $\sqrt{s} = 7$  TeV proton-proton collisions”, *Phys.Lett.* **B701** (2011) 186–203, [doi:10.1016/j.physletb.2011.05.061](https://doi.org/10.1016/j.physletb.2011.05.061), [arXiv:1102.5290](https://arxiv.org/abs/1102.5290).
- [106] ATLAS Collaboration, “Expected Performance of the ATLAS Experiment - Detector, Trigger and Physics”, [arXiv:0901.0512](https://arxiv.org/abs/0901.0512).
- [107] R. L. Arnowitt and P. Nath, “Loop corrections to radiative breaking of electroweak symmetry in supersymmetry”, *Phys.Rev.* **D46** (1992) 3981–3986, [doi:10.1103/PhysRevD.46.3981](https://doi.org/10.1103/PhysRevD.46.3981).
- [108] K. L. Chan, U. Chattopadhyay, and P. Nath, “Naturalness, weak scale supersymmetry and the prospect for the observation of supersymmetry at the Tevatron and at the CERN LHC”, *Phys.Rev.* **D58** (1998) 096004, [doi:10.1103/PhysRevD.58.096004](https://doi.org/10.1103/PhysRevD.58.096004), [arXiv:hep-ph/9710473](https://arxiv.org/abs/hep-ph/9710473).
- [109] U. Chattopadhyay, A. Corsetti, and P. Nath, “WMAP constraints, SUSY dark matter and implications for the direct detection of SUSY”, *Phys.Rev.* **D68** (2003) 035005, [doi:10.1103/PhysRevD.68.035005](https://doi.org/10.1103/PhysRevD.68.035005), [arXiv:hep-ph/0303201](https://arxiv.org/abs/hep-ph/0303201).
- [110] J. L. Feng, K. T. Matchev, and T. Moroi, “Multi - TeV scalars are natural in minimal supergravity”, *Phys.Rev.Lett.* **84** (2000) 2322–2325, [doi:10.1103/PhysRevLett.84.2322](https://doi.org/10.1103/PhysRevLett.84.2322), [arXiv:hep-ph/9908309](https://arxiv.org/abs/hep-ph/9908309).

- [111] H. Baer, C. Balazs, A. Belyaev et al., “Updated reach of the CERN LHC and constraints from relic density,  $b \rightarrow s\gamma$  and  $a(\mu)$  in the mSUGRA model”, *JHEP* **0306** (2003) 054, [arXiv:hep-ph/0304303](#).
- [112] S. Akula, M. Liu, P. Nath et al., “Naturalness, Supersymmetry and Implications for LHC and Dark Matter”, *Phys.Lett.* **B709** (2012) 192–199, [doi:10.1016/j.physletb.2012.01.077](#), [arXiv:1111.4589](#).
- [113] D. Feldman, K. Freese, P. Nath et al., “Predictive Signatures of Supersymmetry: Measuring the Dark Matter Mass and Gluino Mass with Early LHC data”, *Phys.Rev.* **D84** (2011) 015007, [doi:10.1103/PhysRevD.84.015007](#), [arXiv:1102.2548](#).
- [114] S. Akula, P. Nath, and G. Peim, “Implications of the Higgs Boson Discovery for mSUGRA”, *Phys.Lett.* **B717** (2012) 188–192, [doi:10.1016/j.physletb.2012.09.007](#), [arXiv:1207.1839](#).
- [115] F. Feroz, K. Cranmer, M. Hobson et al., “Challenges of Profile Likelihood Evaluation in Multi-Dimensional SUSY Scans”, *JHEP* **1106** (2011) 042, [doi:10.1007/JHEP06\(2011\)042](#), [arXiv:1101.3296](#).
- [116] Y. Akrami, P. Scott, J. Edsjo et al., “A Profile Likelihood Analysis of the Constrained MSSM with Genetic Algorithms”, *JHEP* **1004** (2010) 057, [doi:10.1007/JHEP04\(2010\)057](#), [arXiv:0910.3950](#).
- [117] S. Akula, B. Altunkaynak, D. Feldman et al., “Higgs Boson Mass Predictions in SUGRA Unification, Recent LHC-7 Results, and Dark Matter”, *Phys.Rev.* **D85** (2012) 075001, [doi:10.1103/PhysRevD.85.075001](#), [arXiv:1112.3645](#).
- [118] A. Hoecker, “The Hadronic Contribution to the Muon Anomalous Magnetic Moment and to the Running Electromagnetic Fine Structure Constant at MZ - Overview and Latest Results”, *Nucl.Phys.Proc.Suppl.* **218** (2011) 189–200, [doi:10.1016/j.nuclphysbps.2011.06.031](#), [arXiv:1012.0055](#).
- [119] N. Chen, D. Feldman, Z. Liu et al., “Low Mass Gluino within the Sparticle Landscape, Implications for Dark Matter, and Early Discovery Prospects at LHC-7”, *Phys.Rev.* **D83** (2011) 035005, [doi:10.1103/PhysRevD.83.035005](#), [arXiv:1011.1246](#).
- [120] S. Akula, D. Feldman, Z. Liu et al., “New Constraints on Dark Matter from CMS and ATLAS Data”, *Mod.Phys.Lett.* **A26** (2011) 1521–1535, [doi:10.1142/S0217732311036292](#), [arXiv:1103.5061](#).